

159

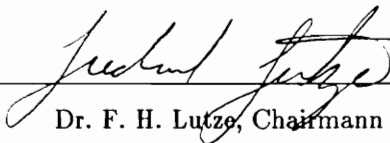
PARAMETER OPTIMIZATION OF ATMOSPHERIC SKIP TRAJECTORIES FOR USE IN MINIMUM FUEL USAGE TRANSFER ORBITS

by

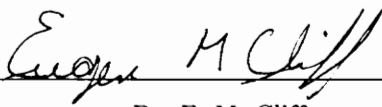
Craig Alan Martell

Thesis submitted to the Faculty of the
Virginia Polytechnic Institute and State University
in partial fulfillment of the requirements for the degree of
Master of Science
in
Aerospace and Ocean Engineering

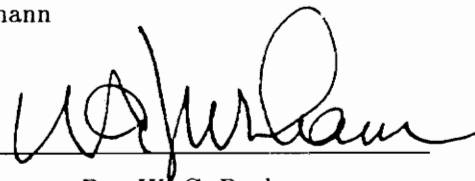
APPROVED:



Dr. F. H. Lutze, Chairmann



Dr. E. M. Cliff



Dr. W. C. Durham

March 28, 1991

Blacksburg, Virginia

02

LD

5655

V855

1991

M378

0.2

PARAMETER OPTIMIZATION OF ATMOSPHERIC SKIP TRAJECTORIES FOR USE IN MINIMUM FUEL USAGE TRANSFER ORBITS

by

Craig Alan Martell

Dr. F. H. Lutze, Chairman

Aerospace and Ocean Engineering

(ABSTRACT)

The problem of developing a generalized impulse as a function of a set of parameters is investigated. The proposed generalized impulse alters an existing orbit by producing, over some period of time, a change in velocity, $\Delta\vec{V}$, as well as a change in position, $\Delta\vec{r}$. The generalized impulse is described by parameters associated with an instantaneous change in velocity as well as parameters associated with an atmospheric skip trajectory. Closed form solutions are obtained through several changes of independent variable, the use of modified Chapman variables and the consequent analytical integration of the uncoupled equations. The closed form solutions contain between two and six parameters depending on the complexity of the desired skip trajectory. Fuel optimal transfer orbits are obtained using the generalized impulse along with Keplerian arcs and instantaneous changes in velocity. Families of coplanar and noncoplanar transfers for circular orbit to circular orbit are numerically generated. The generated transfer trajectories involve the rendezvous of two vehicles. The orbits are not globally optimal but rather optimal for the specified number and type of velocity impulses specified. The optimal solution to the nonlinear problem is determined via sequential quadratic programming which satisfies the Kuhn-Tucker optimality conditions for constrained minimization. It is found that for transfer between coplanar and noncoplanar orbits, solutions using the generalized impulse compare favorably with solutions obtained by optimal control theory. Numerical solution to complex problems involving transfer from general orbit to general orbit were not obtained.

Acknowledgements

I am greatly indebted to Dr. Frederick H. Lutze for all of his guidance, encouragement and patience during the past two years. Thanks also goes to Dr. E. M. Cliff and Dr. W. C. Durham for serving on my committee.

This research was supported by the Aerospace and Ocean Engineering department of the Virginia Polytechnic Institute and State University and is gratefully acknowledged.

Acknowledgements also go to Michael C. Brown, Eric D. Bloodworth and Lee H. Hart for their assistance with computer related matters. Thanks goes to Brian G. Thompson, Joeseeph T. Hadden and Michael S. Warner for their support over the past two years.

Finally, this effort is dedicated to Annette Lynn Eisler.

List of Symbols

a	Semi-major axis
C_D	Drag coefficient
C_D^*	Drag coefficient for maximum lift-to-drag ratio
C_{D0}	Zero-lift drag coefficient
C_L	Lift coefficient
C_L^*	Lift coefficient for maximum lift-to-drag ratio
E^*	Maximum Lift-to-Drag ratio
e	Eccentricity
g	Constraint
h	Altitude (km)
i	Orbital plane inclination
J	Cost function
K	Induced drag factor
k^2	Atmospheric constant (βr)
m	Mass (kg)
n	Exponent for the generalized drag polar
r	Radial distance from center of Earth
s	Dimensionless arc length
R	Gas constant for air
S	Vehicle reference area (m^2)

t	Time (s)
v	Dimensionless velocity
V	Velocity (km/s)
Z	Dimensionless altitude
$\Delta\vec{V}$	Change in velocity vector
DU	Distance units
LEO	Low-Earth orbit
GEO	Geosynchronous Earth orbit
SU	Speed units
TOF	Time of flight

Greek Symbols

α	Right ascension
β	Inverse scale Height
γ	Flight path angle
δ	Declination
η	Keplerian coasting arc
θ	Longitude or downrange angle
λ	Scaled lift coefficient
μ	Gravitational parameter (km ³ /s ²)
ν	True anomaly
ρ	Density (kg/m ³)
σ	Bank angle
ϕ	Latitude or lateral range angle

χ	Ratio of interceptor to target circular radii
ψ	Heading angle
ω_e	Angular rate of the Earth (rad/s)
ω	Argument of perigee
Ω	Longitude of the ascending node

Subscripts

a	Ascent subarc
c	Constant altitude subarc
d	Descent subarc
e	Entry conditions into the atmosphere
f	Exit conditions from the atmosphere
o	Sea-level reference values
I	Inertial coordinate system
E	Earth fixed coordinate system
T	Tracking coordinate system
W	Wind axes coordinate system
G	Geocentric-equatorial coordinate system
atm	Atmospheric related values
min	Designates minimum values

Table of Contents

Chapter 1: Introduction and Background	1
Chapter 2: Problem Formulation	6
2.1: Overview	6
2.2: General Point-Mass Model	7
2.2.1: Basic Vector Mechanics	7
2.2.2: Angular Motion	11
2.2.3: Acceleration Relative to Earth Fixed Axes	12
2.2.4: General Forces	13
2.2.5: General Equations of Motion for Atmospheric Flight	15
2.3: Problem Statement	16
2.4: Skip Trajectory Point-Mass Model	18
2.4.1: Aerodynamic Forces	19
2.4.2: Atmospheric Model	22
2.4.3: Skip Trajectory Equations of Motion	23
2.4.4: Skip Trajectory Dimensionless Equations of Motion	25
2.5: Closed Form Solutions	28
2.5.1: Method of Performing Skip Trajectory	29
2.5.2: Boundary Conditions for Constant Altitude Subarc	29
2.5.3: Closed Form Solutions to the Constant Altitude Subarc	30
2.5.4: Boundary Conditions for Descent and Ascent Subarcs	33
2.5.5: Closed Form Solutions for the Descent and Ascent Subarcs	34
2.6: Skip Trajectory Parameters	38

Chapter 3: Skip Trajectory Implementation	40
3.1: Overview	40
3.2: Previous Orbit Calculation Procedures	40
3.3: Calculating the Generalized Impulse for an Aeroassisted Maneuver	41
3.3.1: Coordinate Systems	41
3.3.2: Calculation of Entrance Conditions	42
3.3.3: Changes in Position due to Aeroassisted Maneuver	43
3.3.4: Exit Orbit Determination	47
3.4: The Generalized Impulse	50
Chapter 4: Numerical Results	51
4.1: Overview	51
4.2: Validation of Closed Form Solutions	52
4.3: Validation of Skip Trajectory Implementation	53
4.4: Two Impulse Orbit Transfers	55
4.4.1: Parameters and Constraints for Two Impulse Transfer	56
4.4.2: Coplanar Two Impulse Transfers	58
4.4.3: Noncoplanar Two Impulse Transfers	61
Chapter 5: Conclusion and Recommendation	72
5.1: Conclusions	72
5.2: Recommendations for Future Research	73

Appendix A: Partial Derivatives and Integrals	74
A.1: Partial Derivatives	74
A.1.1: Z Chapman Variable	74
A.1.2: v Chapman Variable	75
A.2: Integrals	76
A.2.1: Latitude and Longitude	76
A.2.2: Time	80
References	84
Vita	136

List of Figures

Figure 1.	Earth Fixed and Tracking Coordinate Systems	86
Figure 2.	Wind Axes Coordinate System	87
Figure 3.	Lift, Drag and Gravitational Forces Acting on a Vehicle	88
Figure 4.	Altitude vs. Atmospheric Density	89
Figure 5.	Geocentric-Equatorial Coordinate System	90
Figure 6.	Right Ascension-Declination Coordinate System	91
Figure 7.	Definition of Reference Planes for a General Skip Trajectory	92
Figure 8.	Orbital Elements and the Geocentric-Equatorial Coordinate System	93
Figure 9.	Inclination Change Due to an Aeroassisted Maneuver	94
Figure 10.	Orbital Path for a Two Impulse Transfer	95
Figure 11.	Altitude vs. Time for 10°, 20°, 30° and 40° Heading Change Maneuvers	96
Figure 12.	Altitude vs. Time for $\chi = 5.75$ (Coplanar)	97
Figure 13.	Normal G-Load vs. Time for $\chi = 5.75$ (Coplanar)	98
Figure 14.	Convective Heating Rate vs. Time for $\chi = 5.75$ (Coplanar)	99
Figure 15.	Flight Path Angle vs. Time for $\chi = 5.75$ (Coplanar)	100
Figure 16.	Dynamic Pressure vs. Time for $\chi = 5.75$ (Coplanar)	101
Figure 17.	Velocity vs. Time for $\chi = 5.75$ (Coplanar)	102
Figure 18.	Altitude vs. Time for $\chi = 2.61$ (Coplanar)	103
Figure 19.	Normal G-Load vs. Time for $\chi = 2.61$ (Coplanar)	104
Figure 20.	Convective Heating Rate vs. Time for $\chi = 2.61$ (Coplanar)	105

Figure 21.	Flight Path Angle vs. Time for $\chi = 2.61$ (Coplanar)	106
Figure 22.	Dynamic Pressure vs. Time for $\chi = 2.61$ (Coplanar)	107
Figure 23.	Velocity vs. Time for $\chi = 2.61$ (Coplanar)	108
Figure 24.	Altitude vs. Time for $\chi = 1.30$ (Coplanar)	109
Figure 25.	Normal G-Load vs. Time for $\chi = 1.30$ (Coplanar)	110
Figure 26.	Convective Heating Rate vs. Time for $\chi = 1.30$ (Coplanar)	111
Figure 27.	Flight Path Angle vs. Time for $\chi = 1.30$ (Coplanar)	112
Figure 28.	Dynamic Pressure vs. Time for $\chi = 1.30$ (Coplanar)	113
Figure 29.	Velocity vs. Time for $\chi = 1.30$ (Coplanar)	114
Figure 30.	Altitude vs. Time for $\chi = 5.75$ (Noncoplanar $\Delta i = 5^\circ$)	115
Figure 31.	Normal G-Load vs. Time for $\chi = 5.75$ (Noncoplanar $\Delta i = 5^\circ$)	116
Figure 32.	Convective Heating Rate vs. Time for $\chi = 5.75$ (Noncoplanar $\Delta i = 5^\circ$)	117
Figure 33.	Flight Path Angle vs. Time for $\chi = 5.75$ (Noncoplanar $\Delta i = 5^\circ$)	118
Figure 34.	Dynamic Pressure vs. Time for $\chi = 5.75$ (Noncoplanar $\Delta i = 5^\circ$)	119
Figure 35.	Velocity vs. Time for $\chi = 5.75$ (Noncoplanar $\Delta i = 5^\circ$)	120
Figure 36.	Altitude vs. Time for $\chi = 2.61$ (Noncoplanar $\Delta i = 5^\circ$)	121
Figure 37.	Normal G-Load vs. Time for $\chi = 2.61$ (Noncoplanar $\Delta i = 5^\circ$)	122
Figure 38.	Convective Heating Rate vs. Time for $\chi = 2.61$ (Noncoplanar $\Delta i = 5^\circ$)	123
Figure 39.	Flight Path Angle vs. Time for $\chi = 2.61$ (Noncoplanar $\Delta i = 5^\circ$)	124
Figure 40.	Dynamic Pressure vs. Time for $\chi = 2.61$ (Noncoplanar $\Delta i = 5^\circ$)	125
Figure 41.	Velocity vs. Time for $\chi = 2.61$ (Noncoplanar $\Delta i = 5^\circ$)	126
Figure 42.	Altitude vs. Time for $\chi = 1.30$ (Noncoplanar $\Delta i = 5^\circ$)	127
Figure 43.	Normal G-Load vs. Time for $\chi = 1.30$ (Noncoplanar $\Delta i = 5^\circ$)	128
Figure 44.	Convective Heating Rate vs. Time for $\chi = 1.30$ (Noncoplanar $\Delta i = 5^\circ$)	129
Figure 45.	Flight Path Angle vs. Time for $\chi = 1.30$ (Noncoplanar $\Delta i = 5^\circ$)	130
Figure 46.	Dynamic Pressure vs. Time for $\chi = 1.30$ (Noncoplanar $\Delta i = 5^\circ$)	131

Figure 47. Velocity vs. Time for $\chi = 1.30$ (Noncoplanar $\Delta i = 5^\circ$)	132
Figure 48. Cost Function vs. χ for Coplanar Transfer Methods	133
Figure 49. Cost Function vs. χ for Noncoplanar Transfer Methods ($\Delta i = 5^\circ$)	134
Figure 50. Coplanar and Noncoplanar Generalized Impulse Cost Functions vs. χ	135

Chapter 1: Introduction and Background

The general problem of determining orbital transfer trajectories using minimum fuel requires characterization of the manner in which the transfer trajectory is produced. Since changes in an orbit are produced by some manner of propulsive action, the type of the propulsive burn determines the amount of fuel expended. Propulsive burns can be applied continuously over some period of time according to a control law which specifies their magnitude and direction or they can be approximated by an impulse which acts instantaneously in a defined direction. Determining the optimal control during thrusting arcs is difficult and requires complex numerical calculations and is not discussed in this paper. For a comprehensive discussion of optimal space maneuvers see [9]. This paper concentrates on determining a simple, yet accurate, approximation to a continuous thrusting arc in the form of a generalization of the impulse approximation mentioned previously.

Determining transfer orbits is made easier by parameterizing the entire transfer trajectory with instantaneously applied propulsive burns commonly called delta-v's, $\Delta\vec{V}_{inst}$, separated by Keplerian coasting arcs through the angle, η . In general, the $\Delta\vec{V}_{inst}$ has components in three dimensional space and these three components become a set of three parameters to be used along with the coasting angle η to describe each subarc of the transfer orbit. Using the $\|\Delta\vec{V}_{inst}\|$ as a means to measure the propulsive burns, the total fuel expended is related to the cost function, J , by

$$J = \sum_{i=1}^n \|(\Delta\vec{V}_{inst})_i\|$$

where n is the number of instantaneous delta- v 's. Motion of the space vehicle during the Keplerian arcs is well known and is not discussed in detail in this paper. However, a thorough discussion of Keplerian motion is found in [1,2]. The combination of the parameters describing the Keplerian arc angle and the instantaneous changes in velocity is sufficient to parameterize the amount of fuel used in an orbit transfer problem.

The pure impulsive approximation to a thrusting maneuver as described above is applied instantaneously while the position of the vehicle is assumed constant. This research proposes a generalized impulse which produces a change in velocity as well as a change in position that is not instantaneous but occurs over some finite period of time. The generalized impulse produces these changes in position and velocity as a function of a set of generalized impulse parameters, \vec{x}_g , as follows:

$$\vec{V}^+ = \vec{V}^- + \Delta\vec{V}(\vec{x}_g)$$

$$\vec{r}^+ = \vec{r}^- + \Delta\vec{r}(\vec{x}_g)$$

$$t^+ = t^- + \Delta t(\vec{x}_g)$$

where $+$ indicates the state after application of the generalized impulse and $-$ indicates the state prior to the application of the generalized impulse.

This paper concentrates on the problem of representing an aeroassist maneuver as a generalized impulse and determining the changes in position and velocity as functions of the generalized impulse parameters, \vec{x}_g associated with this maneuver. This aeroassisted maneuver involves a space trajectory of which part dips into the atmosphere. It is well known that these types of maneuvers can reduce the amount of fuel needed for certain orbit transfer problems. In particular, the types of orbit transfers that take advantage of atmospheric flight to reduce the amount of fuel used include orbital plane, orbital size and orbital energy change maneuvers.

Trajectories which use the combination of propulsive maneuvers in space along with aerodynamic maneuvers in the upper portion of the atmosphere to produce these orbital changes are classified under the title of synergistic space flight.

The maneuver sequence is initiated by the application of an appropriate instantaneous $\Delta\vec{V}_{inst}$ to an existing exoatmospheric Keplerian orbit. As a result of this instantaneous delta-v, whose components are only part of the entire set of generalized impulse parameters, a new Keplerian orbit is generated. The new orbit generated is designated as the deboost orbit and as the vehicle moves along the deboost orbit, it is forced to enter the atmosphere. The space vehicle's motion from atmospheric entry to atmospheric exit is mapped by the remaining parameters of the generalized impulse. These parameters are designated by the vector of atmospheric parameters, \vec{x}_a and are determined from the atmospheric flight equations. Exit from the atmosphere terminates the changes described by the generalized impulse.

Solution for the state and control variables related to the atmospheric flight using optimal control theory proves unsatisfactory because the solution method requires numerical integration of the coupled nonlinear system of flight equations. While the problem of determining optimal transfers involving the atmosphere has been widely investigated using optimal control theory, simplification of the problem to a parameter optimization problem has generally been ignored. References [3-7, 10-15, 17-19] provide discussion on atmospheric modeling, atmospheric flight and the optimal control laws used for several different types of optimal control problems related to aeroassisted transfers.

Previous work in Hull [4] poses and solves via optimal control theory the problem which uses an aeroassisted maneuver for the transfer between two noncoplanar circular orbits of the same radius. In this reference, Hull proposes a transfer using instantaneous delta-v's applied tangential to the flight path at three distinct points along the transfer orbit. The first instantaneous delta-v is a tangential retroburn applied to inject the vehicle into an elliptical

orbit that causes atmospheric entry. The second impulse is applied tangential to the flight path at the exit from the atmosphere to raise the exit orbit's apogee to the radius corresponding to the initial circular orbit. The third instantaneous delta-v is applied tangentially at apogee to recircularize at the target radius. Because this research concentrates on two impulse maneuvers, only the atmospheric portion of the aforementioned transfer orbit is of interest to the current research. The results presented by Hull [4] show that atmospheric flight occurs at a nearly constant angle-of-attack corresponding to maximum Lift-to-Drag for all cases presented. The change in latitude is small and the entire pass through the atmosphere is made at small flight path angles. Hull [4] notes that for orbital plane changes exceeding twenty degrees, that the gravitational and apparent lift forces become important to the calculation of the state variables associated with atmospheric flight. As related to the current research, this suggests that exclusion of the gravitational and apparent lift forces produces valid answers for maneuvers which change the orbital plane inclination by less than twenty degrees.

In the work of Vinh and Mease [14], minimum fuel usage transfer orbits between two coplanar circular orbits are determined by optimal control theory. However, the circular orbits are not of the same radius allowing for the use of two impulses rather than the three required by Hull [4], thus more closely paralleling the current research. Similar to Hull [4], the first instantaneous delta-v is a tangential retroburn applied to inject the vehicle from a high-Earth orbit (HEO) into an elliptical orbit that causes atmospheric entry. After the atmospheric pass, and subsequent exit from the atmosphere followed by a Keplerian coast, the second instantaneous delta-v is applied to circularize at the radius corresponding the low-Earth orbit (LEO) target orbit. The presented results show that the atmospheric pass occurs at small flight path angles and that when a heating rate constraint is added to their optimal control problem, flight also occurs at a constant lift coefficient. Because the orbit transfer in [14] and the present work is performed with two impulses, the atmospheric skip trajectories calculated in [14] and the current research are compared. Comparison between the time histories in [14] for heating rate, dynamic

pressure and normal g-load provide a measure of the validity between results obtained using the proposed generalized impulse and optimal control theory.

As part of determining the generalized impulse and the associated parameters as an alternative to solution by optimal control theory, this research effort determines closed form solutions to the atmospheric state variables. These closed form solutions are then applied to the problem of finding minimum fuel rendezvous transfer orbits. In obtaining these closed form solutions, assumptions on the nature of flight through the atmosphere and the form of the vehicle control laws are made. Parameters which completely describe the skip trajectory are proposed. Using these parameters along with the parameters defining the rest of the generalized impulse and the set of parameters defining the Keplerian space flight, the constrained parameter optimization problem is formulated and solved. The solutions to the constrained parameter optimization problem provide a quick, yet accurate, method of producing answers to initial questions associated with designing transfer orbits using an aeroassisted trajectory or generating an initial guess for finding a solution to an optimal control problem.

The following chapter reiterates the formulation of the generalized impulse as a function of a set of parameters. Closed form solutions involving parameters for the atmospheric portion of the aeroassisted transfer orbit are developed. Chapter 3 discusses the conversion of the scalar skip trajectory results to vector form which is used with existing Keplerian orbits to determine the exact position of the vehicle. Chapter 3 also discusses previously existing and added methods used in calculating parameterized transfer orbits. Chapter 4 presents the numerical results which validate the closed form solutions as well as presenting numerical solutions to several minimum fuel transfer orbit problems. Finally, Chapter 5 makes conclusions about the present research effort as well as giving some ideas for future research. Analytical evaluation for several of the partial derivatives used and evaluation of selected important integrals is presented in Appendix A.

Chapter 2: Problem Formulation

2.1: Overview

This chapter states the problem of forming an orbit transfer trajectory as a function of a set of parameters. As part of this formulation, a generalized impulse is presented which takes the form of an aeroassisted maneuver. The generalized impulse, which produces a change in velocity, $\Delta\vec{V}$, a change in position, $\Delta\vec{r}$, and a change in time, Δt , involves flight through space and the atmosphere. A review of the parameterization of the exoatmospheric equations as done in reference 8 is presented and will be used in developing the generalized impulse. Focus is on the formulation of the generalized impulse as a function of a set of parameters.

The formulation of the generalized impulse requires the development of the atmospheric differential equations of motion, an atmospheric model, and finding the closed form solutions to the equations of motion. Once determined, the closed form solutions reveal the parameters needed for the generalized impulse. The newly formed generalized impulse can then be included as part of a parameter optimization problem. The optimization problem may be loosely stated as to find the set of parameters which describes a transfer orbit sequence so that an interceptor will rendezvous with a target and at the same time minimize fuel expenditure.

2.2: General Point-Mass Model

As a basis for formulating the parameter optimization problem, a general point-mass model of the differential equations of motion governing the atmospheric flight portion is developed. The equations of motion governing space flight are already well known and are not presented here; however a complete discussion of the equations of motion for a vehicle under Keplerian motion is found in references [1,2]. The following sections give the equations of motion governing the atmospheric flight in thier most general form as derived from basic physical laws and then these equations are simplified for application to skip trajectories.

2.2.1: Basic Vector Mechanics

A coordinate system $O_I X_I Y_I Z_I$ is fixed in inertial space, while another coordinate system xyz rotates relative to the fixed coordinate system with angular rate $\vec{\omega}$. The arbitrary vector \vec{A} is represented in the rotating system as $\vec{A} = A_x \hat{i} + A_y \hat{j} + A_z \hat{k}$. In order to take the time derivative of \vec{A} as observed from the fixed coordinate system, the time derivatives of the unit vectors fixed in the rotating system need to be evaluated. The following determines the rate of change of \vec{A} , represented in the rotating system, as observed from the inertial system $O_I X_I Y_I Z_I$.

$$\frac{d\vec{A}}{dt} = \frac{dA_x}{dt} \hat{i} + \frac{dA_y}{dt} \hat{j} + \frac{dA_z}{dt} \hat{k} + A_x \frac{d\hat{i}}{dt} + A_y \frac{d\hat{j}}{dt} + A_z \frac{d\hat{k}}{dt}.$$

By definition a fixed vector \vec{r} , which rotates with angular rate $\vec{\omega}$ has the following linear velocity $\vec{V} = \frac{d\vec{r}}{dt} = \vec{\omega} \times \vec{r}$. By defining $\vec{r} = \hat{i} + \hat{j} + \hat{k}$, Poisson's equations are obtained

$$\frac{d\hat{i}}{dt} = \vec{\omega} \times \hat{i}$$

$$\frac{d\hat{j}}{dt} = \vec{\omega} \times \hat{j}$$

$$\frac{d\hat{\mathbf{k}}}{dt} = \vec{\omega} \times \hat{\mathbf{k}}$$

Therefore, substituting the above relations into the equation for $\frac{d\vec{\mathbf{A}}}{dt}$ and grouping the appropriate terms

$$\frac{d\vec{\mathbf{A}}}{dt} = \left. \frac{\delta\vec{\mathbf{A}}}{\delta t} \right|_{oxyz} + \vec{\omega} \times \vec{\mathbf{A}}$$

where $\left. \frac{\delta\vec{\mathbf{A}}}{\delta t} \right|_{oxyz}$ denotes the rate of change of $\vec{\mathbf{A}}$ as observed from the rotating system *oxyz*.

This principle is now applied to Newton's Second Law for a rotating Earth relative to the inertial reference frame $O_I X_I Y_I Z_I$. Setting the angular rotation rate of the Earth, $\vec{\omega}_e = \vec{\omega} =$ constant and $\vec{\mathbf{r}} = \vec{\mathbf{A}}$.

$$\frac{d\vec{\mathbf{r}}}{dt} = \left. \frac{\delta\vec{\mathbf{r}}}{\delta t} \right|_{oxyz} + \vec{\omega}_e \times \vec{\mathbf{r}}$$

$$\frac{d\vec{\mathbf{V}}_I}{dt} = \frac{d}{dt} \left(\frac{d\vec{\mathbf{r}}}{dt} \right) = \frac{\delta}{\delta t} \left(\left. \frac{\delta\vec{\mathbf{r}}}{\delta t} \right|_{oxyz} + \vec{\omega}_e \times \vec{\mathbf{r}} \right) + \vec{\omega}_e \times \left(\left. \frac{\delta\vec{\mathbf{r}}}{\delta t} \right|_{oxyz} + \vec{\omega}_e \times \vec{\mathbf{r}} \right)$$

$$\frac{d\vec{\mathbf{V}}_I}{dt} = \left. \frac{\delta^2\vec{\mathbf{r}}}{\delta t^2} \right|_{oxyz} + 2 \left(\vec{\omega}_e \times \left. \frac{\delta\vec{\mathbf{r}}}{\delta t} \right|_{oxyz} \right) + \vec{\omega}_e \times (\vec{\omega}_e \times \vec{\mathbf{r}})$$

where $\vec{\mathbf{V}}_I$ is the absolute inertial velocity vector. Using the expression for $\frac{d\vec{\mathbf{V}}_I}{dt}$ in Newton's Second Law we have

$$m \frac{d\vec{\mathbf{V}}_I}{dt} = \vec{\mathbf{F}}$$

$$m \left. \frac{\delta^2\vec{\mathbf{r}}}{\delta t^2} \right|_{oxyz} = \vec{\mathbf{F}} - 2m \left(\vec{\omega}_e \times \left. \frac{\delta\vec{\mathbf{r}}}{\delta t} \right|_{oxyz} \right) - m \vec{\omega}_e \times (\vec{\omega}_e \times \vec{\mathbf{r}})$$

where $\vec{\mathbf{F}}$ is the vector of external forces acting on the vehicle.

The rotating reference frame is designated as the Earth fixed coordinate system and has its origin at the center of the Earth. This system is defined with the Z_E axis aligned with the rotation vector of the Earth. The $X_E Y_E$ plane is in the plane of the equator and defines the Z_E axis by the right hand rule. The Earth fixed system rotates with the Earth with angular velocity $\vec{\omega}_e$ about Z_E . Newton's Second Law now becomes

$$m \frac{d\vec{V}_E}{dt} = \vec{F} - 2m(\vec{\omega}_e \times \vec{V}_E) - m\vec{\omega}_e \times (\vec{\omega}_e \times \vec{r}) \quad (2.1)$$

Defining \vec{V}_E as the velocity vector relative to the Earth fixed rotating reference frame and \vec{r} as the position vector to the vehicle, then

$$\left. \frac{\delta \vec{r}}{\delta t} \right|_{xyz} \equiv \vec{V}_E \quad (2.2)$$

In the above definition, $\frac{\delta \vec{r}}{\delta t}$, denotes the relative derivative of the position vector with respect to the Earth fixed coordinate system and henceforth will indicate the change in position relative to the Earth fixed reference frame.

The position vector \vec{r} is defined in the Earth fixed coordinate system by its magnitude, by the longitude angle θ , measured in the $X_E Y_E$ plane positive from the Greenwich meridian about the Z_E axis and by the latitude angle ϕ , measured along a meridian positive northward from the equatorial plane as seen in Figure 1. Evaluation of the terms in equations 2.1 and 2.2 is made easier using the vector components along a rotating coordinate system whose origin is at the center of the Earth and whose X axis moves with the vehicle. Hence the X_T axis is coincident with the position vector to the vehicle. The Y_T axis is defined to be in the Earth fixed coordinate system's $X_E Y_E$ plane and orthogonal to the X_T axis pointing in an easterly direction. The Z_T axis is obtained from the right hand rule. Let γ be the angle between the local horizontal plane, that is the plane passing through the vehicle located at the point M and orthogonal to the position vector \vec{r} , and the velocity vector \vec{V}_E as shown in Figure 1. The angle

γ is the flight path angle and is positive when the velocity vector \vec{V}_E is above the local horizontal plane. The angle ψ is the heading angle and is the angle between the local parallel of the latitude and the projection of the velocity vector \vec{V}_E on the local horizontal plane. The heading angle ψ is measured positive for a right handed rotation of the velocity vector \vec{V}_E about the position vector \vec{r} . This coordinate system is designated as the vehicle tracking system. Figure 1 shows the relationship between the Earth fixed and the vehicle tracking coordinate systems.

Defining \hat{i} , \hat{j} , and \hat{k} as unit vectors along the vehicle tracking system axes, the position vector \vec{r} and the velocity vector \vec{V}_E are given by

$$\vec{r} = r \hat{i} \quad (2.3)$$

$$\vec{V}_E = (V \sin \gamma) \hat{i} + (V \cos \gamma \cos \psi) \hat{j} + (V \cos \gamma \sin \psi) \hat{k} \quad (2.4)$$

where the magnitude of \vec{V}_E is denoted as V to simplify notation. The angular rate of the Earth fixed system written in the tracking system is

$$\vec{\omega}_e = (\omega_e \sin \phi) \hat{i} + (\omega_e \cos \phi) \hat{k}$$

Therefore, calculating the cross products for the Coriolis acceleration $\vec{\omega}_e \times \vec{V}_E$ and the transport acceleration $\vec{\omega}_e \times (\vec{\omega}_e \times \vec{r})$ we have

$$\begin{aligned} \vec{\omega}_e \times \vec{V}_E = & \\ & -\omega_e V (\cos \gamma \cos \psi \cos \phi) \hat{i} + \omega_e V (\cos \phi \sin \gamma - \cos \gamma \sin \psi \sin \phi) \hat{j} + \omega_e V (\sin \phi \cos \gamma \cos \psi) \hat{k} \end{aligned} \quad (2.5)$$

$$\vec{\omega}_e \times (\vec{\omega}_e \times \vec{r}) = -(r \omega_e^2 \cos^2 \phi) \hat{i} + (r \omega_e^2 \sin \phi \cos \phi) \hat{k} \quad (2.6)$$

where equations 2.5 and 2.6 are for use in the right hand side of equation 2.1

2.2.2: Angular Motion

In order to write $\frac{d\vec{V}_E}{dt}$ and $\frac{d\vec{r}}{dt}$ using the position and velocity vector components along the tracking system, we need to relate the angular rate of the tracking system to Earth fixed coordinate system. Using the Earth fixed coordinates ϕ and θ , the angular rate of the tracking system is given by decomposing the angular rates $\frac{d\phi}{dt}$ and $\frac{d\theta}{dt}$ to their components along the tracking coordinate system. The angular rate of the tracking system, $\vec{\Omega}$, written as components along the tracking coordinate system is given by

$$\vec{\Omega} = (\sin\phi \frac{d\theta}{dt}) \hat{i} + (-\frac{d\phi}{dt}) \hat{j} + (\cos\phi \frac{d\theta}{dt}) \hat{k}$$

From Poisson's equations, the time derivatives of the tracking system unit vectors as observed from the Earth fixed coordinate system is

$$\frac{d\hat{i}}{dt} = \vec{\Omega} \times \hat{i} = (\cos\phi \frac{d\theta}{dt}) \hat{j} + \frac{d\phi}{dt} \hat{k} \quad (2.7a)$$

$$\frac{d\hat{j}}{dt} = \vec{\Omega} \times \hat{j} = (-\cos\phi \frac{d\theta}{dt}) \hat{i} + (\sin\phi \frac{d\theta}{dt}) \hat{k} \quad (2.7b)$$

$$\frac{d\hat{k}}{dt} = \vec{\Omega} \times \hat{k} = (-\frac{d\phi}{dt}) \hat{i} - (\sin\phi \frac{d\theta}{dt}) \hat{j} \quad (2.7c)$$

The change in the components of the position vector \vec{r} represented in the tracking system as observed from the Earth fixed system are obtained using equations 2.2, 2.3 and 2.7.

$$\vec{V}_E = \frac{d\vec{r}}{dt}$$

$$\vec{V}_E = \frac{d(r\hat{i})}{dt}$$

$$\vec{V}_E = (\frac{dr}{dt}) \hat{i} + r(\frac{d\hat{i}}{dt})$$

$$\vec{V}_E = (\frac{dr}{dt}) \hat{i} + (r\cos\phi \frac{d\theta}{dt}) \hat{j} + (r\frac{d\phi}{dt}) \hat{k} \quad (2.8)$$

Matching components from equation 2.4 and 2.8, the kinematic expressions are

$$\frac{dr}{dt} = V \sin \gamma \quad (2.9)$$

$$\frac{d\theta}{dt} = \frac{V \cos \gamma \cos \psi}{r \cos \phi} \quad (2.10)$$

$$\frac{d\phi}{dt} = \frac{V \cos \gamma \sin \psi}{r} \quad (2.11)$$

2.2.3: Acceleration Relative to Earth Fixed Axes

Using the velocity vector \vec{V}_E as defined in the tracking system from equation 2.4, the vehicle acceleration $\frac{d\vec{V}_E}{dt}$ is obtained as follows. The time derivative of equation 2.4 is calculated and equations 2.7 and 2.9 - 2.11 substituted to eliminate the time derivatives of the unit vectors. After collecting trigonometric terms and applying the appropriate trigonometric identities, the vehicle acceleration with respect to the Earth fixed axes system can be written out in component form along the tracking system as follows:

$$\frac{d\vec{V}_E}{dt} = \quad (2.12)$$

$$(\sin \gamma \frac{dV}{dt} + V \cos \gamma \frac{d\gamma}{dt} - \frac{V^2}{r} \cos^2 \gamma) \hat{i} +$$

$$(\cos \gamma \cos \psi \frac{dV}{dt} - V \sin \gamma \cos \psi \frac{d\gamma}{dt} - V \cos \gamma \sin \psi \frac{d\psi}{dt} + \frac{V^2}{r} \cos \gamma \cos \psi (\sin \gamma - \cos \gamma \sin \psi \tan \phi)) \hat{j} +$$

$$(\cos \gamma \sin \psi \frac{dV}{dt} - V \sin \gamma \sin \psi \frac{d\gamma}{dt} + V \cos \gamma \cos \psi \frac{d\psi}{dt} + \frac{V^2}{r} \cos \gamma (\sin \gamma \sin \psi + \cos \gamma \cos^2 \psi \tan \phi)) \hat{k}$$

where equation 2.12 is used in the left hand side of equation 2.1

2.2.4: General Forces

As a summary, all components of the vector equations 2.1 and 2.2, except the forces acting on the vehicle, have been written as components along the tracking coordinate system. Therefore, the forces acting on the vehicle need to be decomposed along the vehicle tracking system. In the most general case, the forces acting on the vehicle include aerodynamic, thrusting and gravitational forces. In determining the aerodynamic force components acting on the vehicle, the vertical plane of the vehicle is defined as containing the position vector \vec{r} and the velocity vector \vec{V}_E . It is convenient to designate aerodynamic forces acting on the vehicle in a coordinate system with the Y_W axis aligned with the velocity vector and the X_W axis in the vertical plane pointing radially outward and orthogonal to the Y_W axis. The Z_W axis completes the right handed system as shown in Figure 2. The $X_W Y_W Z_W$ system described is designated as the wind axes coordinate system as given in Vinh [17].

The aerodynamic forces acting on the vehicle are composed of a tangential and normal force. The tangential force is along the velocity vector \vec{V}_E and the normal force is perpendicular to the velocity vector \vec{V}_E and in general directed at an angle σ out of the vertical plane. The angle σ is the bank angle and is positive for a rotation of the normal force vector about $-\vec{V}_E$ (i.e. left banking as observed from the rear of the vehicle). Written in the wind axes, these forces are given as

$$\vec{F}_{aero} = \vec{F}_t + \vec{F}_n \quad (2.13)$$

$$\vec{F}_n = (F_n \cos \sigma) \hat{i} + (F_n \sin \sigma) \hat{k} \quad (2.14)$$

$$\vec{F}_t = (F_t) \hat{j} \quad (2.15)$$

To resolve aerodynamic force components from the wind coordinate system to the vehicle tracking system, two coordinate system rotations are needed. First, a γ rotation about the Z_W

wind axes to align the X_W wind axis with the X_T tracking system axis. Secondly a $-\psi$ rotation about the X_T axis aligns the wind and tracking system axes [17]. The following transformation matrix transforms a vector in the wind axes to the appropriate vector in the vehicle tracking system.

$$\begin{bmatrix} x \\ y \\ z \end{bmatrix}^{tracking} = \begin{bmatrix} \cos\gamma & \sin\gamma & 0 \\ -\sin\gamma\cos\psi & \cos\gamma\cos\psi & -\sin\psi \\ -\sin\gamma\sin\psi & \cos\gamma\sin\psi & \cos\psi \end{bmatrix} \begin{bmatrix} x \\ y \\ z \end{bmatrix}^{wind} \quad (2.16)$$

The gravity force acting on the vehicle is given by the following relation written in the vehicle tracking system as

$$\vec{F}_{grav} = (-mg(r)) \hat{i} \quad (2.17)$$

where gravity is a function of the radial distance from the center of the Earth.

Resolution of the aerodynamic and thrusting forces from the wind axes to the vehicle tracking coordinate system, accounting for the out-of-plane bank angle σ , is done using equations 2.13 - 2.16. Figure 2 shows the relationship between the wind axes, the vertical plane and the vehicle tracking system. The gravity force as given in equation 2.17 and the resolved aerodynamic forces using equation 2.16 determine the complete force vector acting on the vehicle. Written as components along the vehicle tracking axes, the force vector is

$$\begin{aligned} \vec{F} = & \\ & (F_n \cos\gamma \cos\sigma + F_t \sin\gamma - mg) \hat{i} - (F_n(\sin\sigma \sin\psi + \sin\gamma \cos\psi \cos\sigma) - F_t \cos\gamma \cos\psi) \hat{j} \\ & + (F_n(\sin\sigma \cos\psi - \sin\gamma \sin\psi \cos\sigma) + F_t \cos\gamma \sin\psi) \hat{k} \end{aligned} \quad (2.18)$$

where equation 2.18 is used in the right hand side of equation 2.1.

2.2.5: General Equations of Motion for Atmospheric Flight

From equations 2.5, 2.6, 2.12 and 2.18 the vector equation 2.1 can be written using components along the vehicle tracking axes as equations 2.19, 2.20 and 2.21.

(2.19)

$$\sin\gamma\frac{dV}{dt} + V\cos\gamma\frac{d\gamma}{dt} - \frac{V^2}{r}\cos^2\gamma = \frac{1}{m}(F_n\cos\gamma\cos\sigma + F_t\sin\gamma - mg) + 2\omega_e V\cos\gamma\cos\psi\cos\phi + r\omega_e^2\cos^2\phi$$

(2.20)

$$\cos\gamma\cos\psi\frac{dV}{dt} - V\sin\gamma\cos\psi\frac{d\gamma}{dt} - V\cos\gamma\sin\psi\frac{d\psi}{dt} + \frac{V^2}{r}\cos\gamma\cos\psi(\sin\gamma - \cos\gamma\sin\psi\tan\phi) = \frac{1}{m}(F_t\cos\gamma\cos\psi - F_n(\sin\sigma\sin\psi + \sin\gamma\cos\psi\cos\sigma)) - 2\omega_e V(\cos\phi\sin\gamma - \cos\gamma\sin\psi\sin\phi)$$

(2.21)

$$\cos\gamma\sin\psi\frac{dV}{dt} - V\sin\gamma\sin\psi\frac{d\gamma}{dt} + V\cos\gamma\cos\psi\frac{d\psi}{dt} + \frac{V^2}{r}\cos\gamma(\sin\gamma\sin\psi + \cos\gamma\cos^2\psi\tan\phi) = \frac{1}{m}(F_n(\sin\sigma\cos\psi - \sin\gamma\sin\psi\cos\sigma) + F_t\cos\gamma\sin\psi) - 2\omega_e V\sin\phi\cos\gamma\cos\psi - r\omega_e^2\sin\phi\cos\phi$$

To isolate $\frac{dV}{dt}$ equation 2.19 is multiplied by $\sin\gamma$, equation 2.20 is multiplied by $\cos\gamma\cos\psi$ and equation 2.21 is multiplied by $\cos\gamma\sin\psi$. The three equations are then added together component by component. In a similar manner, equation 2.19 is multiplied by $-\cos\gamma$, equation 2.20 is multiplied by $\sin\gamma\cos\psi$ and equation 2.21 is multiplied by $\sin\gamma\sin\psi$. The three equations are added together to isolate $\frac{d\gamma}{dt}$. To isolate $\frac{d\psi}{dt}$, equation 2.20 is multiplied by $-\sin\gamma$ and equation 2.21 is multiplied by $\cos\psi$. The two equations are then added together. By grouping appropriate trigonometric identities during the addition, the following relations for $\frac{dV}{dt}$, $\frac{d\gamma}{dt}$ and $\frac{d\psi}{dt}$ are obtained.

$$\frac{dV}{dt} = \frac{1}{m}F_t - g\sin\gamma + r\omega_e^2\cos\phi(\sin\gamma\cos\phi - \cos\gamma\sin\psi\sin\phi) \quad (2.22)$$

$$V \frac{d\gamma}{dt} = \quad (2.23)$$

$$\frac{1}{m} F_n \cos \sigma - g \cos \gamma + \frac{V^2}{r} \cos \gamma + 2\omega_e V \cos \psi \cos \phi + r\omega_e^2 \cos \phi (\cos \gamma \cos \phi + \sin \gamma \sin \psi \sin \phi)$$

$$V \frac{d\psi}{dt} = \quad (2.24)$$

$$\frac{1}{m} \frac{F_n \sin \sigma}{\cos \gamma} - \frac{V^2}{r} \cos \gamma \cos \psi \tan \phi + 2\omega_e V (\tan \gamma \sin \psi \cos \phi - \sin \phi) - \frac{r\omega_e^2}{\cos \gamma} \cos \phi \sin \phi \cos \psi$$

$$\frac{dr}{dt} = V \sin \gamma$$

$$\frac{d\theta}{dt} = \frac{V \cos \gamma \cos \psi}{r \cos \phi}$$

$$\frac{d\phi}{dt} = \frac{V \cos \gamma \sin \psi}{r}$$

The force equations 2.22 - 2.24, along with the three kinematics equations restated above constitute the complete equations of motion over a spherical rotating Earth. From this general point-mass model, equations will be developed which satisfy requirements for the problem formulation.

2.3: Problem Statement

The overall problem is to determine a set of parameters which describes the rendezvous orbit transfer between two vehicles, initially in different orbits, with minimum fuel expenditure. A convenient choice of parameters is a combination of instantaneously applied changes in velocity, $\Delta \vec{V}_{inst}$, and the angle along the Keplerian coasting arcs, η . Inclusion of an aeroassisted maneuver using this model cannot be done, hence a generalized impulse is proposed which allows for the inclusion of the aeroassisted maneuver which changes the velocity as well as the position. Parameterization using the $\Delta \vec{V}_{inst}$ and the Keplerian coasting arcs was done by Lutze and Cliff [8] and will be used in part together with the proposed generalized impulse described as

$$\vec{V}^+ = \vec{V}^- + \Delta\vec{V}(\vec{x}_g)$$

$$\vec{r}^+ = \vec{r}^- + \Delta\vec{r}(\vec{x}_g)$$

$$t^+ = t^- + \Delta t(\vec{x}_g)$$

where $-$ indicates the state prior to the application of the generalized impulse and the $+$ indicates the state after the application of the generalized impulse. The parameters used in the generalized impulse are given by the vector \vec{x}_g . The generalized impulse parameters, \vec{x}_g , are given as

$$\vec{x}_g^T = \{(\Delta V_x)_{inst}, (\Delta V_y)_{inst}, (\Delta V_z)_{inst}, \vec{x}_a\}$$

where $(\Delta V_x)_{inst}$, $(\Delta V_y)_{inst}$, and $(\Delta V_z)_{inst}$ are the components of the instantaneously applied change in velocity and the vector \vec{x}_a contains parameters related to the atmospheric portion of the trajectory. Determination of the vector of atmospheric parameters, \vec{x}_a , is a sub-problem of the overall problem of determining the parameters \vec{x} .

Therefore, using the generalized impulse, the complete set of parameters used for orbit transfer calculation is

$$\vec{x}^T = \{\eta_1, \eta_2, \dots, \eta_{n+1}, (\Delta\vec{V}_1)_{inst}, (\Delta\vec{V}_2)_{inst}, \dots, (\Delta\vec{V}_{n-1})_{inst}, \vec{x}_g^T\}$$

where η denotes an angle along a Keplerian coasting arc and $(\Delta\vec{V})_{inst}$, which contains the three components $(\Delta V_x)_{inst}$, $(\Delta V_y)_{inst}$, and $(\Delta V_z)_{inst}$, denotes a pure instantaneous change in velocity and \vec{x}_g^T is the vector containing the generalized impulse parameters which includes one particular deboost delta-v. Using the parameters given above, a transfer trajectory consists of the first coasting arc followed by an impulse, a second coasting arc followed by an impulse and so on up to the number of allowed impulses. The last impulse is used by the interceptor to match velocities at the rendezvous point. The last impulse is not a parameter, as it does not

influence the trajectory, but it is included in calculating the amount of fuel needed to accomplish the transfer orbit. The performance index used to measure the amount of fuel expended is given as

$$J = \sum_{i=1}^n \|(\Delta \vec{V}_{inst})_i\|$$

where n is the number of allowed impulses. The value of n is specified before each trajectory is calculated and does not appear as a parameter. Now that the performance index and the parameters have been defined the general minimization problem, using the proposed parameters, is stated in a formal manner as follows

Minimize $J(\vec{x})$ subject to

$$g_i(\vec{x}) = 0 \quad i = 1 \dots m_e$$

$$g_j(\vec{x}) \geq 0 \quad j = m_e + 1 \dots m$$

where the following boundary conditions apply

$$\vec{x}(0) = \vec{x}_o$$

$$\text{where } \vec{x} \in \mathfrak{R}^n, \vec{x}_g \subseteq \vec{x} \text{ and } \vec{x}_a \subseteq \vec{x}_g$$

and all functions are continuously differentiable.

In the above statement, m_e is the number of equality constraints and m is the total number of constraints and the vectors \vec{x} , \vec{x}_g and \vec{x}_a are as defined previously.

2.4: Skip Trajectory Point-Mass Model

In order to solve the general minimization problem and to solve for the elapsed time, the change in position and change in velocity that occur during the atmospheric portion of the generalized impulse need to be determined. Formally stated, this sub-problem is

Given the dynamical system of equations 2.9 - 2.11 and 2.22 - 2.24, determine a set of parameters, \vec{x}_a , which allows for the analytic solution of each state variable and the associated time of flight.

As a first step in solving the sub-problem, the general point-mass model has to be simplified. This section develops a set of simplified atmospheric flight equations by making assumptions relative to the skip trajectory flight regime, the physical properties of the Earth, and the properties of the Earth's atmosphere. The simplified flight equations can then be integrated in closed form. These closed form solutions contain the required set of parameters.

2.4.1: Aerodynamic Forces

Since we are only concerned with unpowered skip trajectories through the atmosphere, the thrust forces are zero and the normal and tangential forces in the force equations 2.22 - 2.24 are composed of lift and drag given as

$$F_n = L(r, V_E, C_L) \quad (2.25)$$

$$F_t = -D(r, V_E, Re, C_D) \quad (2.26)$$

The drag force acts opposite to the velocity vector while the lift force acts orthogonal to the velocity vector in the direction defined for the normal force. Assuming that the atmosphere is at rest with respect to the Earth, then the Earth and its atmosphere rotate at the same constant angular rate $\vec{\omega}_e$ and there are no wind shear forces produced by a moving atmosphere. Figures 2 and 3 show the relationship between the lift, drag and gravitational forces. A lateral force on the vehicle is generated when the normal force is rotated out of the vertical plane via such vehicle controls as the ailerons. Choosing the usual definitions for the drag and lift forces as

$$D = \frac{1}{2}\rho(r)V_E^2 S C_D(\alpha, M, Re) \quad (2.27)$$

$$L = \frac{1}{2}\rho(r)V_E^2 S C_L(\alpha, M) \quad (2.28)$$

where ρ is the atmospheric density as a function of radial position, S is the vehicle reference planform area, C_D and C_L are the drag and lift coefficients. The following general drag polar relation between lift and drag will be used

$$C_D = C_{DO}(M, Re) + K(M, Re) C_L^n(\alpha, M) \quad (2.29)$$

The zero lift drag coefficient, C_{DO} , is the drag due to the profile and wave drag of the vehicle. The induced drag factor, K , results from the effects of lift. In general these two drag factors are a function of the flight regime, where M is the Mach number and Re is the Reynolds number. The exponent n can be set according to the appropriate flight regime. Since skip trajectories involve flight at high hypersonic velocities, C_{DO} and K are assumed as constants. To ease future calculations, the lift coefficient, C_L , is chosen as the control variable instead of the angle-of-attack, α . In order to form convenient ratios for use in the equations of motion 2.22 - 2.24, general expressions for the lift coefficient for maximum lift-to-drag, C_L^* , the drag coefficient for maximum lift-to-drag, C_D^* , and the maximum Lift-to-Drag ratio, E^* , are determined. The Lift-to-Drag ratio, E , is defined as

$$E = \frac{C_L}{C_D} = \frac{C_L}{C_{DO} + K C_L^n} \quad (2.30)$$

For the maximum Lift-to-Drag ratio, E^* , we need to minimize the expression given in equation 2.30. Taking the partial derivative of E with respect to C_L and using one dimensional minimization, calculus gives the lift coefficient for maximum lift-to-drag, C_L^* as

$$\frac{\partial E}{\partial C_L} = 0$$

$$(C_{DO} + K C_L^n) - (C_L)(nK C_L^{n-1}) = 0$$

$$C_L^* = \left[\frac{C_{DO}}{K(n-1)} \right]^{\frac{1}{n}} \quad (2.31)$$

where $n \neq 1$. Substituting equation 2.31 into the general drag polar equation 2.29 we obtain the drag coefficient for maximum lift-to-drag, C_D^* , which is given as

$$\begin{aligned} C_D^* &= C_{DO} + K(C_L^*)^n = C_{DO} + \frac{C_{DO}}{(n-1)} \\ C_D^* &= \frac{nC_{DO}}{(n-1)} \end{aligned} \quad (2.32)$$

Combining C_L^* and C_D^* to form E^*

$$\begin{aligned} E^* &= \frac{C_L^*}{C_D^*} \\ E^* &= \left[\frac{C_{DO}}{K(n-1)} \frac{(n-1)^n}{(nC_{DO})^n} \right]^{\frac{1}{n}} \\ E^* &= \left[\frac{C_{DO}^{(1-n)} (n-1)^{(n-1)}}{K n^n} \right]^{\frac{1}{n}} \end{aligned} \quad (2.33)$$

Defining the scaled lift coefficient, λ , as

$$\lambda = \frac{C_L}{C_L^*} \quad (2.34)$$

and substituting into the general drag polar equation 2.29 and using equations 2.31 and 2.32

$$\begin{aligned} C_D &= C_{DO} + K(\lambda C_L^*)^n \\ C_D &= \frac{(n-1)}{n} C_D^* + K \left(\lambda \left[\frac{C_D^*}{nK} \right]^{\frac{1}{n}} \right)^n \\ \frac{C_D}{C_D^*} &= \frac{(n-1) + \lambda^n}{n} \end{aligned} \quad (2.35)$$

The ratios $\frac{C_L}{C_L^*}$ and $\frac{C_D}{C_D^*}$ are useful in reducing the force equations of motion 2.22 - 2.24.

2.4.2: Atmospheric Model

Because the lift, drag and gravitational forces are functions of altitude, a model of the density and gravity field needs to be determined. Newton's inverse square law

$$g(r) = \frac{g_0 r_0^2}{r^2} \quad (2.36)$$

determines the gravity field, where g_0 is the standard sea-level reference value for the acceleration due to gravity and r_0 is the mean radius of the Earth. Assuming an ideal gas law relation, the equation of state is

$$p = \rho R T \quad (2.37)$$

where R is the gas constant for air. Using the fact that the atmospheric pressure at any point is proportional to the amount of atmosphere above that point, the following relation holds

$$dp = -\rho g dr \quad (2.38)$$

From the equation of state

$$\frac{d\rho}{\rho} = \frac{dp}{p} - \frac{dT}{T}$$

and using equation 2.38 the differential equation of state is

$$\frac{d\rho}{\rho} = - \left[\frac{g(r)}{R T(r)} + \frac{1}{T(r)} \frac{dT(r)}{dr} \right] dr$$

in the above relation the term in brackets is defined as the inverse scale height $\beta(r)$ [3, 17, 18].

$$\beta(r) = \frac{g(r)}{R T(r)} + \frac{1}{T(r)} \frac{dT(r)}{dr}$$

Therefore, the differential equation of state is

$$\frac{d\rho}{\rho} = -\beta(r)dr \quad (2.39)$$

Integration of equation 2.39 is possible under the assumption that the quantity βr is a constant. Reference [3] discusses in detail the properties of the constant βr atmospheric model. Other possible assumptions on the type of atmosphere are the strict exponential and the isothermal atmosphere [17, 18]. From equation 2.39 $\beta = \beta(r)$, however since $\frac{1}{\beta(r)}$ has a large average value, considering the inverse scale height, β , as a constant introduces an error on the order of $\frac{1}{\beta r}$ into equation 2.39. Since βr is a large value the introduced error is small compared to unity. Therefore, the $\beta r = \text{constant}$ atmosphere is retained while also holding β constant. The choice of the $\beta r = \text{constant}$ atmosphere is convenient for simplification of the force and kinematic flight equations. Performing the integration of equation 2.39 yields

$$\int \frac{d\rho}{\rho} = -\beta r \int \frac{dr}{r}$$

$$\ln(\rho) - \ln(\rho_o) = -\beta r [\ln(r) - \ln(r_o)]$$

$$\frac{\rho}{\rho_o} = \left(\frac{r}{r_o}\right)^{-\beta r} \quad (2.40)$$

where ρ_o is the sea-level density of air. The value of $k^2 = \beta r = 900$ will be used as derived from reference [3] for flight in the Earth's atmosphere. Figure 4 shows altitude versus density for the constant βr atmosphere.

2.4.3: Skip Trajectory Equations of Motion

Looking at the magnitudes of the terms from equation 2.1, the transport acceleration term has a maximum value when the vehicle is at the equator. The Coriolis acceleration has a maximum value when the vehicle is traveling in the equatorial plane. For the Earth, which has an angular rate of 7.292×10^{-5} radians per second, terms involving $r\omega_e^2$ are on the order of one percent of sea-level gravity when evaluated at the Earth's surface. For near orbital flight speeds at an

altitude of 60 kilometers (200,000 ft), terms involving $2\omega_e V$ are on the order of one tenth sea level gravity. Therefore, the $r\omega_e^2$ and $2\omega_e V$ terms will be neglected. Under this assumption the force equations of motion 2.22 - 2.24 reduce to

$$\frac{dV}{dt} = \frac{1}{m}F_t - g\sin\gamma$$

$$V \frac{d\gamma}{dt} = \frac{1}{m}F_n \cos\sigma - \left(g - \frac{V^2}{r}\right)\cos\gamma$$

$$V \frac{d\psi}{dt} = \frac{1}{m} \frac{F_n \sin\sigma}{\cos\gamma} - \frac{V^2}{r} \cos\gamma \cos\psi \tan\phi$$

Next, the expressions for the normal and tangential forces from equations 2.25 - 2.28 are substituted into the above equations yielding the force equations of motion for a nonthrusting vehicle over a spherical nonrotating Earth.

$$\frac{dV}{dt} = -\frac{\rho V^2 S C_D}{2m} - g\sin\gamma \quad (2.41)$$

$$V \frac{d\gamma}{dt} = \frac{\rho V^2 S C_L}{2m} \cos\sigma - \left(g - \frac{V^2}{r}\right)\cos\gamma \quad (2.42)$$

$$V \frac{d\psi}{dt} = \frac{\rho V^2 S C_L}{2m} \frac{\sin\sigma}{\cos\gamma} - \frac{V^2}{r} \cos\gamma \cos\psi \tan\phi \quad (2.43)$$

Equations 2.41 - 2.43 along with the previously derived kinematic equations

$$\frac{dr}{dt} = V\sin\gamma \quad (2.44)$$

$$\frac{d\theta}{dt} = \frac{V\cos\gamma\cos\psi}{r\cos\phi} \quad (2.45)$$

$$\frac{d\phi}{dt} = \frac{V\cos\gamma\sin\psi}{r} \quad (2.46)$$

are the set of six scalar equations necessary to completely describe the motion of the vehicle.

2.4.4: Skip Trajectory Dimensionless Equations of Motion

In order to further simplify the six differential equations 2.41 - 2.46, Vinh [17] proposed several dimensionless variables. These dimensionless variables let the equations become decoupled and allow for solution by closed form integration. The first of the variables proposed by Vinh is the dimensionless arc length, s , which is defined as

$$s = \int_0^t \frac{V}{r} \cos \gamma \, dt \quad (2.47)$$

where t is the time of flight. Using the above equation to change the independent variable from time to arc length, the kinematic equations 2.44 - 2.46 become

$$\frac{dr}{ds} = r \tan \gamma \quad (2.48)$$

$$\frac{d\theta}{ds} = \frac{\cos \psi}{\cos \phi} \quad (2.49)$$

$$\frac{d\phi}{ds} = \sin \psi \quad (2.50)$$

while the force equations 2.41 - 2.43 become

$$\frac{dV}{ds} = \left(-\frac{\rho V^2 S C_D}{2m \cos \gamma} - g \tan \gamma \right) \frac{r}{V} \quad (2.51)$$

$$\frac{d\gamma}{ds} = \left(\frac{\rho V^2 S C_L}{2m} \frac{\cos \sigma}{\cos \gamma} - \left(g - \frac{V^2}{r} \right) \right) \frac{r}{V^2} \quad (2.52)$$

$$\frac{d\psi}{ds} = \left(\frac{\rho V^2 S C_L}{2m} \frac{\sin \sigma}{\cos \gamma} - \frac{V^2}{r} \cos \gamma \cos \psi \tan \phi \right) \frac{r}{V^2 \cos \gamma} \quad (2.53)$$

As proposed by Vinh [17], the following modified nondimensional Chapman variables are defined as follows to further simplify the equations of motion.

$$Z = \frac{\rho S C_L^*}{2m} \sqrt{\frac{r}{\beta}} \quad (2.54)$$

$$v = \frac{V^2}{gr} \quad (2.55)$$

where g and ρ are determined from 2.36 and 2.40 respectively. Equations 2.54 and 2.55 are used to replace r and V respectively in equations of motion, 2.48 - 2.53. In their most general form, since the Chapman variables $Z = Z(\rho(r), r, \beta(r))$ and $v = v(V, g(r), r)$ chain rule differentiation is used to rewrite the equations of motion using the dimensionless Chapman variables. The partial derivatives needed are found in Appendix A. For completeness, inclusion of $\beta = \beta(r)$ is presented in the process of rewriting the equations with the assumption of β as a constant being used at the end of the rewriting process and in any following equations. Using the partial derivatives from Appendix A and forming the dimensionless variables the following transformation for the altitude related state variable Z , occurs

$$\begin{aligned} \frac{dZ}{ds} &= \frac{\partial Z}{\partial \rho} \frac{\partial \rho}{\partial r} \frac{\partial r}{\partial s} + \frac{\partial Z}{\partial r} \frac{\partial r}{\partial s} + \frac{\partial Z}{\partial \beta} \frac{\partial \beta}{\partial r} \frac{\partial r}{\partial s} \\ \frac{dZ}{ds} &= \left(-\beta Z + \frac{Z}{2r} - \frac{Z}{2\beta} \frac{\partial \beta}{\partial r} \right) r \tan \gamma \\ \frac{dZ}{ds} &= -\beta r Z \left[1 - \frac{1}{2\beta r} + \frac{1}{2\beta^2} \frac{\partial \beta}{\partial r} \right] \tan \gamma \end{aligned} \quad (2.56)$$

for the constant $\beta r = 900$ atmosphere, the term in brackets from equation 2.56 is approximately unity [17, 18]. Therefore, equation 2.56 reduces to

$$\frac{dZ}{ds} = -k^2 Z \tan \gamma \quad (2.57)$$

In a similar manner, with the substitution for C_D , the transformation of the velocity state variable leads to

$$\frac{dv}{ds} = \frac{\partial v}{\partial V} \frac{\partial V}{\partial s} + \frac{\partial v}{\partial g} \frac{\partial g}{\partial r} \frac{\partial r}{\partial s} + \frac{\partial v}{\partial r} \frac{\partial r}{\partial s}$$

$$\frac{dv}{ds} = \frac{-2vZk}{E^* \cos \gamma} \left[\frac{n-1+\lambda^n}{n} \right] - (2-v)\tan \gamma \quad (2.58)$$

The other four state equations involve angles which are already dimensionless and only require that the dimensionless variables be formed. These four equations are as follows

$$\frac{d\gamma}{ds} = \frac{Z\lambda k \cos \sigma}{\cos \gamma} + \left(1 - \frac{1}{v} \right) \quad (2.59)$$

$$\frac{d\theta}{ds} = \frac{\cos \psi}{\cos \phi} \quad (2.60)$$

$$\frac{d\phi}{ds} = \sin \psi \quad (2.61)$$

$$\frac{d\psi}{ds} = \frac{Z\lambda k \sin \sigma}{\cos^2 \gamma} - \cos \psi \tan \phi \quad (2.62)$$

Further simplification of the kinematic and force equations is possible by making some assumptions on the properties of the vehicle's trajectory. For atmospheric skip trajectories in the upper portion of the atmosphere, speeds are near orbital velocity. In equation 2.52, the gravitational acceleration nearly cancels the generated centrifugal relief term. Therefore, in equation 2.59 the term $\left(1 - \frac{1}{v} \right)$ will be neglected. Since the skip trajectory occurs at small flight path angles, $\tan \gamma$ is small. Therefore, the component of gravity tangent to the flight path is small compared to the generated aerodynamic forces. With this assumption, the gravity term $\frac{gr}{V} \tan \gamma$ as given in equation 2.51 or the same term when transformed to $(2-v)\tan \gamma$ as given in equation 2.58 will be neglected. Using these two assumptions, the equations of motion become

$$\frac{dZ}{ds} = -k^2 Z \tan \gamma \quad (2.63)$$

$$\frac{dv}{ds} = \frac{-2vZk}{E^* \cos \gamma} \left[\frac{n-1+\lambda^n}{n} \right] \quad (2.64)$$

$$\frac{d\gamma}{ds} = \frac{Z\lambda k \cos \sigma}{\cos \gamma} \quad (2.65)$$

$$\frac{d\theta}{ds} = \frac{\cos\psi}{\cos\phi} \quad (2.66)$$

$$\frac{d\phi}{ds} = \sin\psi \quad (2.67)$$

$$\frac{d\psi}{ds} = \frac{Z\lambda k \sin\sigma}{\cos^2\gamma} - \cos\psi \tan\phi \quad (2.68)$$

A third assumption is that the skip trajectory covers a small cross range. Using this assumption, a small angle approximation involving ϕ can be used. Therefore, in equation 2.66, $\cos\phi \approx 1$. Also, the term $\cos\psi \tan\phi$ will be neglected in equation 2.68. The reduced dimensionless equations of motion are now written as

$$\frac{dZ}{ds} = -k^2 Z \tan\gamma \quad (2.69)$$

$$\frac{dv}{ds} = \frac{-2vZk}{E^* \cos\gamma} \left[\frac{n-1+\lambda^n}{n} \right] \quad (2.70)$$

$$\frac{d\theta}{ds} = \cos\psi \quad (2.71)$$

$$\frac{d\phi}{ds} = \sin\psi \quad (2.72)$$

$$\frac{d\psi}{ds} = \frac{Z\lambda k \sin\sigma}{\cos^2\gamma} \quad (2.73)$$

$$\frac{d\gamma}{ds} = \frac{Z\lambda k \cos\sigma}{\cos\gamma} \quad (2.74)$$

where the equation for the time of flight is given by

$$\frac{ds}{dt} = \frac{V}{r} \cos\gamma \quad (2.75)$$

2.5: Closed Form Solutions

As a first step in solving the formulated general problem, the solutions to the equations of motion are reduced to closed form. The set of closed form solutions consist of an analytic equation for each state variable that depends only on the initial and final values of the

independent variable. Included in the closed form equations are parameters which influence the state variable. When the parameter's value is changed, at any given time any state variable which depends on that parameter is also changed. The solutions also depend upon the physical characteristics of the vehicle.

2.5.1: Method of Performing the Skip Trajectory

The first step in determining the closed form solutions is to formulate how the skip will be performed. A general atmospheric skip trajectory is proposed which contains three flight subarcs. The first subarc begins with an initial velocity and flight path angle (V_e, γ_e) at the altitude defined as the boundary to the atmosphere. This subarc, called the descent arc, continues until the flight path angle equals zero. The second subarc is determined by holding constant altitude at a zero flight path angle for some specified amount of time. The third subarc, called the ascent arc, begins with zero flight path angle and exits the atmosphere with the final speed and flight path angle determined when the exit altitude equals the entrance altitude. The following sections present the boundary conditions and the set of closed form flight equations for each of the three arcs described above.

2.5.2: Boundary Conditions for the Constant Altitude Subarc

Solution to the differential flight equations along a constant altitude subarc requires the following boundary conditions

$v_e =$ Given by v_f at the end of the descent subarc

$Z_e =$ Given by Z_f at the end of the descent subarc

$\gamma_e = 0$

$\psi_e = 0$

$$\phi_e = 0$$

$$\theta_e = 0$$

$$s_e = 0$$

$$v_f = \text{free}$$

$$Z_f = \text{Same as } Z_e$$

$$\gamma_f = 0$$

$$\psi_f = \text{free}$$

$$\phi_f = \text{free}$$

$$\theta_f = \text{free}$$

$$s_f = \text{free}$$

2.5.3: Closed Form Solutions for Constant Altitude Subarc

As proposed for the general skip trajectory, inclusion of a subarc at constant altitude is possible. This subarc is developed for cases where there is a minimum altitude constraint on the skip trajectory. The equation for the dimensionless arc length, 2.75 is also used to include time as a relevant variable. For constant altitude flight, two conditions must be satisfied. These two conditions being that the altitude does not change over time and that the flight path angle is constant. These conditions are given by the equations

$$\frac{dZ}{ds} = 0 = -k^2 Z \tan \gamma \quad (2.76)$$

$$\frac{d\gamma}{ds} = 0 = \frac{Z \lambda k \cos \sigma}{\cos \gamma} \quad (2.77)$$

Equation 2.76 is satisfied for the condition

$$\gamma = 0 \quad (2.78a)$$

Equation 2.77 is satisfied under either of the two conditions

$$\lambda = 0 \quad (2.78b)$$

$$\sigma = \pm \frac{\pi}{2} \quad (2.78c)$$

The sign on the bank angle used along a constant altitude subarc is not a parameter but is chosen apriori to solving the orbit transfer problem.

Using the condition 2.78a, solutions for the state variables are given by direct integration as

$$\ln \left[\frac{v}{v_e} \right] = \frac{-2Zk[n-1+\lambda^n]}{E^*n} s \quad (2.79)$$

$$\psi = Z\lambda k \sin \sigma s \quad (2.80)$$

$$\theta = \frac{1}{Z\lambda k \sin \sigma} \sin [Z\lambda k \sin \sigma s] \quad (2.81)$$

$$\phi = \frac{1}{Z\lambda k \sin \sigma} [1 - \cos [Z\lambda k \sin \sigma s]] \quad (2.82)$$

Equations 2.81 and 2.82 are obtained by substituting the expression from equation 2.80 in for the heading angle before integration. Substituting equation 2.79 into the expression for time, given by equation 2.75, yields

$$\frac{ds}{dt} = \frac{\exp \left[\frac{-Zk[n-1+\lambda^n]}{E^*n} s \right] \sqrt{v_e \mu \beta^3}}{k^3}$$

After separation of variables and integration, the expression for the arc length as a function of time is given as

$$s = \left[\frac{E^*n}{Zk[n-1+\lambda^n]} \right] \ln \left[\left[\frac{Zk[n-1+\lambda^n] \sqrt{v_e \mu \beta^3}}{n E^*k^3} \right] t + 1 \right] \quad (2.83)$$

Although we usually would like to use $t = t(s)$, equation 2.83 is used because time has a more physical meaning and is easier to specify than the arc length. Equations 2.79 - 2.82 are the general closed form equations used for flight at constant altitude. The equation for time, 2.83, holds for either condition 2.78b or 2.78c. When the condition given by $\sigma = \pm \frac{\pi}{2}$ applies, the parameterized flight equations are given as

$$\ln \left[\frac{v}{v_e} \right] = \frac{-2Zk[n - 1 + \lambda^n]}{E^*n} s \quad (2.84)$$

$$\psi = \pm Z\lambda k s \quad (2.85)$$

$$\theta = \frac{1}{Z\lambda k} \sin [Z\lambda k s] \quad (2.86)$$

$$\phi = \pm \frac{1}{Z\lambda k} [1 - \cos [Z\lambda k s]] \quad (2.87)$$

where a positive or negative sign results from a positive or negative bank angle respectively. Equations 2.84 - 2.87 apply when a heading change is necessary along the constant altitude subarc. In order to produce the change in heading along the constant altitude subarc, $\lambda \neq 0$. When the condition corresponding to $\lambda = 0$ applies, the flight equations along a constant altitude subarc are given as

$$\ln \left[\frac{v}{v_e} \right] = \frac{-2Zk[n - 1]}{E^*n} s \quad (2.88)$$

$$\psi = 0 \quad (2.89)$$

$$\theta = s \quad (2.90)$$

$$\phi = 0 \quad (2.91)$$

Since terms involving gravity have been assumed out of the problem, the results given by equations 2.84 - 2.91 describe two methods of flight along a constant altitude subarc neglecting gravitational effects. For the case where $\sigma = \pm \frac{\pi}{2}$, all lift is out of the vertical plane, thus the choice for the lift coefficient is arbitrary and the equations of motion are given by equations 2.84 - 2.87. For $\lambda = 0$, there is no generated lift force, thus the bank orientation of the vehicle is

irrelevant and no plane change can occur. The equations of motion corresponding to $\lambda = 0$ are given by equations 2.88 - 2.91.

2.5.4: Boundary Conditions for the Descent and Ascent Subarcs

Solution to the differential flight equations along the descent and ascent subarcs require that each subarc have appropriate boundary conditions. The following boundary conditions are used for the descent subarc

$v_e =$ Specified by the Keplerian orbit at the entrance to the atmosphere

$Z_e =$ Specified by the altitude for the outer edge of the atmosphere

$\gamma_e =$ Specified by the Keplerian orbit at the entrance to the atmosphere

$\psi_e = 0$

$\phi_e = 0$

$\theta_e = 0$

$t_e = 0$

$v_f =$ free

$Z_f =$ free

$\gamma_f = 0$

$\psi_f =$ free

$\phi_f =$ free

$\theta_f =$ free

$t_f =$ free

The following boundary conditions are used for the ascent subarc

$v_e =$ Specified by v_f from the constant altitude subarc

Z_e = Specified by the altitude of the constant altitude subarc

$$\gamma_e = 0$$

$$\psi_e = 0$$

$$\phi_e = 0$$

$$\theta_e = 0$$

$$t_e = 0$$

$$v_f = \text{free}$$

Z_f = Specified by the altitude for the outer edge of the atmosphere

γ_f = Specified by Z_e , Z_f and γ_e needed to reach the outer edge of the atmosphere

$$\psi_f = \text{free}$$

$$\phi_f = \text{free}$$

$$\theta_f = \text{free}$$

$$t_f = \text{free}$$

2.5.5: Closed Form Solutions for the Descent and Ascent Subarcs

The proposed method of the skip trajectory indicates that an appropriate independent variable is the flight path angle γ rather than the dimensionless arc length s as given in section 2.4. Therefore changing the independent variable to γ by dividing equations 2.69 - 2.73 by equation 2.74 the dimensionless equations of motion become

$$\frac{dZ}{d\gamma} = -\frac{k \sin\gamma}{\lambda \cos\sigma} \quad (2.92)$$

$$\frac{dv}{d\gamma} = \frac{-2v}{E^* \cos\sigma} \left[\frac{n-1}{n} + \lambda^n \right] \quad (2.93)$$

$$\frac{d\psi}{d\gamma} = \frac{\tan\sigma}{\cos\gamma} \quad (2.94)$$

$$\frac{d\theta}{d\gamma} = \frac{\cos\psi\cos\gamma}{kZ\lambda\cos\sigma} \quad (2.95)$$

$$\frac{d\phi}{d\gamma} = \frac{\sin\psi\cos\gamma}{kZ\lambda\cos\sigma} \quad (2.96)$$

In addition to the state variables, the time of flight also is calculated for later use in the transfer orbit calculations. From equation 2.75, and after forming the modified Chapman variables, the dimensionless differential equation for time is

$$\frac{dt}{d\gamma} = \frac{k^2}{\lambda Z \cos\sigma \sqrt{\beta^3 \mu v}} \quad (2.97)$$

where μ is the gravitational parameter for the Earth. The above equations can now be integrated in closed form if assumptions are made about the vehicle controls, λ and σ , as functions of the independent variable γ . The following assumption is used to obtain the parameterized closed form solutions.

Assume that the vehicle controls for lift (λ) and bank (σ) are held constant throughout each subarc of the skip trajectory.

Using this assumption and performing direct integration on equations 2.92 - 2.94, the following equations for the descent and ascent arcs are obtained

$$Z = Z_e - \frac{k}{\lambda \cos\sigma} (\cos\gamma - \cos\gamma_e) \quad (2.98)$$

$$\ln\left[\frac{v}{v_e}\right] = \frac{-2(n-1 + \lambda^n)}{E^* n \lambda \cos\sigma} (\gamma - \gamma_e) \quad (2.99)$$

$$\psi = \tan\sigma \left[\ln\left(\tan\left\{\frac{\pi}{4} + \frac{\gamma}{2}\right\}\right) - \ln\left(\tan\left\{\frac{\pi}{4} + \frac{\gamma_e}{2}\right\}\right) \right] \quad (2.100)$$

Because the expressions 2.95 and 2.96 contain Z and ψ , the results from 2.98 and 2.100 must be substituted into the equations before integration can be performed. However, since equations

2.98 and 2.100 contain γ in a nonlinear form, a small angle approximation for γ will be applied to equations 2.92 and 2.94 before they are integrated and substituted into equations 2.95 and 2.96. Using the small angle approximation, equations for Z and ψ are

$$Z = Z_e - \frac{k}{2\lambda\cos\sigma}(\gamma^2 - \gamma_e^2) \quad (2.101)$$

$$\psi = \tan\sigma(\gamma - \gamma_e) \quad (2.102)$$

Substituting equations 2.101 and 2.102 into equation 2.95, the following differential equation for θ along the descent and ascent arcs is obtained

$$\frac{d\theta}{d\gamma} = \frac{\cos(\psi_e + \tan\sigma(\gamma - \gamma_e))}{k\lambda\cos\sigma(Z_e - \frac{k}{2\lambda\cos\sigma}(\gamma^2 - \gamma_e^2))} \quad (2.103)$$

Likewise, when equations 2.101 and 2.102 are substituted into equation 2.96, the following differential equation for ϕ along the descent and ascent arcs is obtained

$$\frac{d\phi}{d\gamma} = \frac{\sin(\psi_e + \tan\sigma(\gamma - \gamma_e))}{k\lambda\cos\sigma(Z_e - \frac{k}{2\lambda\cos\sigma}(\gamma^2 - \gamma_e^2))} \quad (2.104)$$

Also, when equations 2.99 and 2.101 for v and Z are substituted into the differential equation for time, 2.97, the following equation is obtained

$$\frac{dt}{d\gamma} = \frac{k^2}{\lambda\cos\sigma \left[Z_e - \frac{k}{2\lambda\cos\sigma}(\gamma^2 - \gamma_e^2) \right] \sqrt{\beta^3 \mu v_e \exp \left[\frac{-2(n-1+\lambda^n)}{E^* n \lambda \cos\sigma} (\gamma - \gamma_e) \right]}} \quad (2.105)$$

Equations 2.103 - 2.105 are now functions only of the entrance conditions and the independent variable γ and can be integrated under suitable assumptions. Details of the integration and the approximations used to obtain the following solutions are given in Appendix A, with the results given as

$$\phi = \quad (2.106)$$

$$\begin{aligned} & \frac{C_1}{720} \left[(\tan^6 \sigma) \frac{\gamma^5}{5} - (30 \tan^4 \sigma - C_2 \tan^6 \sigma) \frac{\gamma^3}{3} - (30 C_2 \tan^4 \sigma - C_2^2 \tan^6 \sigma - 360 \tan^2 \sigma) \gamma \right]_{\gamma_e}^{\gamma} \\ & + \frac{C_1}{720} \left[\frac{720 - 360 C_2 \tan^2 \sigma + 30 C_2^2 \tan^4 \sigma - C_2^3 \tan^6 \sigma}{2 \sqrt{C_2}} \ln \left[\frac{\sqrt{C_2} + \gamma}{\sqrt{C_2} - \gamma} \right] \right]_{\gamma_e}^{\gamma} + \\ & \frac{C_3}{5040} \left[(\tan^7 \sigma) \frac{\gamma^6}{6} - (42 \tan^5 \sigma - C_2 \tan^7 \sigma) \frac{\gamma^4}{4} - (42 C_2 \tan^5 \sigma - C_2^2 \tan^7 \sigma - 840 \tan^3 \sigma) \frac{\gamma^2}{2} \right]_{\gamma_e}^{\gamma} \\ & - \frac{C_3}{5040} \left[\frac{5040 \tan \sigma - 840 C_2 \tan^3 \sigma + 42 C_2^2 \tan^5 \sigma - C_2^3 \tan^7 \sigma}{2} \ln(C_2 - \gamma^2) \right]_{\gamma_e}^{\gamma} \end{aligned}$$

$$\theta = \quad (2.107)$$

$$\begin{aligned} & \frac{C_1}{720} \left[(\tan^6 \sigma) \frac{\gamma^5}{5} - (30 \tan^4 \sigma - C_2 \tan^6 \sigma) \frac{\gamma^3}{3} - (30 C_2 \tan^4 \sigma - C_2^2 \tan^6 \sigma - 360 \tan^2 \sigma) \gamma \right]_{\gamma_e}^{\gamma} \\ & + \frac{C_1}{720} \left[\frac{720 - 360 C_2 \tan^2 \sigma + 30 C_2^2 \tan^4 \sigma - C_2^3 \tan^6 \sigma}{2 \sqrt{C_2}} \ln \left[\frac{\sqrt{C_2} + \gamma}{\sqrt{C_2} - \gamma} \right] \right]_{\gamma_e}^{\gamma} - \\ & \frac{C_3}{5040} \left[(\tan^7 \sigma) \frac{\gamma^6}{6} - (42 \tan^5 \sigma - C_2 \tan^7 \sigma) \frac{\gamma^4}{4} - (42 C_2 \tan^5 \sigma - C_2^2 \tan^7 \sigma - 840 \tan^3 \sigma) \frac{\gamma^2}{2} \right]_{\gamma_e}^{\gamma} \\ & + \frac{C_3}{5040} \left[\frac{5040 \tan \sigma - 840 C_2 \tan^3 \sigma + 42 C_2^2 \tan^5 \sigma - C_2^3 \tan^7 \sigma}{2} \ln(C_2 - \gamma^2) \right]_{\gamma_e}^{\gamma} \end{aligned}$$

$$t = \frac{C_6 \exp(-C_2 \gamma)}{2C_7} \ln \left[\frac{C_7 + \gamma}{C_7 - \gamma} \right]_{\gamma_e}^{\gamma} + \quad (2.108)$$

$$\frac{C_6 C_2 \exp(C_2 C_7)}{2C_7} \left[\frac{\exp(a_1 x_1) \ln(x_1)}{a_1} - \frac{1}{a_1} \left[\ln(x_1) + \frac{a_1 x_1}{1!} + \frac{(a_1 x_1)^2}{2 \cdot 2!} + \dots + \frac{(a_1 x_1)^7}{7 \cdot 7!} \right] \right]_{\gamma_e}^{\gamma} +$$

$$\frac{C_6 C_2 \exp(-C_2 C_7)}{2C_7} \left[\frac{\exp(a_2 x_2) \ln(x_2)}{a_2} - \frac{1}{a_2} \left[\ln(x_2) + \frac{a_2 x_2}{1!} + \frac{(a_2 x_2)^2}{2 \cdot 2!} + \dots + \frac{(a_2 x_2)^7}{7 \cdot 7!} \right] \right]_{\gamma_e}^{\gamma}$$

where the constants are defined in Appendix A. Equations 2.98 - 2.100 and 2.106 - 2.108 are the closed form solutions for Z , v , ψ , ϕ , θ and t along the descent and ascent arcs, with the flight path angle γ as the independent variable.

2.6: Skip Trajectory Parameters

From the closed form solutions, the parameters describing an atmospheric skip trajectory can now be stated. In the most general case, as postulated in obtaining the closed form solutions, there are three subarcs of flight. Each subarc can be described by entry conditions and a group of parameters. Because the skip trajectory is being separated into three separate regions, the assumption that the vehicle controls can change instantaneously as we go from one region to the next will be used. The parameters for the descent and ascent subarcs are the scaled lift coefficient, λ , and the bank angle σ . For the constant altitude subarc, by choosing the scaled lift coefficient parameter as zero, the bank angle is arbitrary and is not a parameter; by choosing the scaled lift coefficient to be a nonzero parameter, the bank angle is forced to be either positive or negative ninety degrees and is not a parameter but is chosen a priori to solving for the optimal parameter values. Using these conditions regarding the scaled lift coefficient and

specifying the time to remain in flight at constant altitude gives the parameters for the constant altitude subarc.

Therefore, by choosing various degrees of complexity for the skip trajectory, the flight through the atmosphere could have between two and six parameters. The six parameters are defined in the following manner

σ_d - Descent subarc bank angle (2.109)

λ_d - Descent subarc scaled lift coefficient

λ_c - Constant altitude subarc scaled lift coefficient

t_c - Constant altitude subarc time of flight

σ_a - Ascent subarc bank angle

λ_a - Ascent subarc scaled lift coefficient

Chapter 3: Skip Trajectory Implementation

3.1: Overview

This chapter discusses the incorporation of the closed form skip trajectory flight equations into an existing computer algorithm. The capabilities of the previous computer algorithm are detailed and modifications required to accommodate development of the computer algorithm for the aeroassisted trajectory are presented. The cost function and constraints associated with the aeroassisted transfer trajectories are discussed for application to the proposed problem of generating minimum fuel rendezvous transfer orbits.

3.2: Previous Orbit Calculation Procedure

A basis for the present research effort is to add to the computer algorithm developed at Virginia Polytechnic Institute and State University, Blacksburg, Virginia [8]. Prior to this research, the algorithm was capable of determining optimal transfer orbits using the components of velocity impulses ($\Delta\vec{V}_{inst}$) as parameters. The algorithm is based on selecting a set of these parameters, calculating a cost function, a set of constraints and applying a nonlinear parameter optimization routine to update the parameters selected until all constraints are satisfied and the cost function is as small as possible. The present research replaces one of the velocity impulses, $\Delta\vec{V}_{inst}$, by the generalized impulse which includes an aeroassisted maneuver to change velocity and position. The parameters associated with the generalized impulse in combination with those

associated with pure velocity impulse Δv 's and the angles associated with Keplerian coasting arcs are the parameters used to describe the transfer orbit.

The generalized impulse must be incorporated in a compatible manner with the existing method of function and constraint evaluation. In particular, the current procedure determines the initial conditions of one Keplerian coasting arc based on the final conditions of the previous Keplerian coasting arc in the following manner

$$r^+ = r^-$$

$$V^+ = V^- + \Delta \vec{V}$$

$$t^+ = t^-$$

3.3: Calculating the Generalized Impulse for an Aeroassisted Maneuver

This section covers the incorporation of the scalar skip trajectory equations into the previously existing algorithm. The conversion of the Keplerian orbital elements at the edge of the atmosphere to useful entrance conditions for the skip trajectory is covered. After the skip trajectory is executed, discussion of the conversion performed to determine the new Keplerian orbit is presented. The result enables the generalized impulse to be calculated as

$$r^+ = r^- + \Delta \vec{r}$$

$$V^+ = V^- + \Delta \vec{V}$$

$$t^+ = t^- + \Delta t$$

3.3.1: Coordinate Systems

During the calculation of the Keplerian orbits, an inertial coordinate system useful for calculation of orbital elements and the vehicle's position in space needs to be defined. The

inertial coordinate system used is called the geocentric-equatorial coordinate system. This system has its origin at the Earth's center. The $X_G Y_G$ plane is the Earth's equatorial plane with the X_G axis pointing to the vernal equinox. The Z_G axis completes the right handed system and points to the north pole. As a note, since the developed atmospheric flight equations in Chapter 2 neglect the rotational effects of the Earth, the Earth fixed coordinate system and the geocentric-equatorial coordinate system are identical if the Greenwich meridian specified by X_E is aligned with the vernal equinox. The reference X_E axis is therefore chosen to coincide with the X_G axis. To exactly locate the vehicle in space, two angles and the radial distance are used. The two angles are called the right ascension (α) and the declination (δ). The right ascension is measured positive from the X_G axis about the Z_G axis in the $X_G Y_G$ plane to the projection of the position vector on the $X_G Y_G$ plane. The declination is measured positive northward from the $X_G Y_G$ plane along a meridian to the position vector of the vehicle. Figure 5 shows the geocentric-equatorial coordinate system. Figure 6 shows the definition of the right ascension and declination.

3.3.2: Calculation of Entrance Conditions

When an aeroassisted orbit is generated, the orbital properties of the vehicle at the entrance to the atmosphere are used to calculate the initial conditions for the skip trajectory equations. These are usually given as position and velocity vector components in the geocentric-equatorial coordinate system and are converted to the needed scalar quantities. Conversion to the scalar entrance velocity and initial flight path at the radius corresponding to the outer edge of the atmosphere is done as follows:

$$V_e = \|\vec{V}_e\| \tag{3.1}$$

$$\gamma_e = -\cos^{-1} \left[\frac{\|\vec{r}_e \times \vec{V}_e\|}{\|\vec{r}_e\| \|\vec{V}_e\|} \right] \tag{3.2}$$

where the e subscript denotes conditions at entrance to the atmosphere. For execution of a skip trajectory to occur, the initial flight path angle is always negative. Given these two initial conditions and the set of parameters from equations 2.109 designating the type of skip trajectory, the entire aeroassisted portion of the transfer orbit is calculated and the resulting changes in position, velocity and time are determined.

3.3.3: Changes in Position Due to the Aeroassisted Maneuver

As stated in Chapter 2, the skip trajectory through the atmosphere is completely described by up to six parameters. In the general case of six parameters, the skip trajectory consists of three portions; the descent arc, the constant altitude subarc and the ascent subarc. Inclusion of the skip trajectory calculations in the general form dictates that the changes in the state variables be accounted for even if a simpler type of trajectory is chosen. Determining the changes in position due to the aeroassisted maneuver requires modified use of the tracking coordinate system described in section 2.2.1.

The tracking system defined in section 2.2.1 was chosen because the definition of the Earth fixed axes relied on the rotation vector of the Earth. It was convenient to align the Earth fixed Z_E axis with the rotation vector of the Earth which in turn influenced the choice of orientation for the vehicle tracking coordinate system. Since the Earth's rotation has been assumed out of the problem, an arbitrary choice of the orientation of the vehicle tracking coordinate system relative to the Earth fixed coordinate system is more convenient. In particular, new reference planes can be defined which include the initial position and velocity at the beginning of each portion of the skip trajectory. It is convenient to think of each new reference plane that is defined as a new "equator" and its corresponding vehicle tracking coordinate system determining the changes in state variables relative to the new "equator". In order to determine overall changes in

longitude, latitude and heading an original reference plane is defined and the relationship between the original reference and any subsequent reference planes must be established.

As related to the proposed skip trajectory, the original reference plane is the Keplerian orbit at the point of entrance to the atmosphere. The changes in the state variables along the atmospheric descent subarc are measured relative to original reference plane using the boundary conditions pertaining to the descent subarc. At the beginning of the constant altitude subarc, a new reference plane is defined by the position vector, \vec{r} , and the velocity vector, \vec{V}_E , at the point in the skip trajectory where the flight path angle is zero. The new reference plane is related to the initial reference plane by the changes in longitude, latitude and heading produced during the descent subarc. The changes in the state variables along the constant altitude subarc are measured relative to the newly defined reference plane using the boundary conditions pertaining to the constant altitude subarc. At the beginning of the ascent subarc, a new reference plane is defined by the position vector, \vec{r} , and the velocity vector, \vec{V}_E , at the end of the constant altitude subarc. The ascent subarc reference plane is related to the constant altitude reference plane by the changes in longitude, latitude and heading produced during the constant altitude subarc. The changes in the state variables along the ascent subarc are measured relative to the third reference plane using the boundary conditions pertaining to the ascent subarc. Finally, a fourth reference plane is defined by the position vector, \vec{r} , and the velocity vector, \vec{V}_E , at the exit from the atmosphere. This reference plane is the plane of the new Keplerian orbit after exiting the atmosphere. As before, this reference plane is related to the ascent reference plane by changes in longitude, latitude and heading produced during the ascent subarc. Figure 7 shows the general relationship between the original, descent, constant altitude, ascent and exit reference planes for an arbitrary atmospheric entry point.

By storing the changes in longitude, latitude and heading that occur during each subarc, the position and velocity vectors represented in the vehicle tracking coordinate system aligned with

the exit Keplerian orbit at atmospheric exit can be written as components in the vehicle tracking coordinate system aligned with the entry Keplerian orbit at atmospheric entry. Once this is done, and by using the orbital elements of the entry Keplerian orbit, the orbital elements of the new Keplerian orbit can be found and the position vector and velocity vector at the point of atmospheric exit can be written in geocentric-equatorial coordinates. Details of the required procedure follow.

As a first step in calculating the position and velocity vector components in the geocentric-equatorial coordinate system, the total changes in longitude, latitude and heading produced during the atmospheric skip are determined. Transformation of a vector represented in the vehicle tracking coordinate system aligned with the Keplerian orbit at atmospheric entry to the same vector represented in the vehicle tracking coordinate system aligned with the Keplerian orbit at atmospheric exit is given by

$$\mathbf{T} = [\pm\psi_{3x}][\mp\phi_{3y}][\theta_{3z}][\pm\psi_{2x}][\mp\phi_{2y}][\theta_{2z}][\pm\psi_{1x}][\mp\phi_{1y}][\theta_{1z}] \quad (3.3)$$

where the upper and lower row of signs indicate a rotation produced by a positive or negative bank angle respectively. The subscripts 1, 2 and 3 indicate the descent, constant altitude and ascent portions of the skip trajectory respectively. The x , y and z subscripts denote the vehicle tracking system axis of rotation for that transformation. An equivalent transformation to the one given in equation 3.3 is performed using the total changes in longitude, latitude and heading and is given by

$$\mathbf{T}' = [\pm\psi'_x][\mp\phi'_y][\theta'_z] \quad (3.4)$$

where the prime indicates the as yet to be determined total changes in longitude, latitude and heading and the subscripts and signs are as previously defined. The rotation matrices used in 3.3 and 3.4 are given as

$$[\psi_x] = \begin{bmatrix} 1 & 0 & 0 \\ 0 & \cos\psi & \sin\psi \\ 0 & -\sin\psi & \cos\psi \end{bmatrix} \quad (3.5)$$

$$[\phi_y] = \begin{bmatrix} \cos\phi & 0 & -\sin\phi \\ 0 & 1 & 0 \\ \sin\phi & 0 & \cos\phi \end{bmatrix} \quad (3.6)$$

$$[\theta_z] = \begin{bmatrix} \cos\theta & \sin\theta & 0 \\ -\sin\theta & \cos\theta & 0 \\ 0 & 0 & 1 \end{bmatrix} \quad (3.7)$$

Using the above rotation matrices, the transformation matrix \mathbf{T}' written out in component form is

$$\mathbf{T}' = \quad (3.8)$$

$$\begin{bmatrix} \cos\theta'\cos\phi' & \sin\theta'\cos\phi' & \sin\phi' \\ -\sin\theta'\cos\psi' - \cos\theta'\sin\phi'\sin\psi' & \cos\theta'\cos\psi' - \sin\theta'\sin\phi'\sin\psi' & \cos\phi'\sin\psi' \\ \sin\theta'\sin\psi' - \cos\theta'\sin\phi'\cos\psi' & -\cos\theta'\sin\psi' - \sin\theta'\sin\phi'\cos\psi' & \cos\phi'\cos\psi' \end{bmatrix}$$

Since the two rotation matrices, \mathbf{T} and \mathbf{T}' , produce the same transformation, solution for the unknown angles θ' , ϕ' and ψ' is done by isolating components from the transformation matrix \mathbf{T}' , given in equation 3.8. Designating \mathbf{T}_{rc} as elements of the transformation matrix given by 3.3, where r denotes the row and c denotes the column of the matrix. The solution for the unknown angles is given as

$$\tan\theta' = \frac{\mathbf{T}_{12}}{\mathbf{T}_{11}} \quad (3.9)$$

$$\sin\phi' = \mathbf{T}_{13} \quad (3.10)$$

$$\tan\psi' = \frac{\mathbf{T}_{23}}{\mathbf{T}_{33}} \quad (3.11)$$

Equations 3.9 - 3.11 give the change in longitude, latitude and heading respectively as measured from the atmospheric entrance point in the reference plane aligned with the deboost Keplerian orbit which has the X axis coincident with the atmospheric entrance point.

3.3.4: Exit Orbit Determination

Upon exit from the atmosphere, the vehicle will have a new velocity and flight path angle and position as determined by the derived closed form flight equations and the chosen set of parameters. The new position and velocity vector must be converted to the geocentric-equatorial coordinate system for incorporation into the existing algorithm. Written as components along the reference plane coinciding with the Keplerian orbit plane at the exit from the atmosphere, vehicle tracking coordinate system, the position and velocity vectors are given as

$$\vec{\mathbf{r}} = \begin{bmatrix} r_f \\ 0 \\ 0 \end{bmatrix} \quad (3.12)$$

$$\vec{\mathbf{V}} = \begin{bmatrix} V_f \sin \gamma_f \\ V_f \cos \gamma_f \\ 0 \end{bmatrix} \quad (3.13)$$

where the subscript f denotes conditions at the exit from the atmosphere. In order to write the new position and velocity vectors of the vehicle in the geocentric-equatorial coordinate system, two steps are needed. First, using the inverse of \mathbf{T}' with the angles determined by equations 3.9 - 3.11, the vectors given in 3.12 and 3.13 are written in the coordinate system aligned with the Keplerian orbit at the entrance to the atmosphere. Secondly, using the orbital elements of

the Keplerian entrance orbit, the vectors are written in the geocentric-equatorial coordinate system.

Due to the properties of orthogonal coordinate system rotations, the inverse of such a matrix is its transpose. Therefore

$$\mathbf{T}'^{-1} = \mathbf{T}'^T$$

$$\mathbf{T}'^{-1} = \quad (3.14)$$

$$\begin{bmatrix} \cos\theta'\cos\phi' & -\sin\theta'\cos\psi' - \cos\theta'\sin\phi'\sin\psi' & \sin\theta'\sin\psi' - \cos\theta'\sin\phi'\cos\psi' \\ \sin\theta'\cos\phi' & \cos\theta'\cos\psi' - \sin\theta'\sin\phi'\sin\psi' & -\cos\theta'\sin\psi' - \sin\theta'\sin\phi'\cos\psi' \\ \sin\phi' & \cos\phi'\sin\psi' & \cos\phi'\cos\psi' \end{bmatrix}$$

The exit position vector and the exit velocity vector written in the coordinate system aligned with the Keplerian entrance orbit are denoted as \vec{r}' and \vec{V}' respectively. These vectors are obtained using equations 3.12 and 3.13 and the inverse matrix given in equation 3.14, as follows

$$\vec{r}' = \mathbf{T}'^{-1} \begin{bmatrix} r_f \\ 0 \\ 0 \end{bmatrix} \quad (3.15)$$

$$\vec{V}' = \mathbf{T}'^{-1} \begin{bmatrix} V_f \sin\gamma_f \\ V_f \cos\gamma_f \\ 0 \end{bmatrix} \quad (3.16)$$

As the final step in converting the exit position and velocity vector to their components in the geocentric-equatorial coordinate system, the orbital elements of the Keplerian orbit at the entrance to the atmosphere are used. Using the classical orbital elements

a - Semi-major axis

e - Eccentricity

i - Inclination

Ω - Longitude of the ascending node

ω - Argument of perigee

ν - True anomaly

the position of the entrance point is uniquely determined. The orbital elements also uniquely determine the orientation of the corresponding orbital plane. By converting all angles to values between zero and 2π , the following sequence of rotations transforms a vector written in the coordinate system aligned with the Keplerian entrance orbit whose X axis is aligned with the atmospheric entry point to a vector written in geocentric-equatorial coordinate system. Figure 8 shows the relation between the orbital elements and the geocentric-equatorial coordinate system. The transformation of a vector represented in the vehicle tracking system aligned with Keplerian orbit at the point of atmospheric entry to a vector represented in the geocentric-equatorial coordinate system is given as

$$\begin{bmatrix} \text{Geo} \\ \text{ } \\ \text{ } \end{bmatrix} = [-\Omega_z][i_x][-\omega_z][-\nu_z] \begin{bmatrix} \text{ } \\ \text{ } \\ \text{ } \end{bmatrix}, \quad (3.17)$$

Where the prime denotes vectors written in the coordinate system aligned with the Keplerian entrance orbit and Geo denotes the same vector written in the geocentric-equatorial coordinate system. With the exit position and velocity of the vehicle now written in geocentric-equatorial coordinates as given by equations 3.12 - 3.17, the exit Keplerian orbital elements can be calculated. Also, the vehicle's position can be represented in terms of right ascension and declination. For the general skip trajectory involving the use of bank, the orbital plane will change orientation. As seen in Figure 9, the use of bank angle to change the orbital plane inclination also produces a rotation of the line of nodes, Ω .

3.4: The Generalized Impulse

The results of the previous section can now be combined in the form of a generalized impulse. As stated previously, a generalized impulse produces a change in velocity, $\Delta\vec{V}$, as well as a change in position, $\Delta\vec{r}$, given by

$$\vec{V}^+ = \vec{V}^- + \Delta\vec{V}(\Delta V_x)_{inst}, (\Delta V_y)_{inst}, (\Delta V_z)_{inst}, \sigma_d, \lambda_d, \lambda_c, t_c, \sigma_a, \lambda_a) \quad (3.18)$$

$$\vec{r}^+ = \vec{r}^- + \Delta\vec{r}(\Delta V_x)_{inst}, (\Delta V_y)_{inst}, (\Delta V_z)_{inst}, \sigma_d, \lambda_d, \lambda_c, t_c, \sigma_a, \lambda_a)$$

$$t^+ = t^- + \Delta t(\Delta V_x)_{inst}, (\Delta V_y)_{inst}, (\Delta V_z)_{inst}, \sigma_d, \lambda_d, \lambda_c, t_c, \sigma_a, \lambda_a)$$

where $(\Delta V_i)_{inst}$, corresponds to the components of an instantaneously applied change in velocity at the state indicated by the minus sign. The other parameters are those given by equations 2.109 and are associated with the atmospheric skip trajectory.

The parameters of the generalized impulse result in the following the path for the vehicle. By applying the $(\Delta V_x)_{inst}$, $(\Delta V_y)_{inst}$ and $(\Delta V_z)_{inst}$ from equation 3.18, the vehicle, which has velocity, \vec{V}^- , and position, \vec{r}^- , at the end of a previous Keplerian coasting arc, a new orbit is generated. The vehicle travels this new orbit, also called the deboost orbit, until atmospheric penetration occurs. At the point of atmospheric entry, the parameters σ_d , λ_d , λ_c , t_c , σ_a and λ_a describe a skip trajectory which moves the vehicle to a point where it exits the atmosphere. The vehicle's position at the atmospheric exit, \vec{r}^+ , and its velocity, \vec{V}^+ , as determined from the procedure in section 3.3 terminates the path of the generalized impulse at which point a new Keplerian coast begins. A representative path followed by the interceptor as a result of the generalized impulse started as ΔV_1 is given in Figure 10.

The difference between \vec{r}^+ and \vec{r}^- is the change in position, $\Delta\vec{r}(\vec{x}_g)$, produced by the generalized impulse and the difference between \vec{V}^+ and \vec{V}^- is the change in velocity, $\Delta\vec{V}(\vec{x}_g)$, produced by the generalized impulse and the difference between t^+ and t^- is the change in time, $\Delta t(\vec{x}_g)$, produced by the generalized impulse.

Chapter 4: Numerical Results

4.1: Overview

In this chapter, the validity of the developed closed form atmospheric flight equations is determined. By comparing the results of a skip trajectory calculated using the closed form solution with results obtained from the literature, the accuracy of the closed form solutions is demonstrated. Also presented in this chapter are several families of solutions to finding parameter optimized transfer orbits as posed in Chapter 2. These solutions include the use of the closed form atmospheric flight equations. All solutions presented are based on the following assumptions:

- A stationary atmosphere with respect to a nonrotating Earth
- Coriolis and transport accelerations are neglected
- The component of the gravity force tangent to the flight path is small with respect to aerodynamic forces and is neglected
- The centrifugal and the gravity force are nearly equal at the orbital velocities and are considered to cancel each other
- A small cross range angle is covered and the related cross range terms are neglected in the heading equation
- Flight occurs at small flight path angles
- A $\beta r = \text{constant}$ atmosphere is used with the inverse scale height, β , also constant
- $K(M, Re)$ and $C_{DO}(M, Re)$ are constant due to the hypersonic flight Mach numbers
- The exponent in the drag polar is three halves to closer approximate hypersonic flight
- Controls change “instantaneously” with respect to the atmospheric flight time
- Series expansions are used to approximate integrals involving longitude, latitude and time

4.2: Validation of Closed Form Solutions

As a first step in proving the usefulness of the developed closed form atmospheric flight equations, the accuracy of the calculated integrals given in equations 2.98 - 2.100 and 2.106 - 2.108 was checked. A type of trajectory was formulated using the two parameters, λ and σ , to describe the entire skip trajectory rather than the complete set of six parameters detailed in Chapter 2. This type of trajectory is designated as a two parameter skip. Given a set of initial conditions for entrance to the atmosphere [see Table 2] and choosing the value for the lift coefficient as that which yields the maximum lift to drag ratio, manual iteration on the value for the bank angle was performed until the desired final heading change was approximately achieved. Using the corresponding calculated aeroassisted values for the end states, the accuracy of the approximated integrals is checked against a solution obtained by numerical integration. The numerical integration of the state equations 2.92 - 2.97 was performed using the standard IMSL routine DIVPRK with an accuracy of 10^{-10} used for convergence. Cases were generated for changes in the heading angle, ψ , of 10° , 20° , 30° and 40° . Data for the skip vehicle used, atmospheric data and physical constants are given in Table 1. The physical data will be used in all skip trajectory calculations except where noted otherwise. A summary of the initial values for the state variables is given in Table 2. Table 3 gives the final values for the state variables generated using the closed form solutions. Final values for the state variables calculated by numerical integration are given in Table 4. Since the difference between the results of Table 3 and Table 4, as given in Table 5 are negligible, the altitude histories presented in Figure 11 represent the true trajectories, thus validating the accuracy of the state variable closed form solutions given by equations 2.98 - 2.100 and 2.106 - 2.108.

4.3: Validation of Skip Trajectory Implementation

In order to check the validity of the implementation of the skip trajectory discussed in Chapter 3, the following type of trajectory was proposed. At the minimum altitude of the skip trajectory, when the flight path angle is zero, the reference plane was reset using the boundary conditions described in Chapter 2. However, unlike the general skip trajectory discussed in Chapter 2, there is no constant altitude flight subarc. Rather, the final velocity and altitude at the end of the descent subarc are used immediately as the initial conditions for the ascent arc. The values for the parameters λ and σ are kept the same for the descent and ascent flight subarcs. This type of skip trajectory is designated as a four parameter skip. The designation of a four parameter skip is used because even though the respective values for λ and σ are the same for the ascent and descent subarcs, there are four parameters being specified due to the resetting of the reference plane at $\gamma = 0$.

After using the procedure detailed in Chapter 3 for determining the location of the vehicle in the geocentric-equatorial coordinate system, the position of the vehicle resulting from the four parameter skip was calculated. This position and the total change in states were compared to the position and change in states calculated using the two parameter skip described in the section 4.2. Using the same initial conditions for a 10° change in heading given in Table 2, the trajectories were calculated.

Comparison of the calculated end states and the resulting change in plane inclination shows that the two final positions and heading differ significantly. The final velocity, time of flight and exit flight path agree, indicating an error involving latitude, longitude or heading. Because the closed form solutions involve the assumption of a small cross range angle traveled, calculation of the coupled equations given by 2.63 - 2.68 gives a more accurate answer than the closed form solutions. Using DIVPRK, numerical integration was performed on the set of equations 2.63 - 2.68. The flight path is used as the independent variable and the initial conditions are given in

Table 2 as before. The end states for the two parameter method, the four parameter method and the numerically integrated method are given in Table 6.

A comparison of the results obtained by numerically integrating equations 2.63 - 2.68 and the results from the two and four parameter closed form solutions shows that the four parameter skip trajectory is a more accurate method of calculating the change in latitude, longitude and heading. By using the four parameter method versus the two parameter method the error in determining the final position and heading is reduced by 70%.

As a final check on the accuracy of the derived closed form solution, a test case was evaluated against skip trajectory results obtained in Hull [4]. The optimal control used by Hull [4] to determine the skip trajectory state variables uses a parabolic drag polar. Therefore for the comparison test case the value of n in the expression for the atmospheric drag is set to 2.0. Initial conditions for the closed form equations were given to match the case for an optimally guided trajectory to achieve $\psi_f = 10^\circ$, as presented in Hull [4]. As noted in Hull [4], the lift coefficient is nearly constant at the value for maximum Lift-to-Drag, therefore, we choose $C_L = C_L^*$ corresponding to $n = 2$ as one parameter. The bank angle is manually iterated upon to achieve a final change in heading of 10° , and becomes our second parameter. The desired final change in heading is achieved when $\sigma = 87.595^\circ$. The trajectory is calculated using the same values of the two parameters for both the descent and ascent flight subarcs, with the reference plane being reset at $\gamma = 0$ as described earlier. Comparison of the resulting trajectory with the results in Hull [4] show close agreement in all final values of the state variables. Table 7 summarizes the comparison for relevant state variables.

4.4: Two Impulse Orbit Transfers

Now that the generalized impulse has been validated and the results from the aeroassisted maneuver provide accurate changes in position and velocity, the generalized impulse is applied to the minimization problem stated in section 2.3 with the number of impulses, $n = 2$. The two impulse maneuver proposed, transfers an interceptor from one circular orbit to another and allows the interceptor to rendezvous with a target. The interceptor does all the maneuvering while the target remains in its original orbit. The interceptor initial circular orbit has a larger radius than the circular orbit of the target in order to take advantage of the generalized impulse. A transfer from an interceptor circular orbit of smaller radius than the target radius using the generalized impulse is not possible due to the loss of energy encountered during the aeroassisted maneuver.

Given initial orbits and the location within each orbit for both the interceptor and the target, denoted as the epoch conditions, the two impulse maneuver is given as follows. A Keplerian coasting arc in the interceptor epoch circular orbit is terminated by the application of a generalized impulse. After the generalized impulse, described in section 3.4, the interceptor is at the boundary to the atmosphere and begins a second Keplerian coasting arc. This Keplerian coast arc intersects the target orbit and for the rendezvous to occur, the interceptor matches position and velocity with the target by applying an instantaneous delta-v. This instantaneous delta-v completes the orbit transfer.

The generalized impulse to be used in the transfer utilizes the four parameter method of calculation described in section 4.3. The four parameter method calculates the skip trajectory using two subarcs, the descent and ascent subarc, using the parameters λ_d , σ_d , λ_a and σ_a . However, as described in section 4.3, $\lambda_d = \lambda_a$ and $\sigma_a = \sigma_d$, is used to improve accuracy.

4.4.1: Parameters and Constraints for the Two Impulse Transfer

The parameters needed for the two impulse transfer are

η_1	=	Interceptor initial coasting arc
$(\Delta V_x)_{inst}$	=	X component of the instantaneous delta-v used in the generalized impulse
$(\Delta V_y)_{inst}$	=	Y component of the instantaneous delta-v used in the generalized impulse
$(\Delta V_z)_{inst}$	=	Z component of the instantaneous delta-v used in the generalized impulse
λ	=	Scaled lift coefficient used during the skip trajectory
σ	=	Bank angle used during the skip trajectory
η_2	=	Interceptor second coasting arc
η_3	=	Target coasting arc

All of the numerical results for the following aeroassisted maneuvers do not include a constant altitude subarc. The constant altitude subarc is developed for a skip trajectory in general form. The second impulse is applied at the end of the trajectory and is not a parameter of the optimization but is used to calculate the cost function, J .

The equality constraints imposed on the orbit transfer problem are

- X component of the final position for the interceptor and target must match
- Y component of the final position for the interceptor and target must match
- Z component of the final position for the interceptor and target must match
- Total time of flight for the interceptor and the target must be equal

Recall that a velocity match for rendezvous is satisfied by computing the required final delta-v and hence is not an explicit equality constraint.

The inequality constraints imposed on the orbit transfer problem are

- Time of flight for the target must be less than a specified maximum time of flight
- Time of flight for the target must be greater than zero
- Initial coasting arc for the interceptor must be greater than 1°
- Magnitude of $(\Delta \vec{V}_{inst})$ from the generalized impulse must be greater than the magnitude of $(\Delta \vec{V}_{min})$ needed to cause atmospheric entry
- Lift coefficient must be less than or equal to the maximum allowed lift coefficient
- Lift coefficient must be greater than zero

- Bank angle must be less than 90°
- Second interceptor coasting arc must be greater than 1°
- Minimum radius of the second coasting arc must be greater than the radius of the Earth

In order to ensure atmospheric entry, the following procedure was used. For a given interceptor circular orbit, a $\|\Delta\vec{V}_{min}\|$ was determined as the magnitude of the deboost impulse required to perform a Hohmann transfer between the interceptor orbit and a circular orbit of radius h_{atm} . Since the Hohmann transfer is the minimum fuel transfer method between two circular orbits, $\|\Delta\vec{V}_{min}\|$ is the lower bound for impulses to cause atmospheric entry.

After $\|\Delta\vec{V}_{min}\|$ has been calculated and given an initial guess which causes atmospheric entry, the three components of $\Delta\vec{V}_{inst}$ from the generalized impulse are retained. During the optimization process, each iteration of the sequential quadratic programming algorithm produces a complete new set of parameters. If the $\|\Delta\vec{V}_{inst}\|$ of the generalized impulse calculated during the i^{th} iteration is greater than $\|\Delta\vec{V}_{min}\|$, the three components of $\Delta\vec{V}_{inst}$ from the generalized impulse determined during the i^{th} iteration replace the values of $\Delta\vec{V}_{inst}$ from the generalized impulse determined in the $(i^{th} - 1)$ iteration. However, if the $\|\Delta\vec{V}_{inst}\|$ of the generalized impulse calculated during the i^{th} iteration is less than $\|\Delta\vec{V}_{min}\|$, the three components of $\Delta\vec{V}_{inst}$ from the generalized impulse determined in the $(i^{th} - 1)$ iteration replace the values of $\Delta\vec{V}_{inst}$ from the generalized impulse determined during the i^{th} iteration. Thus, by retaining the previous values of the generalized impulse $\Delta\vec{V}_{inst}$ which ensure atmospheric entry, the following iteration will also be ensured of atmospheric entry. With the newly modified parameter vector, a new cost function is evaluated and the process continues until convergence occurs. It is emphasized that all other parameters from iteration to iteration remain unaffected.

The main consideration in using this technique is that the new parameter vector produced by the substitution method described above alters the optimal parameter vector of the current

iteration thus affecting the search for the optimal solution. It should be noted however, that the relative changes in the three components of $\Delta\vec{V}_{inst}$ from the generalized impulse are small from one iteration to the next and that with a reasonable initial guess, the described method works well. It is again emphasized that the other parameters in the parameter vector are never altered using the described method.

4.4.2: Minimum Fuel Two Impulse Coplanar Transfers

Using the parameters listed in section 4.4.1 to minimize the fuel consumed during the transfer

$$J = \sum_{i=1}^n \|(\Delta\vec{V}_{inst})_i\|$$

subject to the constraints given in section 4.4.1, coplanar transfers between the orbits given in Table 8 were performed. To simplify notation, the ratio between the radius of the initial interceptor orbit to the radius of the target orbit is denoted as χ . The chosen target circular orbit corresponds to a LEO of approximately 1000 km in altitude. Tables 9 and 10 give the epoch conditions of the target and interceptor respectively for the coplanar cases that are solved. Solution to the problems were obtained on a VAX mainframe using the IMSL routine DCONF, which is a sequential quadratic programming algorithm based on Schittkowski's method [16]. Table 11 summarizes the overall results obtained for the seven coplanar transfer solutions, with the Total TOF column indicating the total time of flight required to perform the entire transfer and the TOF column denoting the time of flight elapsed during the generalized impulse.

For all of the values of χ investigated, key values pertaining to the atmospheric portion of the generalized impulse used in the coplanar transfers are presented in Table 12. The convective heating rate given is based on a 1 meter radius sphere under the condition of laminar flow. The heating rate is presented to show the trends resulting from the various trajectories rather than the actual heating rates experienced by the skip vehicle. The formula for the heating rate in

Watts/cm² is

$$Q_{Heat} = (3.08 \times 10^{-4}) \sqrt{\rho} V_E^{3.08} \quad (4.1)$$

where the atmospheric density, ρ , is given in kg/km³ and the flight speed, V_E , is given in km/s.

The dynamic pressure is given by

$$q = \frac{1}{2} \rho V_E^2 \quad (4.2)$$

where the atmospheric density, ρ , is given in kg/m³ and the flight speed, V_E , is given in m/s.

The normal g-load is measured in the Lift-Drag plane as defined in Figure 3 and is calculated as

$$g = \frac{\rho V_E^2 S C_L}{2mg} \quad (4.3)$$

Since the results obtained are similar for all of the seven coplanar cases investigated, only three are presented in detail, these three being the transfers corresponding to $\chi = 5.75$, $\chi = 2.61$ and $\chi = 1.30$. Time histories for $\chi = 5.75$, the transfer from GEO, are given in Figures 12 - 17. These figures are the time histories for altitude, normal g-load, convective heating rate, flight path angle, dynamic pressure and velocity respectively. Time histories for the same quantities corresponding to $\chi = 2.61$ are given in Figures 18 - 23 and the time histories for $\chi = 1.30$ are given in Figures 24 - 29.

From Figures 12 - 29, the maximum values for the convective heating rate of 214.95 W/cm², the dynamic pressure of 19.1 KN/m² and the maximum instantaneous normal g-load of 6.97 all occur during the aeroassisted maneuver of the transfer from geosynchronous Earth orbit. This transfer also has the steepest entry flight path angle, -4.17° , and penetrates the deepest into the atmosphere to an altitude of 56.4 km. On the other hand, the orbital transfer corresponding to $\chi = 1.30$ has a maximum heating rate of 107.9 W/cm², a dynamic pressure of 8.4 KN/m² and a maximum instantaneous normal g-load of 3.1. The flight path angle for the $\chi = 1.30$ transfer is -0.722° and only penetrates the atmosphere to an altitude of 60.77 km.

From the results presented above, there is a trend corresponding to the value of χ , this trend being that as the value of χ decreases, the corresponding maximum values presented in Table 12 also decrease. Since the lift coefficient and bank angle are the same for all of the coplanar transfers the trends are related to the atmospheric entrance conditions. As the value of χ decreases, the eccentricity of the deboost orbit decreases causing the values of γ_e and V_e to decrease resulting in shallower skip trajectories. These shallower skip trajectories therefore produce lower heating rates, dynamic pressures and normal g-loads.

A comparison of the results in [14] and the results presented via Figures 12 - 29 show that the closed form solutions and the solutions obtained via optimal control theory are similar. The trends relating to the time histories for altitude, normal-g load, dynamic pressure, convective heating rate and velocity are repeated in Figures 12 - 29 thus further validating the developed closed form solutions and the idea of the generalized impulse.

As a means of comparing the results obtained using the generalized impulse to another two impulse transfer method, the same problem was solved for each value of χ using the Hohmann transfer. The Hohmann transfer is known to be the two impulse method of orbit transfer to minimize fuel when there is no limit on the amount of time needed to transfer orbits. Figure 48 shows the cost function, J , for the two methods. From Figure 48, for values of $\chi \geq 1.3$ the generalized impulse reduces the amount of fuel needed to transfer orbits. For a transfer from GEO to the target radius of 1.15 DU, the savings in fuel expended is 50% relative to the corresponding Hohmann transfer. The percentage of fuel saved decreases as the value of χ decreases to approximately 1.3. It should be noted that the obtained solution for the coplanar transfers using the generalized impulse yielded instantaneously applied delta-v's that were applied in a Hohmann-like manner, i.e. the delta-v's were applied nearly tangent to the flight path and in the plane of the orbit. It should also be noted that the problem was solved with no limit on the maximum allowable time in which to complete the transfer.

From key values presented for the coplanar transfers, the calculated “optimal” fuel skip trajectories all occur at small flight path angles, thus satisfying one of the key assumptions used in obtaining the closed form solutions. The “optimal” skip trajectories all occur at normal g-loads well below human tolerances and the maximum values given are instantaneous rather than sustained values. With the maximum flight time for all of the presented skip trajectories being 25 seconds, these rates of loading are acceptable. It is noted that the lift coefficient determined for all of the coplanar transfers was at the maximum allowable value of 1.5. Flight at the upper bound for the lift coefficient is necessary to slow the vehicle down sufficiently during its atmospheric pass in order to place the interceptor in the proper Keplerian orbit at exit from the atmosphere and to save fuel needed to produce the minimum instantaneous delta-v’s possible.

4.4.3: Minimum Fuel Two Impulse Noncoplanar Transfers

Similar to the coplanar transfers, the cost function to minimize the fuel consumed is given as

$$J = \sum_{i=1}^n \|(\Delta \vec{V}_{inst})_i\|$$

With the constraints given in section 4.4.1, noncoplanar transfers between the orbits given in Table 8 were performed with the difference in plane inclination being 5°. Tables 13 and 14 give the epoch conditions of the target and interceptor respectively for the noncoplanar cases that are solved. Table 15 summarizes the overall results obtained for the seven noncoplanar transfer solutions, with the Total TOF column indicating the total time of flight required to perform the entire transfer and the TOF column denoting the time of flight elapsed during the generalized impulse.

For all of the values of χ investigated, key values pertaining to the atmospheric portion of the generalized impulse used in the noncoplanar transfers are presented in Table 16. Similar to the results presented for the coplanar transfers, the convective heating rate given is based on a 1

meter radius sphere under the condition of laminar flow and is presented to show the trends resulting from the various trajectories rather than the actual heating rates experienced by the skip vehicle. The formula for the heating rate is given in equation 4.1. The dynamic pressure results for the atmospheric portion of the noncoplanar transfers are based on equation 4.2 and the normal g-load is given by equation 4.3.

Since the obtained results are similar for all of the seven noncoplanar cases investigated, only three are presented in detail, these three being the transfers corresponding to $\chi = 5.75$, $\chi = 2.61$ and $\chi = 1.30$. Time histories for $\chi = 5.75$, the transfer from GEO, are given in Figures 30 - 35. These figures are the time histories for altitude, normal g-load, convective heating rate, flight path angle, dynamic pressure and velocity respectively. Time histories for the quantities corresponding to $\chi = 2.61$ are given in Figures 36 - 41 and the time histories for $\chi = 1.30$ are given in Figures 42 - 47.

From Figures 30 - 47 for the noncoplanar orbit transfer, the maximum values for the convective heating rate of 201.36 W/cm^2 and the maximum instantaneous normal g-load of 5.57 occur during the aeroassisted maneuver of the transfer from geosynchronous Earth orbit. The steepest entry flight path angle, -2.33° , occurs during the $\chi = 4.35$ orbit transfer. The deepest penetration into the atmosphere, 56.35 km, occurs during the $\chi = 1.74$ orbit transfer. The maximum dynamic pressure for the noncoplanar transfers, 16.54 KN/m^2 , also occurs during the $\chi = 1.74$ transfer. The maximum flight time during the atmospheric pass, 109.3 seconds, occurs during the $\chi = 1.3$ transfer. The lowest maximum heating rate of, 132.14 W/cm^2 , the lowest maximum dynamic pressure of, 13.69 KN/m^2 and the lowest maximum normal g-load of, .57 all occur during the $\chi = 1.22$ transfer. The shallowest entry flight path angle, $-.941^\circ$, from the noncoplanar trajectories also occurs during the $\chi = 1.22$ orbit transfer. Due to the combined effect of the nonzero bank angle and the lower values for the lift coefficient, the trend

seen in the coplanar orbit transfers corresponding to the value of the ratio χ , is not repeated for the noncoplanar orbit transfers.

As a means of comparing the results for noncoplanar orbit transfer obtained using the generalized impulse to results obtained with other two impulse transfer methods, the same problem was first solved for each value of χ using a combination of the Hohmann transfer required to change the orbital size and the plane change maneuver required to change the orbital inclination. The first delta-v of this two impulse maneuver combines a plane change delta-v, which is applied during the interceptor's orbit at the point when the interceptor crosses the target orbit's line of nodes, with the deboost delta-v of a Hohmann transfer. The equation for performing an instantaneous plane change is

$$\Delta V = 2V \sin\left(\frac{\Delta i}{2}\right) \quad (4.4)$$

Since this delta-v is directly proportional to the existing circular velocity, the pure plane change maneuver is applied at the interceptor radius due to the lower circular velocity at the greater radius. Therefore, the first impulse has components in three dimensions, unlike the pure Hohmann transfer. The second impulse of the two impulse maneuver is the recircularization delta-v of the resulting Hohmann-like transfer and is applied at the radius of the LEO for the target.

The second method of noncoplanar transfer that is compared to the generalized impulse method determines the optimal set of parameters needed to perform a two impulse transfer without a generalized impulse. The parameters of the two impulse maneuver without the generalized impulse are as described earlier with angles through Keplerian coast arcs terminated by an impulsive three dimensional delta-v. The optimal parameters associated with the required two impulse maneuver are determined using the same nonlinear sequential programming routine used to solve the problem when a generalized impulse is included as a set of parameters.

Figure 49 shows the cost function, J , for the three methods. From Figure 49, the aeroassisted maneuver reduces the amount of fuel needed to transfer orbits in all cases. For a transfer from GEO to the target radius of 1.15 DU, the savings in fuel expended is 55% of the fuel required for the corresponding “nonoptimal” two impulse maneuver described above and a 52% savings in fuel compared to the “optimal” nonaeroassisted two impulse maneuver. The percentage in fuel savings decreases as the value of χ decreases. However, unlike the coplanar cases, the generalized impulse produces savings for all cases presented. Finally, Figure 50 compares the coplanar and noncoplanar cost functions that implement the generalized impulse method to solve the aeroassisted transfer. Figure 50 shows that for values of $\chi \geq 1.74$, small plane change transfers using an aeroassisted maneuver require less fuel than the corresponding coplanar orbit transfer that uses an aeroassisted maneuver.

Similar to the key values presented for the coplanar transfers, the noncoplanar “optimal” fuel skip trajectories all occur at small flight path angles. However, unlike the coplanar skip trajectories, not all of the transfers occurred at the maximum allowable value for the lift coefficient. Due to the need to achieve a required change in heading, as the entrance velocity decreases the lift coefficient also decreases to lower the velocity losses during the atmospheric pass. This reduction in the lift coefficient causes the skip trajectory to take longer to achieve the required change in heading. Also, the lower lift coefficient is the cause for the lower normal g-loads experienced by the vehicle. Since the change in orbital plane inclination was 5° for all of the noncoplanar cases, the noncoplanar maneuvers occur at nearly the same bank angle, with a minimum value of $\sigma = 47.85^\circ$ and a maximum value of $\sigma = 55.31^\circ$. Even though the entrance flight path angles are generally lower than those for the corresponding coplanar transfers, the vehicle penetrates deeper into the atmosphere due to the lower lift coefficients and the loss of vertical lift due to the existence of a considerable out of plane bank angle.

Table 1. Physical Data

Symbol	Physical Characteristic	Numerical Value	Units
R_e	Radius of the Earth	6378.145	km
h_{atm}	Altitude of the Atmosphere	60.960	km
β	Inverse Scale Height	7.100	km^{-1}
μ	Gravitational Parameter	3.986×10^5	km^3s^{-2}
ρ_o	Sea-Level Density	1.225	kg m^{-3}
β_r	Atmospheric Constant	900	-
m	Vehicle Mass	4898.805	kg
S	Vehicle Reference Area	11.691	m^2
C_{DO}	Zero Lift Drag Coefficient	0.032	-
K	Induced Drag Factor	1.400	-
n	Exponent in Drag Polar	1.500	-
C_{Lmax}	Maximum Lift Coefficient	1.500	-

Table 2. Initial Conditions for 10°, 20°, 30° and 40° Heading Changes

ψ_f (deg)	γ_e (deg)	σ (deg)	C_L	t_e (s)	V_e (km/s)	ψ_e (deg)	ϕ_e (deg)	θ_e (deg)
10	-1.0000	78.6	0.13	0.0	7.9107	0.0	0.0	0.0
20	-1.5000	81.5	0.13	0.0	7.9107	0.0	0.0	0.0
30	-1.8500	83.0	0.13	0.0	7.9107	0.0	0.0	0.0
40	-2.0875	84.0	0.13	0.0	7.9107	0.0	0.0	0.0

Table 3. Final Conditions Using Closed Form Solutions

γ_f (deg)	t_f (s)	V_f (km/s)	ψ_f (deg)	ϕ_f (deg)	θ_f (deg)
1.0000	249.4159934	6.9229276	9.9193983	1.4323665	16.5065751
1.5000	270.4335809	6.0537450	20.0757621	2.8980739	16.3743975
1.8500	280.5880362	5.3016440	30.1393192	4.1205232	15.3063406
2.0875	294.4709548	4.6726422	39.7312626	5.1721034	14.3180372

Table 4. Final Conditions Using Numerical Integration

γ_f (deg)	t_f (s)	V_f (km/s)	ψ_f (deg)	ϕ_f (deg)	θ_f (deg)
1.0000	249.4159984	6.9229276	9.9193983	1.4323665	16.5065751
1.5000	270.4335425	6.0537450	20.0757621	2.8980735	16.3743952
1.8500	280.5880024	5.3016440	30.1393192	4.1205227	15.3063388
2.0875	294.4709231	4.6726422	39.7312626	5.1721028	14.3180358

Table 5. Error Between Closed Form Solutions and Solutions Using Numerical Integration

γ_f (deg)	$\ \Delta t_f\ $ (s)	$\ \Delta V_f\ $ (km/s)	$\ \Delta \psi_f\ $ (deg)	$\ \Delta \phi_f\ $ (deg)	$\ \Delta \theta_f\ $ (deg)
1.0000	0.0000050	0.0000000	0.0000000	0.0000000	0.0000000
1.5000	0.0000384	0.0000000	0.0000000	0.0000004	0.0000023
1.8500	0.0000338	0.0000000	0.0000000	0.0000005	0.0000018
2.0875	0.0000317	0.0000000	0.0000000	0.0000006	0.0000014

Table 6. Final Conditions Using Various Methods to Calculate the Skip Trajectory

Method	t_f (s)	V_f (km/s)	ψ_f (deg)	ϕ_f (deg)	θ_f (deg)	Δi (deg)
n=1.5, $C_L=0.13$ $\sigma=78.6^\circ$						
2 Parameters	249.41599	6.9229276	9.919398	1.432366	16.50657	10.02125
4 Parameters	249.41599	6.9229276	9.828217	1.427068	16.50828	9.930275
DIVPRK	249.42061	6.9229277	9.793981	1.424145	16.50790	9.895982

Table 7. Comparison to Optimally Guided Trajectory

Method	t_f	V_f	ψ_f	ϕ_f	h_{min}	Δi
n=2. $C_L=.15$ $\sigma=87.6^\circ$	(s)	(km/s)	(deg)	(deg)	(km)	(deg)
Parameterized	401.949	7.3390353	9.727	2.371	57.92602	10.00091
Optimally Guided	400.000	7.3063608	9.930	2.406	59.00928	10.21448

Table 8. Initial Interceptor and Target Circular Radii

χ	Target Radius	Interceptor Radius
5.75	1.15	6.6105
4.35	1.15	5.0000
3.48	1.15	4.0000
2.61	1.15	3.0000
1.74	1.15	2.0000
1.30	1.15	1.5000
1.22	1.15	1.4000

Table 9. Coplanar Epoch Conditions for the Target

χ	a	e	i	Ω	ω	ν
5.75	1.15	0.0	0.0	0.0	0.0	50.0
4.35	1.15	0.0	0.0	0.0	0.0	60.0
3.48	1.15	0.0	0.0	0.0	0.0	270.0
2.61	1.15	0.0	0.0	0.0	0.0	90.0
1.74	1.15	0.0	0.0	0.0	0.0	260.0
1.30	1.15	0.0	0.0	0.0	0.0	335.0
1.22	1.15	0.0	0.0	0.0	0.0	340.0

Table 10. Coplanar Epoch Conditions for the Interceptor

χ	a	e	i	Ω	ω	ν
5.75	6.6105	0.0	0.0	0.0	0.0	350.0
4.35	5.0000	0.0	0.0	0.0	0.0	350.0
3.48	4.0000	0.0	0.0	0.0	0.0	350.0
2.61	3.0000	0.0	0.0	0.0	0.0	350.0
1.74	2.0000	0.0	0.0	0.0	0.0	350.0
1.30	1.5000	0.0	0.0	0.0	0.0	350.0
1.22	1.4000	0.0	0.0	0.0	0.0	350.0

Table 11. Cost Function and Changes Due to the Generalized Impulse (Coplanar)

χ	J (SU)	Total TOF (min)	----- Generalized Impulse -----		
			TOF(min)	$\ \Delta\vec{V}_{atm}\ $ (SU)	$\ \Delta\vec{r}\ $ (DU)
5.75	.23037740	382.00	312.42	.3193	5.4605
4.35	.22796746	276.30	218.38	.2872	3.9904
3.48	.22102576	216.75	165.88	.2565	2.9904
2.61	.20396414	166.68	118.42	.2099	1.9904
1.74	.16121505	112.07	76.67	.1305	0.9904
1.30	.11568558	103.68	58.23	.0654	0.4904
1.22	.10277007	110.69	54.85	.0489	0.3904

Table 12. Max - Min Quantities for Coplanar Skip Trajectories

χ	TOF (s)	γ_e (deg)	C_L	σ (deg)	Q_{max} (W/cm ²)	q_{max} (KN/m ²)	g_{max}	h_{min} (km)
5.75	24.61	-4.170	1.5	0.0	214.95	19.1	6.97	56.414
4.35	23.98	-3.801	1.5	0.0	198.01	17.2	6.27	57.007
3.48	23.14	-3.439	1.5	0.0	183.00	15.5	5.67	57.579
2.61	21.31	-2.872	1.5	0.0	162.18	13.3	4.85	58.444
1.74	16.08	-1.853	1.5	0.0	132.70	10.3	3.77	59.800
1.30	9.22	-0.959	1.5	0.0	112.70	8.7	3.19	60.630
1.22	7.09	-0.722	1.5	0.0	107.90	8.4	3.08	60.770

Table 13. Noncoplanar Epoch Conditions for the Target

χ	a	e	i	Ω	ω	ν
5.75	1.15	0.0	5.0	170.0	0.0	228.0
4.35	1.15	0.0	5.0	170.0	0.0	240.0
3.48	1.15	0.0	5.0	170.0	0.0	95.0
2.61	1.15	0.0	5.0	170.0	0.0	280.0
1.74	1.15	0.0	5.0	170.0	0.0	90.0
1.30	1.15	0.0	5.0	170.0	0.0	165.0
1.22	1.15	0.0	5.0	170.0	0.0	165.0

Table 14. Noncoplanar Epoch Conditions for the Interceptor

χ	a	e	i	Ω	ω	ν
5.75	6.6105	0.0	0.0	0.0	0.0	350.0
4.35	5.0000	0.0	0.0	0.0	0.0	350.0
3.48	4.0000	0.0	0.0	0.0	0.0	350.0
2.61	3.0000	0.0	0.0	0.0	0.0	350.0
1.74	2.0000	0.0	0.0	0.0	0.0	350.0
1.30	1.5000	0.0	0.0	0.0	0.0	350.0
1.22	1.4000	0.0	0.0	0.0	0.0	350.0

Table 15. Cost Function and Changes Due to the Generalized Impulse (Noncoplanar)

χ	J (SU)	Total TOF (min)	----- Generalized Impulse -----		
			TOF(min)	$\ \Delta\vec{V}_{atm}\ $ (SU)	$\ \Delta\vec{r}\ $ (DU)
5.75	.22461882	393.80	319.63	.3204	5.4605
4.35	.22414714	285.97	223.52	.2888	3.9904
3.48	.21827484	224.13	169.59	.2602	2.9904
2.61	.20358296	170.21	120.71	.2202	1.9904
1.74	.16206055	122.34	78.03	.1512	0.9904
1.30	.11823638	104.17	60.43	.1387	0.4904
1.22	.10911130	105.68	57.59	.1233	0.3904

Table 16. Max - Min Quantities for Noncoplanar Skip Trajectories

χ	TOF (s)	γ_e (deg)	C_L	σ (deg)	Q_{max} (W/cm ²)	q_{max} (KN/m ²)	g_{max}	h_{min} (km)
5.75	28.31	-2.317	1.500	55.31	201.36	15.3	5.57	58.14
4.35	26.64	-2.330	1.500	51.29	188.83	14.5	5.29	58.33
3.48	27.21	-2.238	1.402	50.19	177.72	14.0	4.76	58.41
2.61	35.08	-2.313	1.004	47.85	168.96	15.0	3.66	57.56
1.74	56.69	-1.949	0.503	50.26	159.03	16.5	2.02	56.35
1.30	109.30	-1.248	0.172	54.95	154.44	18.1	0.76	55.29
1.22	100.74	-0.941	0.170	54.93	132.14	13.7	0.57	57.19

Chapter 5: Conclusion and Recommendation

5.1 Conclusions

A general set of aeroassisted maneuver parameters, \vec{x}_a , as part of the parameters needed for the generalized impulse was determined. The atmospheric parameters were determined as part of the process in obtaining closed form solutions to the atmospheric flight differential equations of motion. The minimization problem stated in Chapter 2 was solved using the generalized impulse and applied to coplanar and noncoplanar two impulse orbit transfers.

For the atmospheric and gravitational models used, coplanar orbit transfers with an interceptor radius greater than 1.5 DU and a target radius of 1.15 DU, the cost functions using a two impulse maneuver involving an atmospheric assist are lower than the corresponding two impulse Hohmann transfer. For noncoplanar orbit transfers involving small changes of the orbital plane inclination with a target radius of 1.15 DU and $\chi > 1.22$, the cost functions using the two impulse maneuver involving an aeroassist are lower than the corresponding two impulse maneuver described in Chapter 4 that combines a pure plane change maneuver and a Hohmann transfer.

Using an aeroassisted maneuver that involves an atmospheric pass reduces the fuel needed to perform noncoplanar and coplanar orbit transfers and is in agreement with the results from [4,14] for noncoplanar and coplanar transfers, respectively. The developed parameterization allows for quick, yet accurate, solutions to large numbers of minimum fuel orbit transfer

problems. Unlike solutions obtained through the use of optimal control theory and multi point boundary value problem numerical methods, obtaining solutions using parameter optimization is relatively easy and takes little time but does require a “feel” for what takes place during both Keplerian flight and atmospheric flight.

5.2 Recommendations for Future Research

Applying the current research ideas to developing a set of parameters which describe a finite burn in space poses an interesting and challenging extension to the present research. Similar to the present research, this finite burn in space changes position and velocity and occurs during a non-zero period of time, however the choice and implementation of the parameters needed to fully describe the finite burn poses the challenge of future research. Determination of the number of impulses which minimizes the fuel consumption for a given orbit transfer problem and choosing the corresponding impulse types also remains unanswered. Also, investigation into the full capabilities of the developed generalized impulse using all of the proposed six parameters provides an area for further research. Because of the difficulties in ensuring atmospheric entry due to deboost from Keplerian orbits other than circular orbits, application of the generalized impulse to elliptical and hyperbolic orbits also provides an opportunity to expand the generalized impulse idea. Finally, as a result of the search for the minimum, a set of parameters can be determined which does not force atmospheric entry, a method for calculating smooth transition between those trajectories which use atmospheric entry and those which do not and determining if atmospheric entry is even necessary to minimize fuel consumption poses a formidable challenge in extending the current research.

Appendix A: Partial Derivatives and Integrals

A1: Partial Derivatives

The change to the dimensionless variables Chapman variables Z and v in the differential state equations, involves chain rule differentiation and calculation of the following partial derivatives:

A1.1: Z Chapman Variable

$$Z = Z(\rho(r), r, \beta(r))$$

$$Z = \frac{\rho SC_L^*}{2m} \sqrt{\frac{r}{\beta}}$$

$$\rho = \rho_o \left(\frac{r}{r_o}\right)^{-k^2}$$

$$k^2 = \beta r$$

using the above relations for Z and ρ , the following partial derivatives are obtained:

$$\frac{\partial \rho}{\partial r} = -\beta r \rho_o \left(\frac{1}{r_o}\right) \left(\frac{r}{r_o}\right)^{-(k^2+1)}$$

$$\frac{\partial \rho}{\partial r} = -\beta \rho \tag{A.1}$$

$$\frac{\partial Z}{\partial r} = \frac{\rho SC_L^*}{2m} \frac{1}{2\beta} \sqrt{\frac{\beta}{r}}$$

$$\frac{\partial Z}{\partial r} = \frac{\rho SC_L^*}{2m} \frac{1}{2r} \sqrt{\frac{r}{\beta}}$$

$$\frac{\partial Z}{\partial r} = \frac{Z}{2r} \quad (A.2)$$

$$\frac{\partial Z}{\partial \beta} = \frac{\rho SC_L^*}{2m} \left(-\frac{r}{2\beta^2} \right) \sqrt{\frac{\beta}{r}}$$

$$\frac{\partial Z}{\partial \beta} = \frac{\rho SC_L^*}{2m} \left(-\frac{1}{2\beta} \right) \sqrt{\frac{r}{\beta}}$$

$$\frac{\partial Z}{\partial \beta} = -\frac{Z}{2\beta} \quad (A.3)$$

$$\frac{\partial Z}{\partial \rho} = \frac{SC_L^*}{2m} \sqrt{\frac{r}{\beta}} \quad (A.4)$$

A1.2: v Chapman Variable

$$v = v(V, g(r), r)$$

$$v = \frac{V^2}{gr}$$

$$g = \frac{g_0 r_0^2}{r^2}$$

using the above relations for v and g , the following partial derivatives are obtained:

$$\frac{\partial v}{\partial V} = \frac{2V}{gr} \quad (A.5)$$

$$\frac{\partial v}{\partial g} = -\frac{V^2}{rg^2} \quad (A.6)$$

$$\frac{\partial v}{\partial r} = -\frac{V^2}{gr^2} \quad (A.7)$$

$$\frac{\partial g}{\partial r} = -\frac{2g_0 r_0^2}{r^3}$$

$$\frac{\partial g}{\partial r} = -\frac{2g}{r} \quad (A.8)$$

A2: Integrals

Integration of the expressions for latitude, longitude and time requires the use of trigonometric identities, long division and series approximations.

A2.1: Latitude and Longitude

The expressions for latitude and longitude are given as

$$\frac{d\theta}{d\gamma} = \frac{\cos(\psi_e + \tan\sigma(\gamma - \gamma_e))}{k\lambda\cos\sigma(Z_e - \frac{k}{2\lambda\cos\sigma}(\gamma^2 - \gamma_e^2))}$$

$$\frac{d\phi}{d\gamma} = \frac{\sin(\psi_e + \tan\sigma(\gamma - \gamma_e))}{k\lambda\cos\sigma(Z_e - \frac{k}{2\lambda\cos\sigma}(\gamma^2 - \gamma_e^2))}$$

Using trigonometric identities for $\sin(\alpha + \beta)$ and $\cos(\alpha + \beta)$ the above equations can be rewritten as

$$\frac{d\theta}{d\gamma} = \frac{2[\cos(\psi_e - \gamma_e\tan\sigma)\cos(\gamma\tan\sigma) - \sin(\psi_e - \gamma_e\tan\sigma)\sin(\gamma\tan\sigma)]}{k^2\left[\frac{2k\lambda Z_e\cos\sigma + (k\gamma_e)^2}{k^2} - \gamma^2\right]} \quad (\text{A.9})$$

$$\frac{d\phi}{d\gamma} = \frac{2[\sin(\psi_e - \gamma_e\tan\sigma)\cos(\gamma\tan\sigma) + \cos(\psi_e - \gamma_e\tan\sigma)\sin(\gamma\tan\sigma)]}{k^2\left[\frac{2k\lambda Z_e\cos\sigma + (k\gamma_e)^2}{k^2} - \gamma^2\right]} \quad (\text{A.10})$$

Equations A.9 and A.10, have the same form but with different constants. These constants involve the entry states and the constant bank angle σ . Defining the following constants for

equation A.9

$$C_1 = \frac{2}{k^2} \cos(\psi_e - \gamma_e \tan \sigma) \quad (\text{A.11a})$$

$$C_2 = \frac{2k\lambda Z_e \cos \sigma + (k\gamma_e)^2}{k^2} \quad (\text{A.11b})$$

$$C_3 = \frac{2}{k^2} \sin(\psi_e - \gamma_e \tan \sigma) \quad (\text{A.11c})$$

while for equation A.10 the same constants are defined as

$$C_1 = \frac{2}{k^2} \sin(\psi_e - \gamma_e \tan \sigma) \quad (\text{A.11d})$$

$$C_2 = \frac{2k\lambda Z_e \cos \sigma + (k\gamma_e)^2}{k^2} \quad (\text{A.11e})$$

$$C_3 = \frac{2}{k^2} \cos(\psi_e - \gamma_e \tan \sigma) \quad (\text{A.11f})$$

Therefore, using these constants equations A.9 and A.10 are rewritten as

$$\frac{d\theta}{d\gamma} = \frac{C_1 \cos(\gamma \tan \sigma) - C_3 \sin(\gamma \tan \sigma)}{C_2 - \gamma^2} \quad (\text{A.12})$$

$$\frac{d\phi}{d\gamma} = \frac{C_1 \cos(\gamma \tan \sigma) + C_3 \sin(\gamma \tan \sigma)}{C_2 - \gamma^2} \quad (\text{A.13})$$

The equations A.12 and A.13 are now only functions of γ and the constant bank angle σ , but are not directly integrable. A very good approximation of the integral can be obtained if $\sin(\gamma \tan \sigma)$ and $\cos(\gamma \tan \sigma)$ are expanded as the following high order polynomials

$$\cos(\gamma \tan \sigma) = 1 - \frac{(\gamma \tan \sigma)^2}{2!} + \frac{(\gamma \tan \sigma)^4}{4!} - \frac{(\gamma \tan \sigma)^6}{6!} \quad (\text{A.14})$$

$$\sin(\gamma \tan \sigma) = \gamma \tan \sigma - \frac{(\gamma \tan \sigma)^3}{3!} + \frac{(\gamma \tan \sigma)^5}{5!} - \frac{(\gamma \tan \sigma)^7}{7!} \quad (\text{A.15})$$

Substituting equations A.14 and A.15 into the differential equations A.12 and A.13, the terms

on the right hand sides of equations A.12 and A.13 can be rewritten as

$$\frac{C_1 \cos(\gamma \tan \sigma)}{C_2 - \gamma^2} = \frac{C_1 \left[720 - 360(\gamma \tan \sigma)^2 + 30(\gamma \tan \sigma)^4 - (\gamma \tan \sigma)^6 \right]}{720(C_2 - \gamma^2)} \quad (\text{A.16})$$

$$\frac{C_3 \sin(\gamma \tan \sigma)}{C_2 - \gamma^2} = \frac{C_3 \left[5040 \gamma \tan \sigma - 840(\gamma \tan \sigma)^3 + 420(\gamma \tan \sigma)^5 - (\gamma \tan \sigma)^7 \right]}{5040(C_2 - \gamma^2)} \quad (\text{A.17})$$

by performing long division on the right hand side terms of A.16 and A.17, the equations can be rewritten as

$$\frac{C_1 \cos(\gamma \tan \sigma)}{C_2 - \gamma^2} = \quad (\text{A.18})$$

$$\frac{C_1}{720} \left[\gamma^4 \tan^6 \sigma - (30 \tan^4 \sigma - C_2 \tan^6 \sigma) \gamma^2 - (30 C_2 \tan^4 \sigma - C_2^2 \tan^6 \sigma - 360 \tan^2 \sigma) \right] +$$

$$\frac{C_1}{720} \left[\frac{720 - 360 C_2 \tan^2 \sigma + 30 C_2^2 \tan^4 \sigma - C_2^3 \tan^6 \sigma}{C_2 - \gamma^2} \right]$$

$$\frac{C_3 \sin(\gamma \tan \sigma)}{C_2 - \gamma^2} = \quad (\text{A.19})$$

$$\frac{C_3}{5040} \left[\gamma^5 \tan^7 \sigma - (42 \tan^5 \sigma - C_2 \tan^7 \sigma) \gamma^3 - (42 C_2 \tan^5 \sigma - C_2^2 \tan^7 \sigma - 840 \tan^3 \sigma) \right] +$$

$$\frac{C_3}{5040} \left[\frac{5040 \tan \sigma - 840 C_2 \tan^3 \sigma + 42 C_2^2 \tan^5 \sigma - C_2^3 \tan^7 \sigma}{C_2 - \gamma^2} \right]$$

performing the integration of equations A.18 and A.19 for use in equation A.12 and A.13 gives

$$\int \left[\frac{C_1 \cos(\gamma \tan \sigma)}{(C_2 - \gamma^2)} d\gamma \right] = \quad (\text{A.20})$$

$$\frac{C_1}{720} \left[(\tan^6 \sigma) \frac{\gamma^5}{5} - (30 \tan^4 \sigma - C_2 \tan^6 \sigma) \frac{\gamma^3}{3} - (30 C_2 \tan^4 \sigma - C_2^2 \tan^6 \sigma - 360 \tan^2 \sigma) \gamma \right]_{\gamma_e}^{\gamma}$$

$$+ \frac{C_1}{720} \left[\frac{720 - 360 C_2 \tan^2 \sigma + 30 C_2^2 \tan^4 \sigma - C_2^3 \tan^6 \sigma}{2 \sqrt{C_2}} \ln \left[\frac{\sqrt{C_2} + \gamma}{\sqrt{C_2} - \gamma} \right] \right]_{\gamma_e}^{\gamma}$$

$$\int \left[\frac{C_3 \sin(\gamma \tan \sigma)}{(C_2 - \gamma^2)} \right] = \quad (A.21)$$

$$\frac{C_3}{5040} \left[(\tan^7 \sigma) \frac{\gamma^6}{6} - (42 \tan^5 \sigma - C_2 \tan^7 \sigma) \frac{\gamma^4}{4} - (42 C_2 \tan^5 \sigma - C_2^2 \tan^7 \sigma - 840 \tan^3 \sigma) \frac{\gamma^2}{2} \right]_{\gamma_e}^{\gamma}$$

$$- \frac{C_3}{5040} \left[\frac{5040 \tan \sigma - 840 C_2 \tan^3 \sigma + 42 C_2^2 \tan^5 \sigma - C_2^3 \tan^7 \sigma}{2} \ln(C_2 - \gamma^2) \right]_{\gamma_e}^{\gamma}$$

Combining equations A.20 and A.21 to form the solution for the latitude and longitude gives

$$\phi - \phi_e = \quad (A.22)$$

$$\frac{C_1}{720} \left[(\tan^6 \sigma) \frac{\gamma^5}{5} - (30 \tan^4 \sigma - C_2 \tan^6 \sigma) \frac{\gamma^3}{3} - (30 C_2 \tan^4 \sigma - C_2^2 \tan^6 \sigma - 360 \tan^2 \sigma) \gamma \right]_{\gamma_e}^{\gamma}$$

$$+ \frac{C_1}{720} \left[\frac{720 - 360 C_2 \tan^2 \sigma + 30 C_2^2 \tan^4 \sigma - C_2^3 \tan^6 \sigma}{2 \sqrt{C_2}} \ln \left[\frac{\sqrt{C_2} + \gamma}{\sqrt{C_2} - \gamma} \right] \right]_{\gamma_e}^{\gamma} +$$

$$\frac{C_3}{5040} \left[(\tan^7 \sigma) \frac{\gamma^6}{6} - (42 \tan^5 \sigma - C_2 \tan^7 \sigma) \frac{\gamma^4}{4} - (42 C_2 \tan^5 \sigma - C_2^2 \tan^7 \sigma - 840 \tan^3 \sigma) \frac{\gamma^2}{2} \right]_{\gamma_e}^{\gamma}$$

$$- \frac{C_3}{5040} \left[\frac{5040 \tan \sigma - 840 C_2 \tan^3 \sigma + 42 C_2^2 \tan^5 \sigma - C_2^3 \tan^7 \sigma}{2} \ln(C_2 - \gamma^2) \right]_{\gamma_e}^{\gamma}$$

$$\theta - \theta_e = \quad (A.23)$$

$$\begin{aligned} & \frac{C_1}{720} \left[(\tan^6 \sigma) \frac{\gamma^5}{5} - (30 \tan^4 \sigma - C_2 \tan^6 \sigma) \frac{\gamma^3}{3} - (30 C_2 \tan^4 \sigma - C_2^2 \tan^6 \sigma - 360 \tan^2 \sigma) \gamma \right]_{\gamma_e}^{\gamma} \\ & + \frac{C_1}{720} \left[\frac{720 - 360 C_2 \tan^2 \sigma + 30 C_2^2 \tan^4 \sigma - C_2^3 \tan^6 \sigma}{2 \sqrt{C_2}} \ln \left[\frac{\sqrt{C_2} + \gamma}{\sqrt{C_2} - \gamma} \right] \right]_{\gamma_e}^{\gamma} - \\ & \frac{C_3}{5040} \left[(\tan^7 \sigma) \frac{\gamma^6}{6} - (42 \tan^5 \sigma - C_2 \tan^7 \sigma) \frac{\gamma^4}{4} - (42 C_2 \tan^5 \sigma - C_2^2 \tan^7 \sigma - 840 \tan^3 \sigma) \frac{\gamma^2}{2} \right]_{\gamma_e}^{\gamma} \\ & + \frac{C_3}{5040} \left[\frac{5040 \tan \sigma - 840 C_2 \tan^3 \sigma + 42 C_2^2 \tan^5 \sigma - C_2^3 \tan^7 \sigma}{2} \ln(C_2 - \gamma^2) \right]_{\gamma_e}^{\gamma} \end{aligned}$$

Equations A.22 and A.23 are the solutions to the differential equations A.9 and A.10, where the constants are defined from equations A.11.

A2.2: Time

The differential equation for the time of flight along a sub arc is given by

$$\frac{dt}{d\gamma} = \frac{k^2}{\lambda \cos \sigma \left[Z_e - \frac{k}{2 \lambda \cos \sigma} (\gamma^2 - \gamma_e^2) \right] \sqrt{\beta^3 \mu v_e \exp \left[\frac{-2(n-1 + \lambda^n)}{E^* n \lambda \cos \sigma} (\gamma - \gamma_e) \right]}} \quad (A.24)$$

The equation A.24 is now only functions of γ , the entry states and the constant bank angle σ .

Several constants are defined by grouping terms as

$$C_1 = \frac{k^2}{\lambda \cos \sigma \sqrt{\beta^3 \mu}} \quad (\text{A.25a})$$

$$C_2 = \frac{-(n-1 + \lambda^n)}{E^* n \lambda \cos \sigma} \quad (\text{A.25b})$$

$$C_3 = v_e \exp(-2C_2 \gamma_e) \quad (\text{A.25c})$$

$$C_4 = Z_e + \frac{k \gamma_e^2}{2 \lambda \cos \sigma} \quad (\text{A.25d})$$

$$C_5 = \frac{k}{2 \lambda \cos \sigma} \quad (\text{A.25e})$$

Using the constants $C_1 - C_5$ the differential equation A.24 can be rewritten as

$$\frac{dt}{d\gamma} = \frac{C_1 \exp(-C_2 \gamma)}{\sqrt{C_3 C_5 \left[\frac{C_4}{C_5} - \gamma^2 \right]}} \quad (\text{A.26})$$

In order to put equation A.24 in a form that is integrable, two further constants are defined

$$C_6 = \frac{C_1}{\sqrt{C_3 C_5}} \quad (\text{A.27a})$$

$$C_7 = \sqrt{\frac{C_4}{C_5}} \quad (\text{A.27b})$$

Using these two constants, equation A.26 is rewritten as

$$\frac{dt}{d\gamma} = \frac{C_6 \exp(-C_2 \gamma)}{C_7^2 - \gamma^2} \quad (\text{A.28})$$

Performing the integration on equation A.28 by integration by parts,

$$t - t_o = C_6 \left[\frac{\exp(-C_2 \gamma)}{2C_7} \ln \left[\frac{C_7 + \gamma}{C_7 - \gamma} \right] \right]_{\gamma_e}^{\gamma} + \frac{C_2}{2C_7} \int_{\gamma_e}^{\gamma} \exp(-C_2 \gamma) \ln \left[\frac{C_7 + \gamma}{C_7 - \gamma} \right] d\gamma$$

$$t - t_o = \tag{A.29}$$

$$\frac{C_6 \exp(-C_2 \gamma)}{2C_7} \ln \left[\frac{C_7 + \gamma}{C_7 - \gamma} \right]_{\gamma_e}^{\gamma} + \frac{C_6 C_2 \exp(C_2 C_7)}{2C_7} \int_{\gamma_e}^{\gamma} \exp(-C_2(C_7 + \gamma)) \ln(C_7 + \gamma) d\gamma -$$

$$\frac{C_6 C_2 \exp(-C_2 C_7)}{2C_7} \int_{\gamma_e}^{\gamma} \exp(C_2(C_7 - \gamma)) \ln(C_7 - \gamma) d\gamma$$

The integrals in equation A.29 are of the following form

$$\int \exp(ax) \ln(x) dx = \frac{\exp(ax) \ln(x)}{a} - \frac{1}{a} \int \frac{\exp(ax)}{x} dx$$

where the integral on the right hand side is a series expansion. By using the series expansion to higher order terms, a close approximation of equation A.29 can be obtained. The series expansion for the right hand side integral is as follows

$$\int \frac{\exp(ax)}{x} dx = \ln(x) + \frac{ax}{1!} + \frac{(ax)^2}{2 \cdot 2!} + \frac{(ax)^3}{3 \cdot 3!} + \frac{(ax)^4}{4 \cdot 4!} + \frac{(ax)^5}{5 \cdot 5!} + \frac{(ax)^6}{6 \cdot 6!} + \frac{(ax)^7}{7 \cdot 7!}$$

Using the above series expansion and defing new variables from equations A.24 as

$$x_1 = C_7 + \gamma \tag{A.30a}$$

$$x_2 = C_7 - \gamma \tag{A.30b}$$

$$a_1 = -C_2 \tag{A.30c}$$

$$a_2 = C_2 \tag{A.30d}$$

the equation for flight time along a sub arc is given by

$$t - t_o = \frac{C_6 \exp(-C_2 \gamma)}{2C_7} \ln \left[\frac{C_7 + \gamma}{C_7 - \gamma} \right]_{\gamma_e}^{\gamma} + \quad (\text{A.31})$$

$$\frac{C_6 C_2 \exp(C_2 C_7)}{2C_7} \left[\frac{\exp(a_1 x_1) \ln(x_1)}{a_1} - \frac{1}{a_1} \left[\ln(x_1) + \frac{a_1 x_1}{1!} + \frac{(a_1 x_1)^2}{2 \cdot 2!} + \dots + \frac{(a_1 x_1)^7}{7 \cdot 7!} \right] \right]_{\gamma_e}^{\gamma} +$$

$$\frac{C_6 C_2 \exp(-C_2 C_7)}{2C_7} \left[\frac{\exp(a_2 x_2) \ln(x_2)}{a_2} - \frac{1}{a_2} \left[\ln(x_2) + \frac{a_2 x_2}{1!} + \frac{(a_2 x_2)^2}{2 \cdot 2!} + \dots + \frac{(a_2 x_2)^7}{7 \cdot 7!} \right] \right]_{\gamma_e}^{\gamma}$$

where the constants are defined in equations A.25, A.27 and equations A.30.

References

1. Bate, R. R., Mueller, D. D., and White, J. E., *Fundamentals of Astrodynamics*, Dover Publications, New York, 1971.
2. Battin, R. H., *An Introduction to the Mathematics and Methods of Astrodynamics*, AIAA Education Series, New York, 1987.
3. Chapman, D. R., "An Approximate Analytical Method for Studying Entry into Planetary Atmospheres", NASA TR R-11, 1959, pp 3-5.
4. Hull, D. G., Giltner, J. M., Speyer, J. L., and Mapar, J., "Minimum Energy-Loss Guidance for Aeroassisted Orbital Plane Change", *Journal of Guidance, Control and Dynamics*, Vol. 8, No. 4, July-August 1985, pp 487-493.
5. Hull, D. G., and Speyer, J. L., "Optimal Reentry and Plane Change Trajectories", *Journal of the Astronautical Sciences*, Vol. 30, No. 2, April-June 1982, pp 117-130.
6. Hull, D. G., McClendon, J. R., and Speyer, J. L., "Aeroassisted Orbital Plane Change Using an Elliptic Drag Polar", *Journal of the Astronautical Sciences*, Vol. 36, Nos. 1/2, January-June 1988, pp 73-87.
7. London, H. S., "Change of Satellite Orbit Plane by Aerodynamic Maneuvering", *Journal of the Aerospace Sciences*, Vol. 29, 1962, pp 323-332.
8. Lutze, F. H., Cliff, E. M., and Kelley, H. J. "Orbital-Maneuver-Sequence Optimization", AFRPL-TR-85-090, December 1985.
9. Marec, J. P., *Optimal Space Trajectories*, Elsevier Scientific, New York, 1979.

10. Mease, K. D., Lee, J. Y, and Vinh, N. X., "Orbital Changes During Hypersonic Aerocruise", *Journal of the Astronautical Sciences*, Vol. 36, Nos. 1/2, January-June 1988, pp 103-137.
11. Mease, K. D., "Optimization of Aeroassisted Orbital Transfer: Current Status", *Journal of the Astronautical Sciences*, Vol. 36, Nos. 1/2, January-June 1988, pp 7-33.
12. Mease, K. D., and Vinh, N. X., "Minimum Fuel Aeroassisted Coplanar Orbit Transfer Using Lift-Modulation", *Journal of Guidance, Control and Dynamics*, Vol. 8, No. 1, 1985, pp 134-141.
13. Miele, A., *Flight Mechanics: Volume 1 Theory of Flight Paths*, Addison-Wesely, London, 1962
14. Miele, A., Baspur, V. K., and Lee, W. Y., "Optimal Trajectories for Aeroassisted Non-Coplanar Orbital Transfer, *Acta Astronautica*, Vol. 15, No. 6/7, 1987, pp 399-411.
15. Minzer, R. A., Chapman, K. S. W., and Pond, H.L., "The ARDC Model Atmosphere, 1959", United States Air Force Cambridge Research Center, TR No. 59-267, 1959.
16. Schittkowski, K., "NLPQL: A Fortran Subroutine Solving Constrained Nonlinear Programming Problems", *Annals of Operations Research*, Vol. 5, 1986, pp 485-500.
17. Vinh, N. X., *Optimal Trajectories in Atmospheric Flight*, Elsevier Scientific, New York, 1981.
18. Vinh, N. X., Busemann, A., and Culp, R. D., *Hypersonic and Planetary Flight Mechanics*, University of Michigan Press, Ann Arbor, 1980.
19. Vinh, N. X., and Hanson, J. M., "Optimal Aeroassisted Return from High Earth Orbit with Plane Change", *Acta Astronautica*, Vol. 12, No. 1, 1985, pp 11-25.

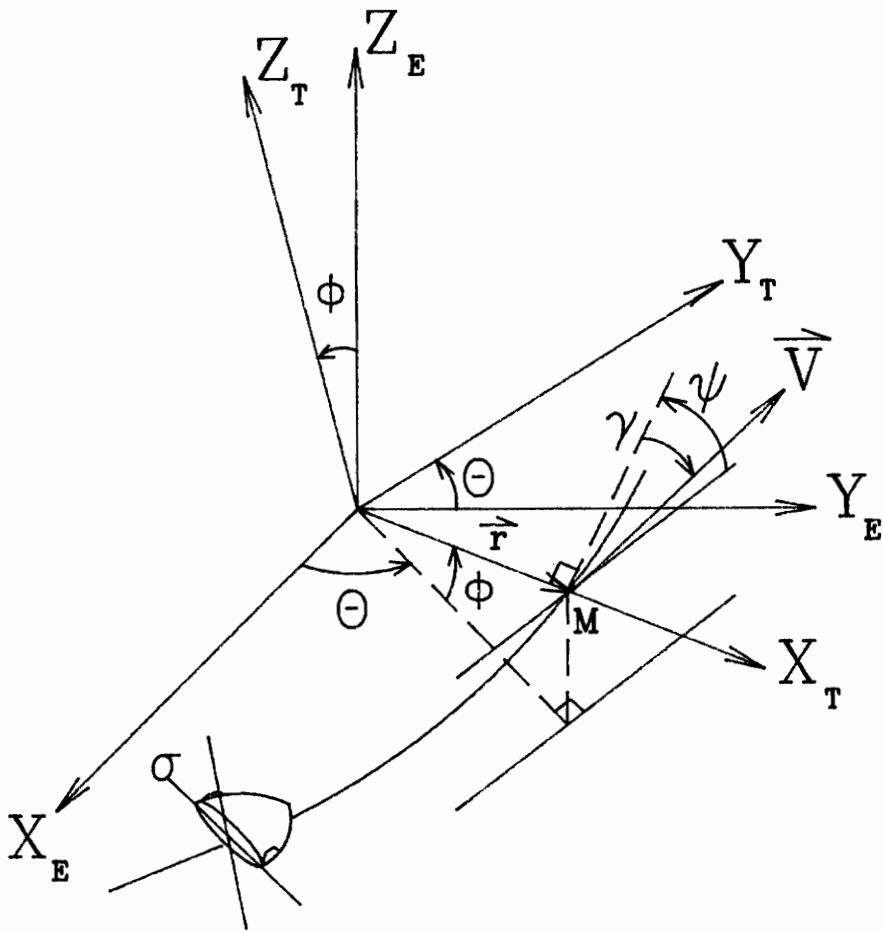


Figure 1. Earth Fixed and Tracking Coordinate Systems

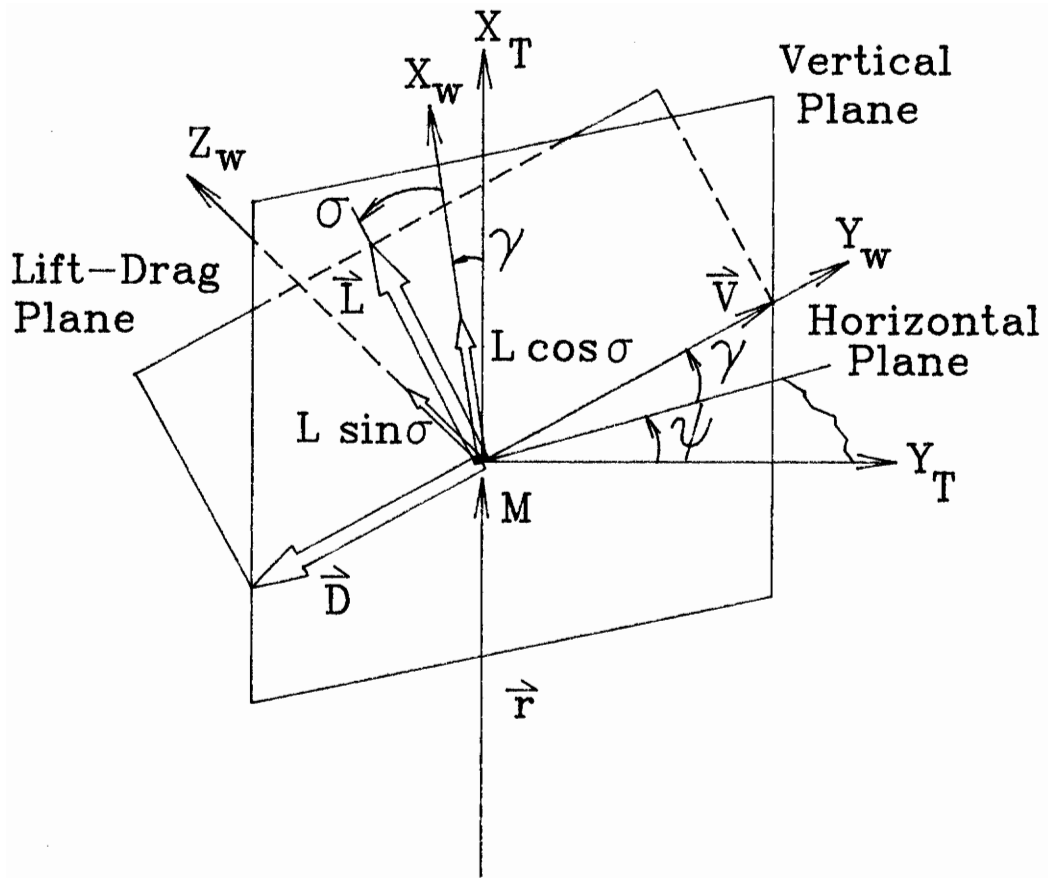


Figure 2. Wind Axes Coordinate System

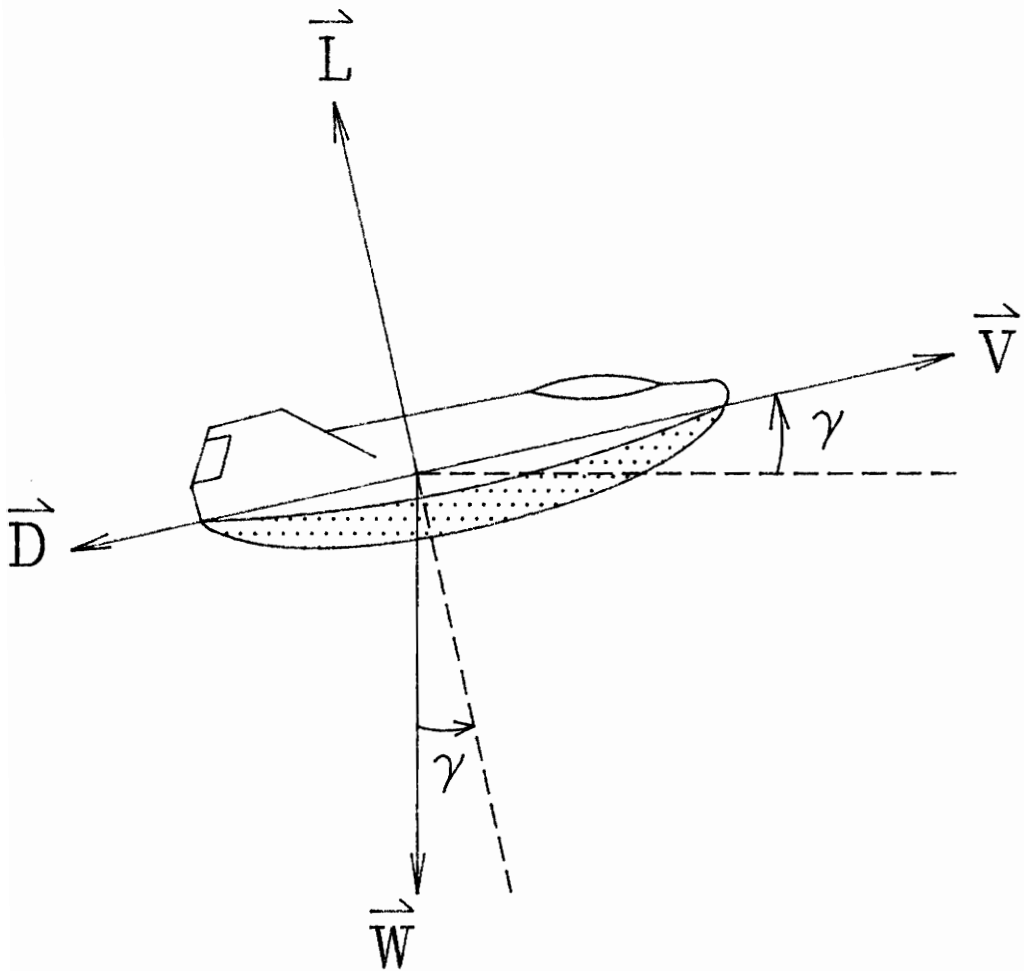


Figure 3. Lift, Drag and Gravitational Forces Acting on a Vehicle

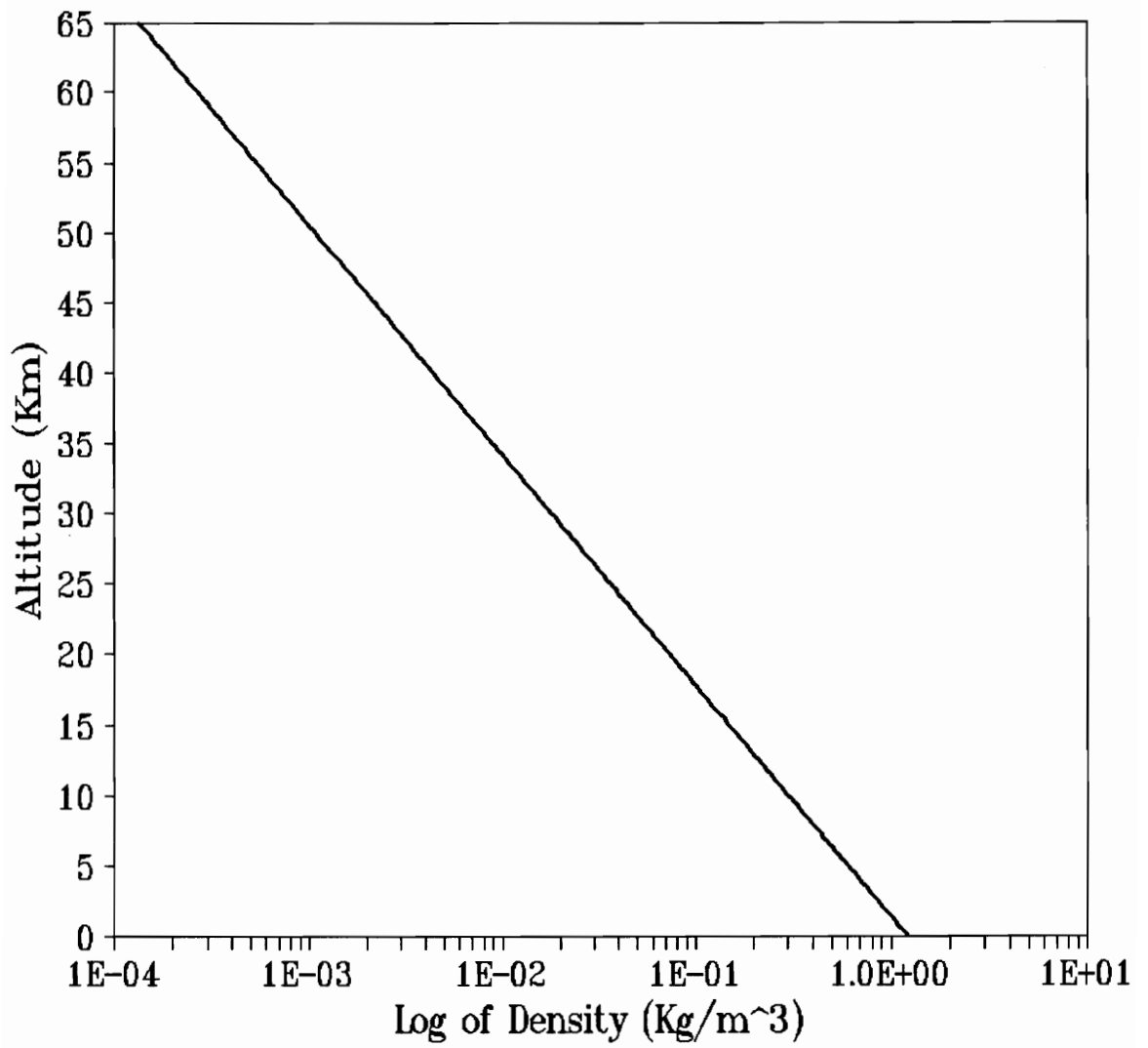


Figure 4. Altitude vs. Atmospheric Density

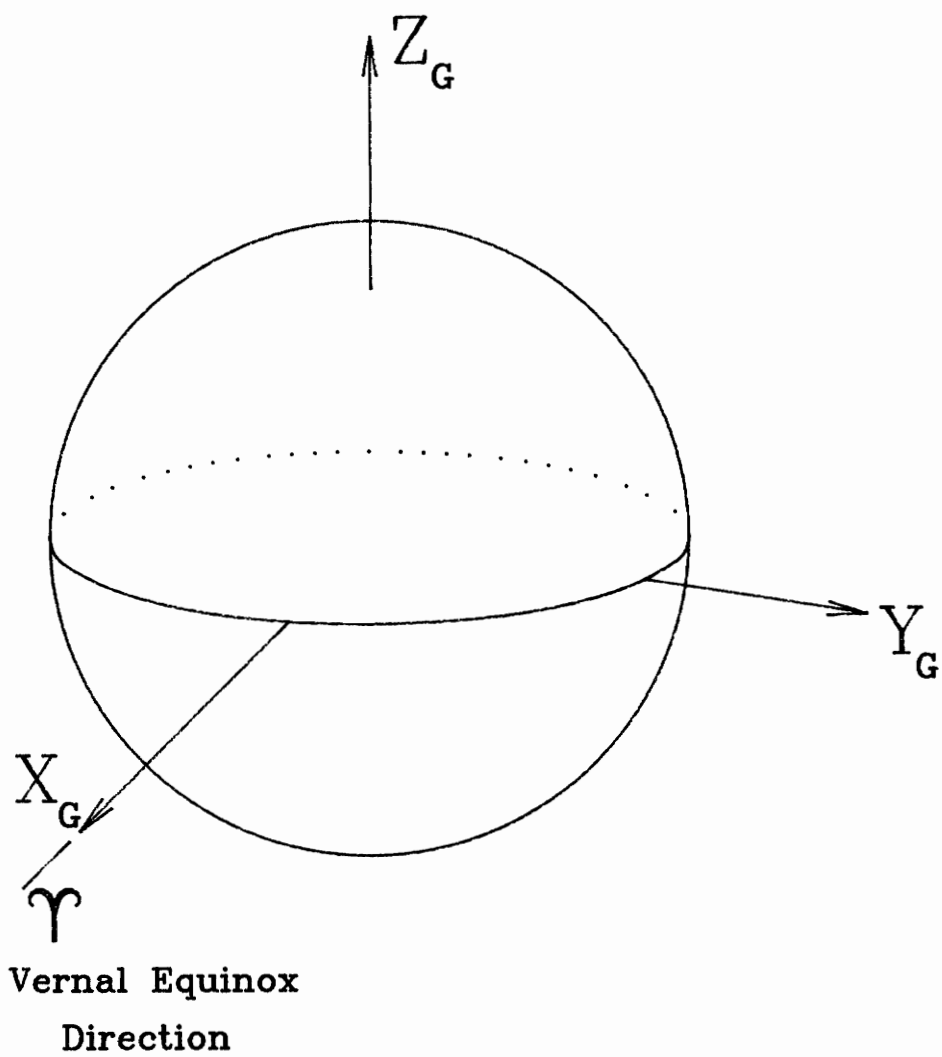


Figure 5. Geocentric-Equatorial Coordinate System

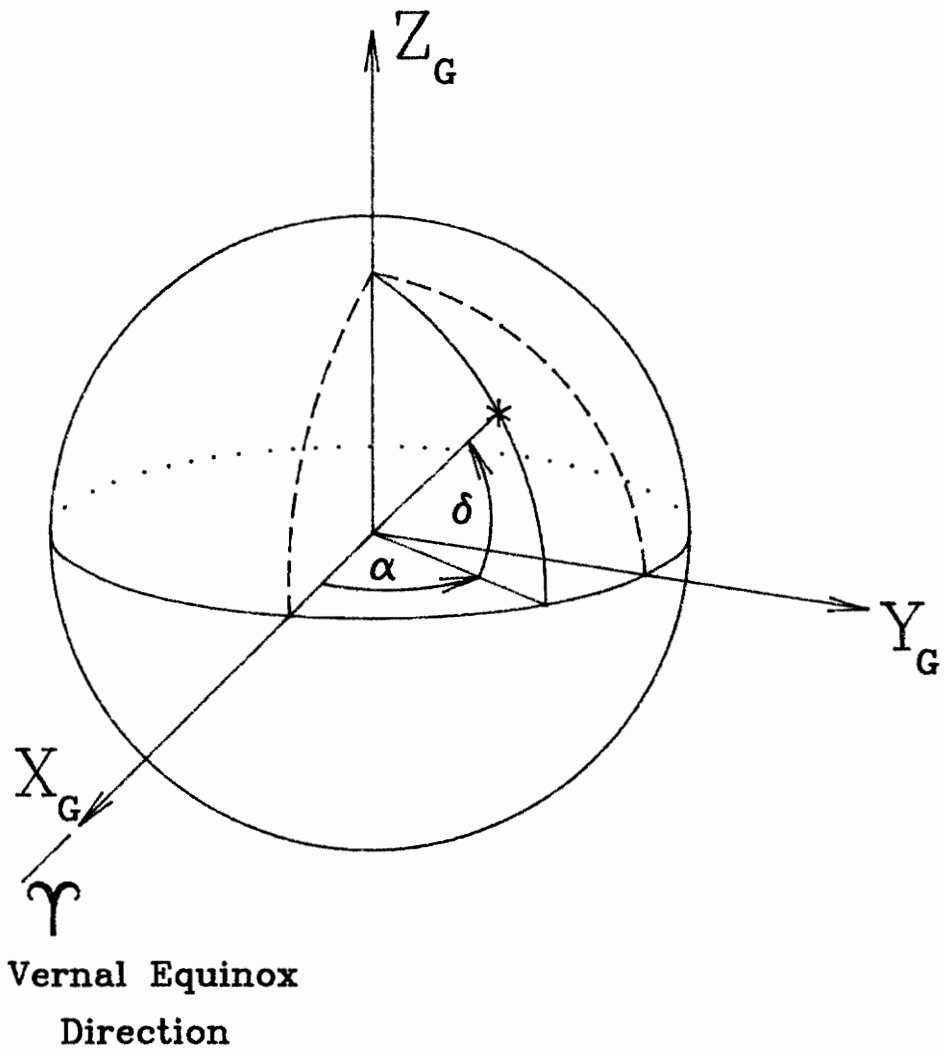


Figure 6. Right Ascension-Declination Coordinate System

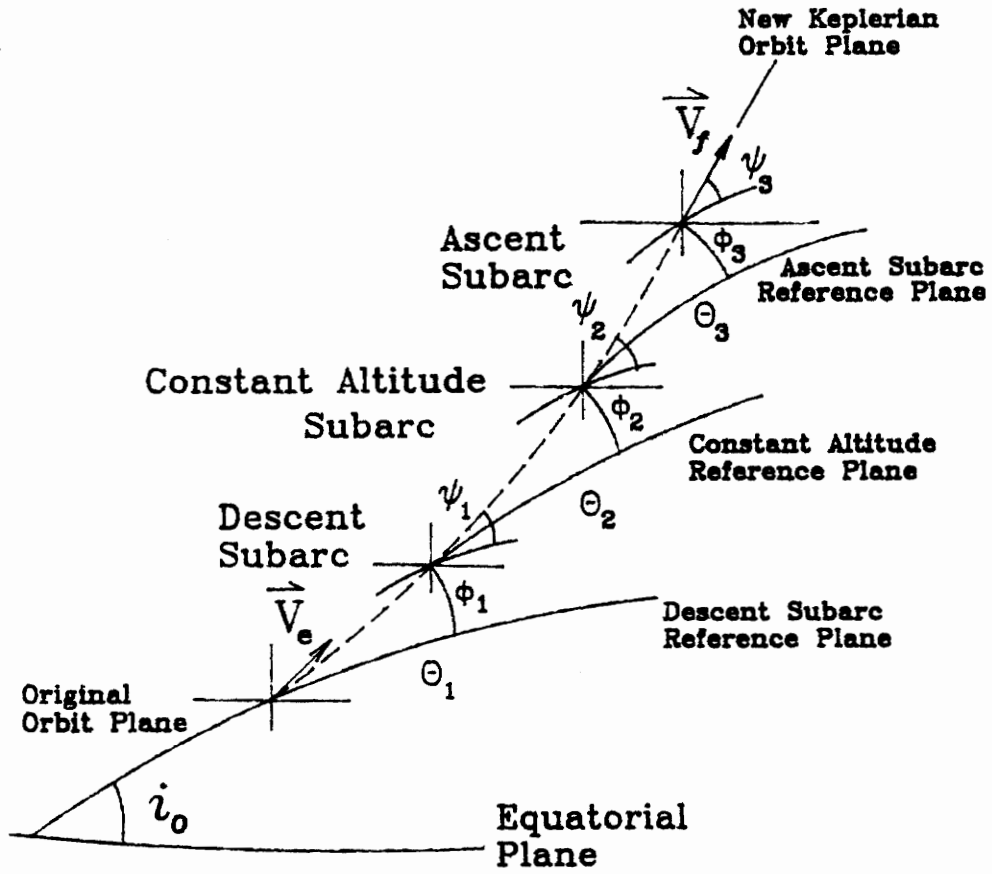


Figure 7. Definition of Reference Planes for a General Skip Trajectory

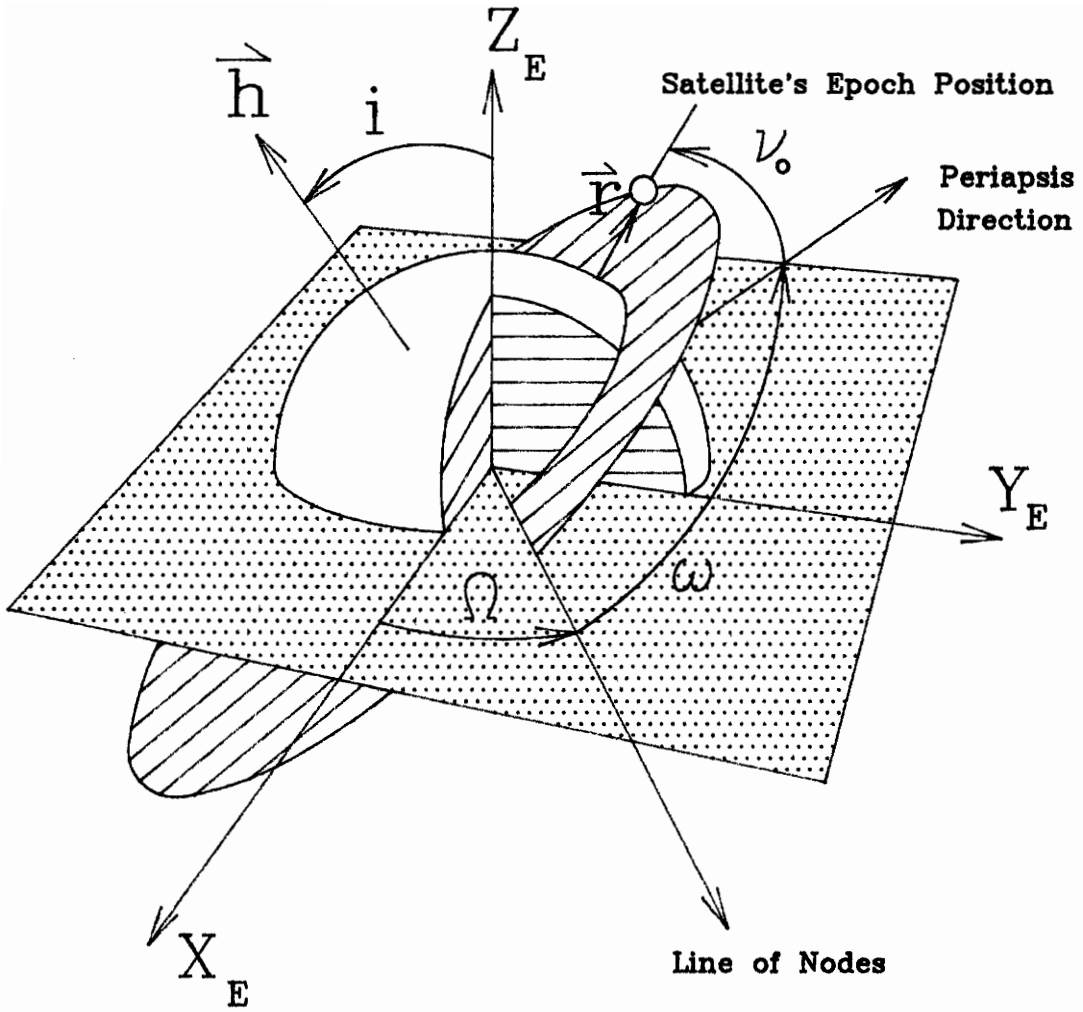


Figure 8. Orbital Elements and the Geocentric-Equatorial Coordinate System

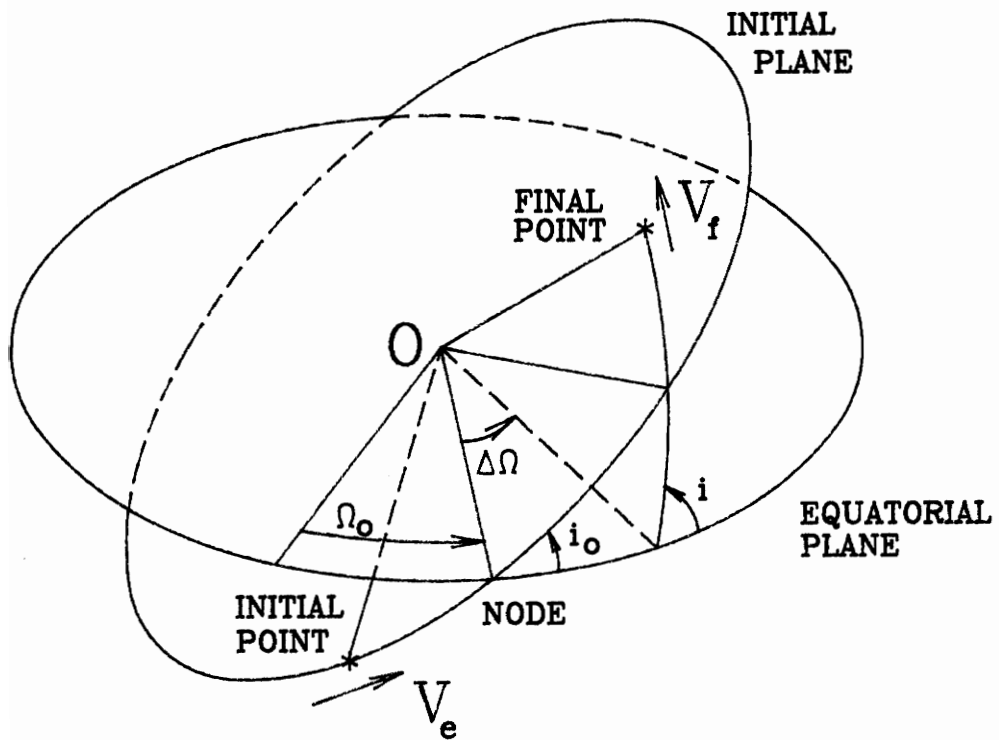


Figure 9. Inclination Change Due to an Aeroassisted Maneuver

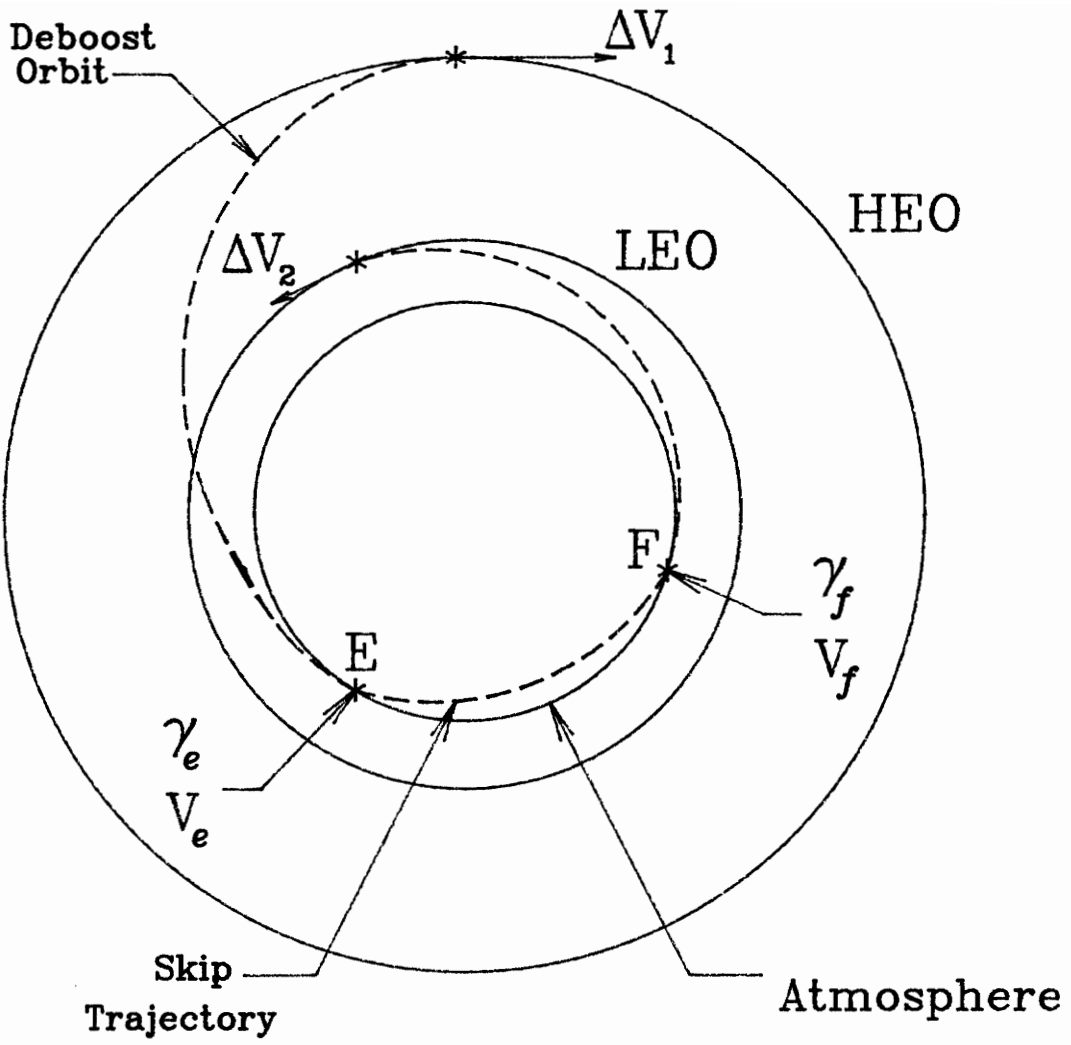


Figure 10. Orbital Path for a Two Impulse Transfer

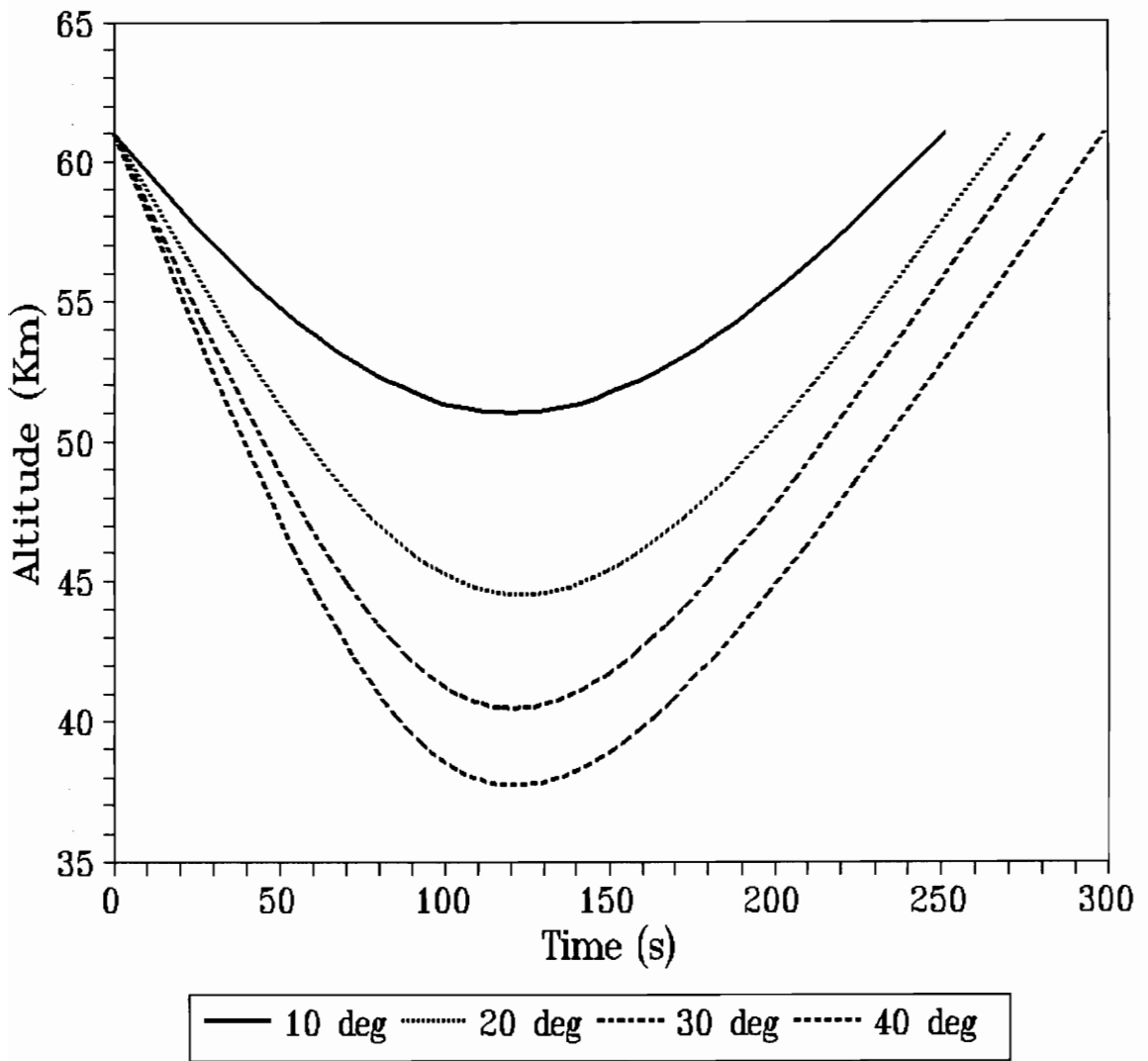


Figure 11. Altitude vs. Time for 10°, 20°, 30° and 40° Heading Change Maneuvers

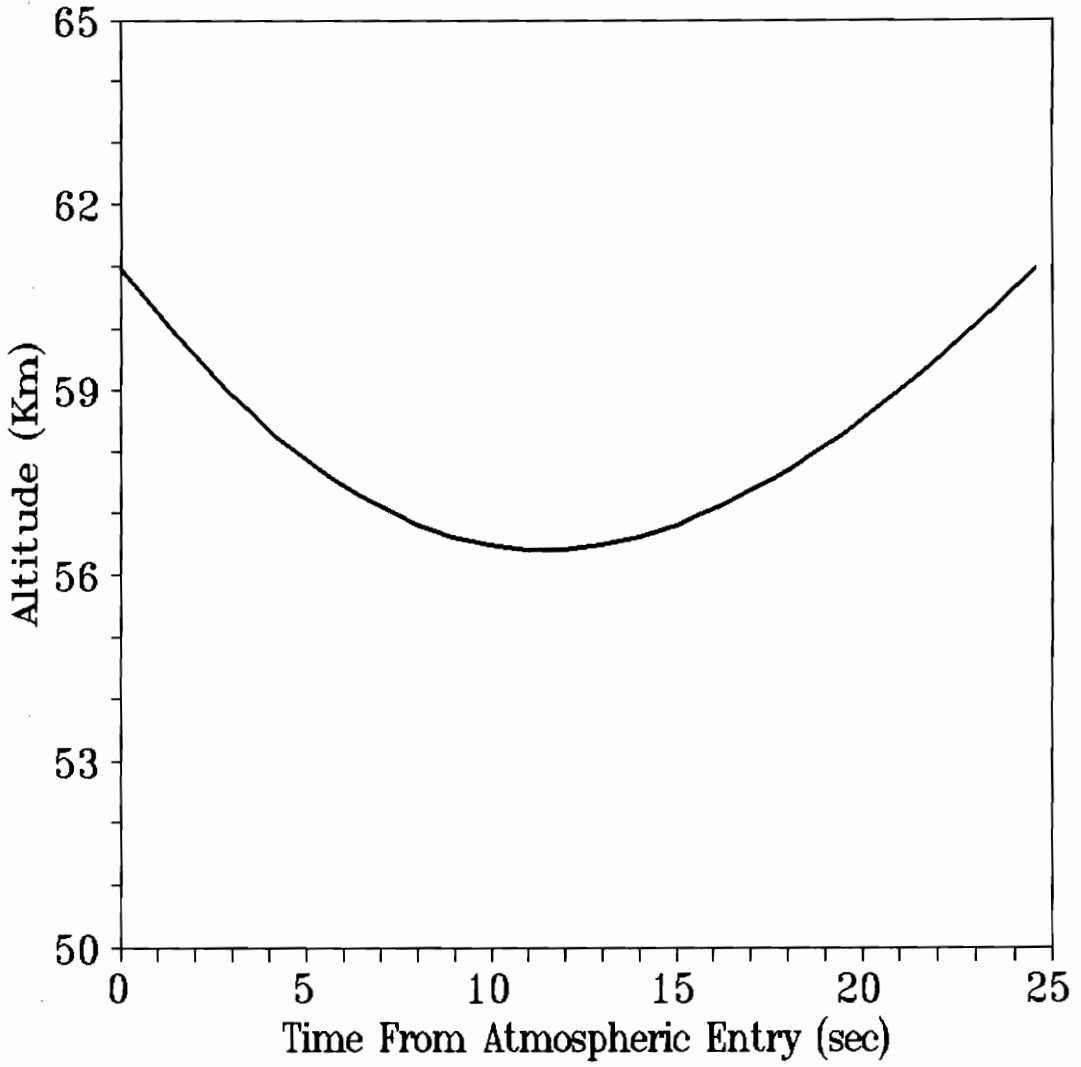


Figure 12. Altitude vs. Time for $\chi = 5.75$ (Coplanar)

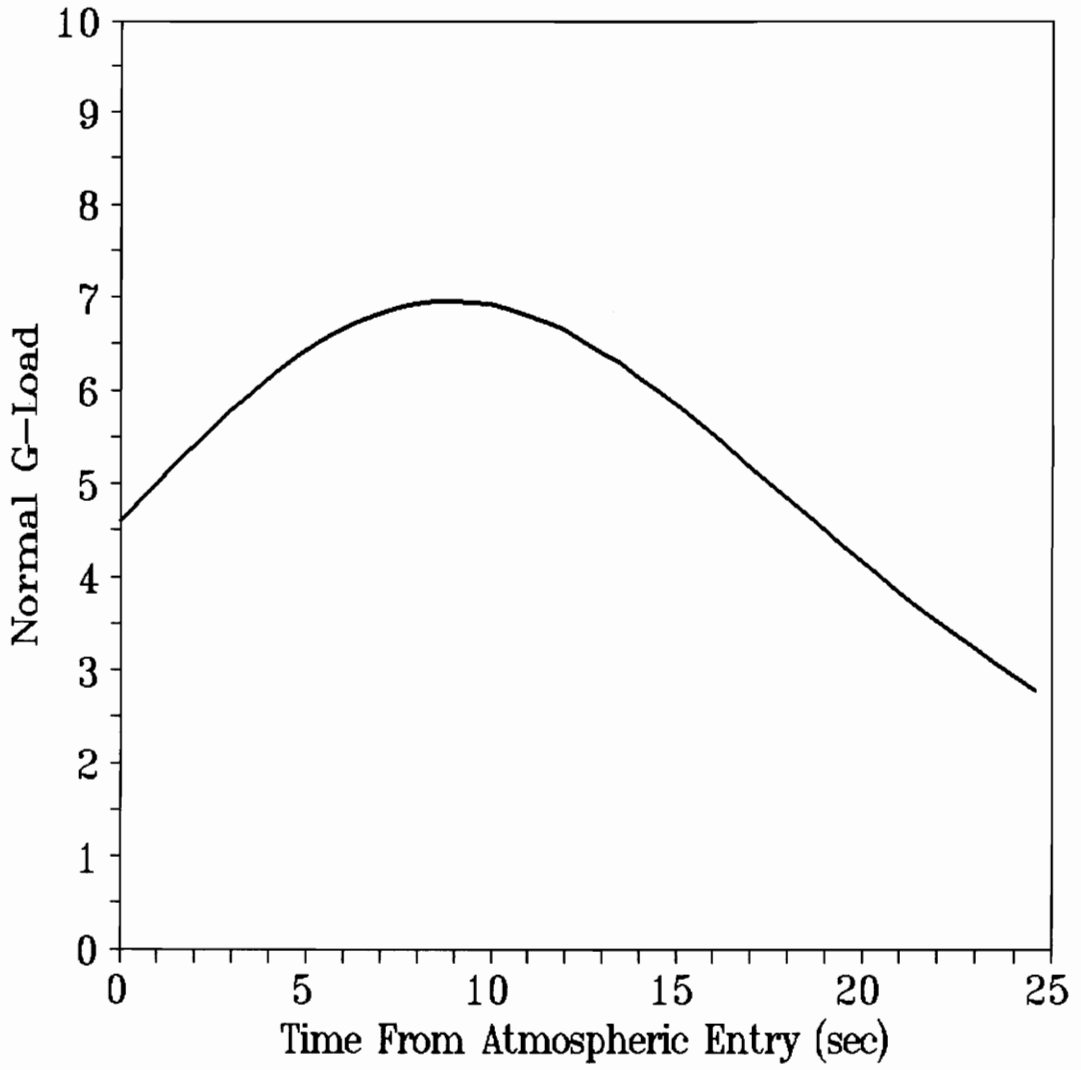


Figure 13. Normal G-Load vs. Time for $\chi = 5.75$ (Coplanar)

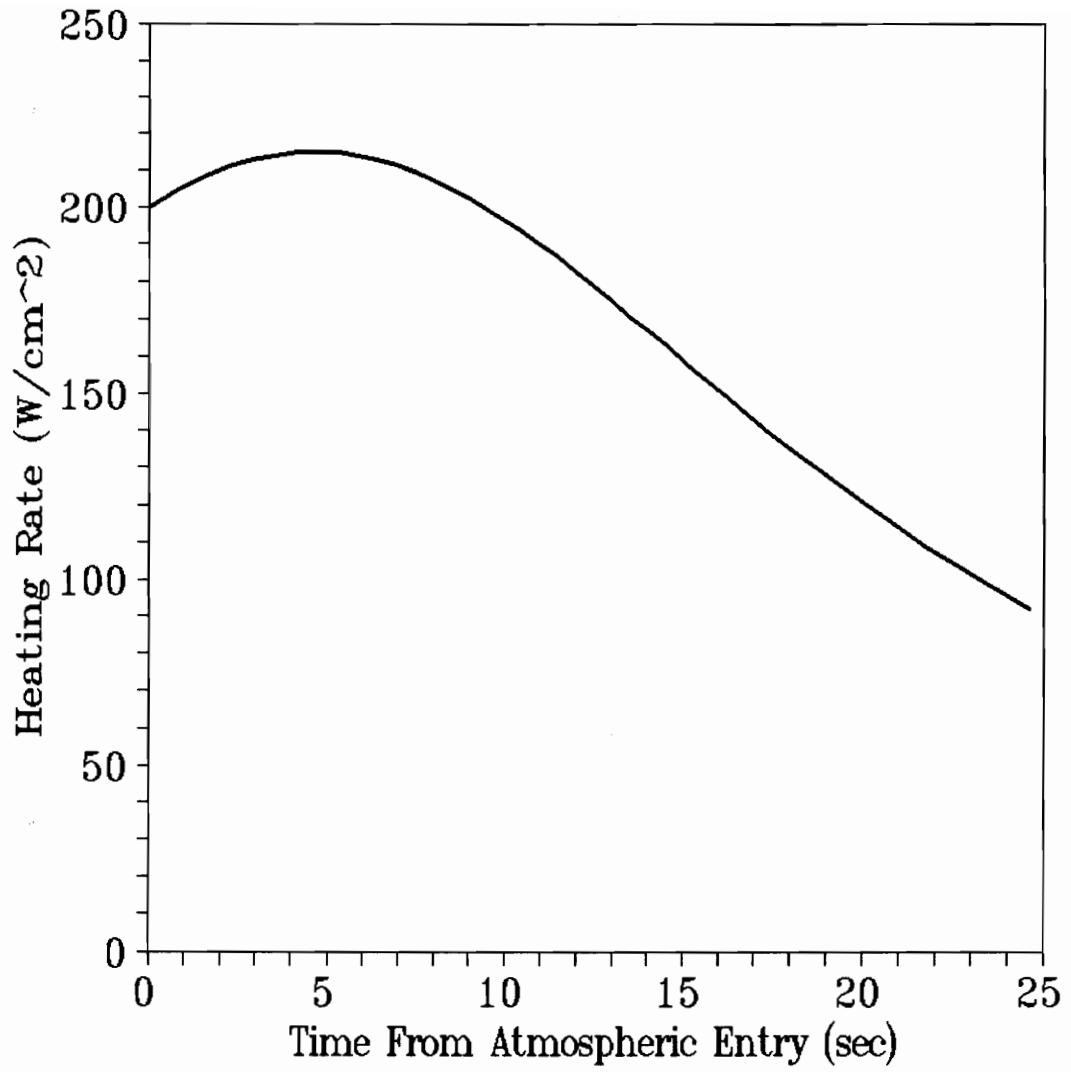


Figure 14. Convective Heating Rate vs. Time for $\chi = 5.75$ (Coplanar)

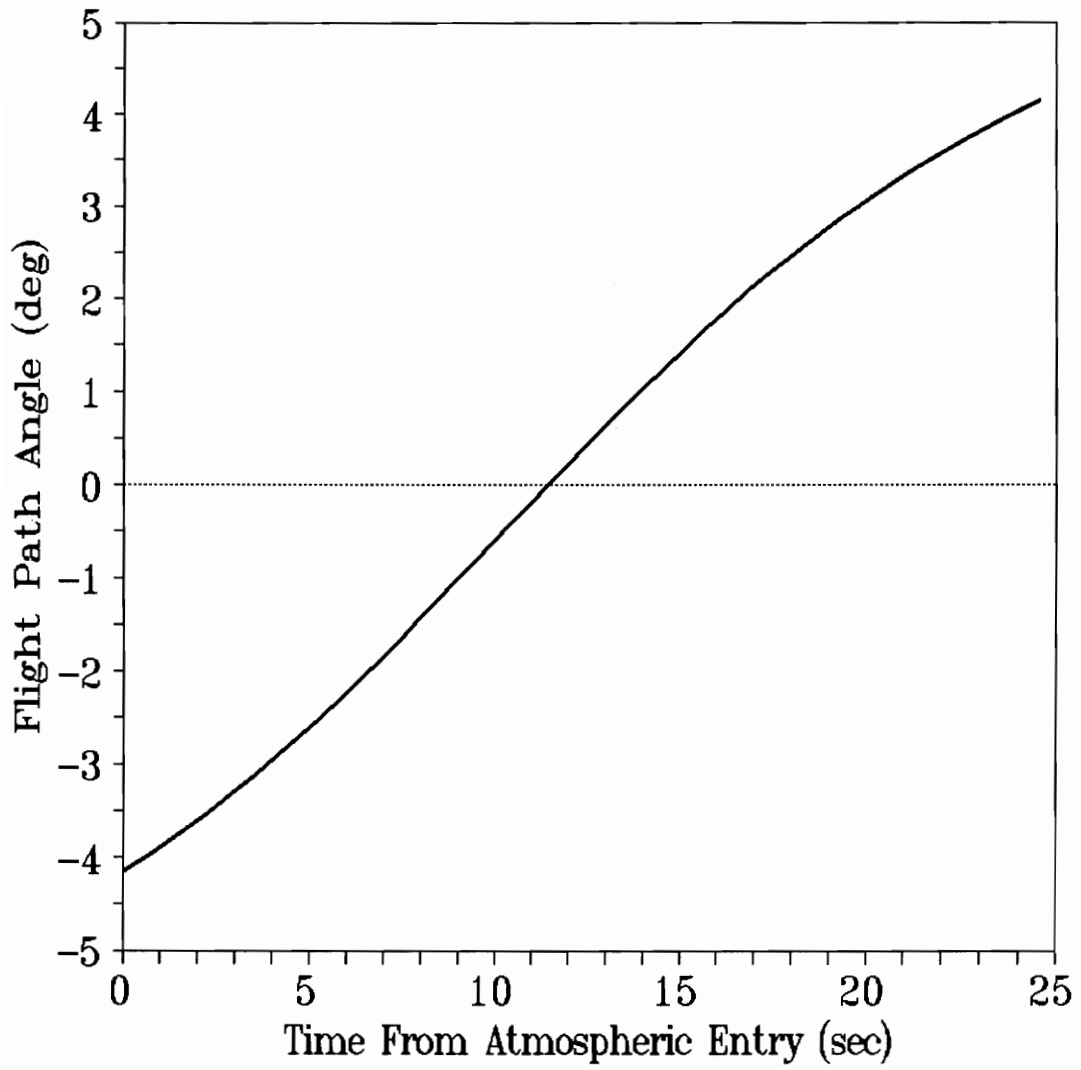


Figure 15. Flight Path Angle vs. Time for $\chi = 5.75$ (Coplanar)

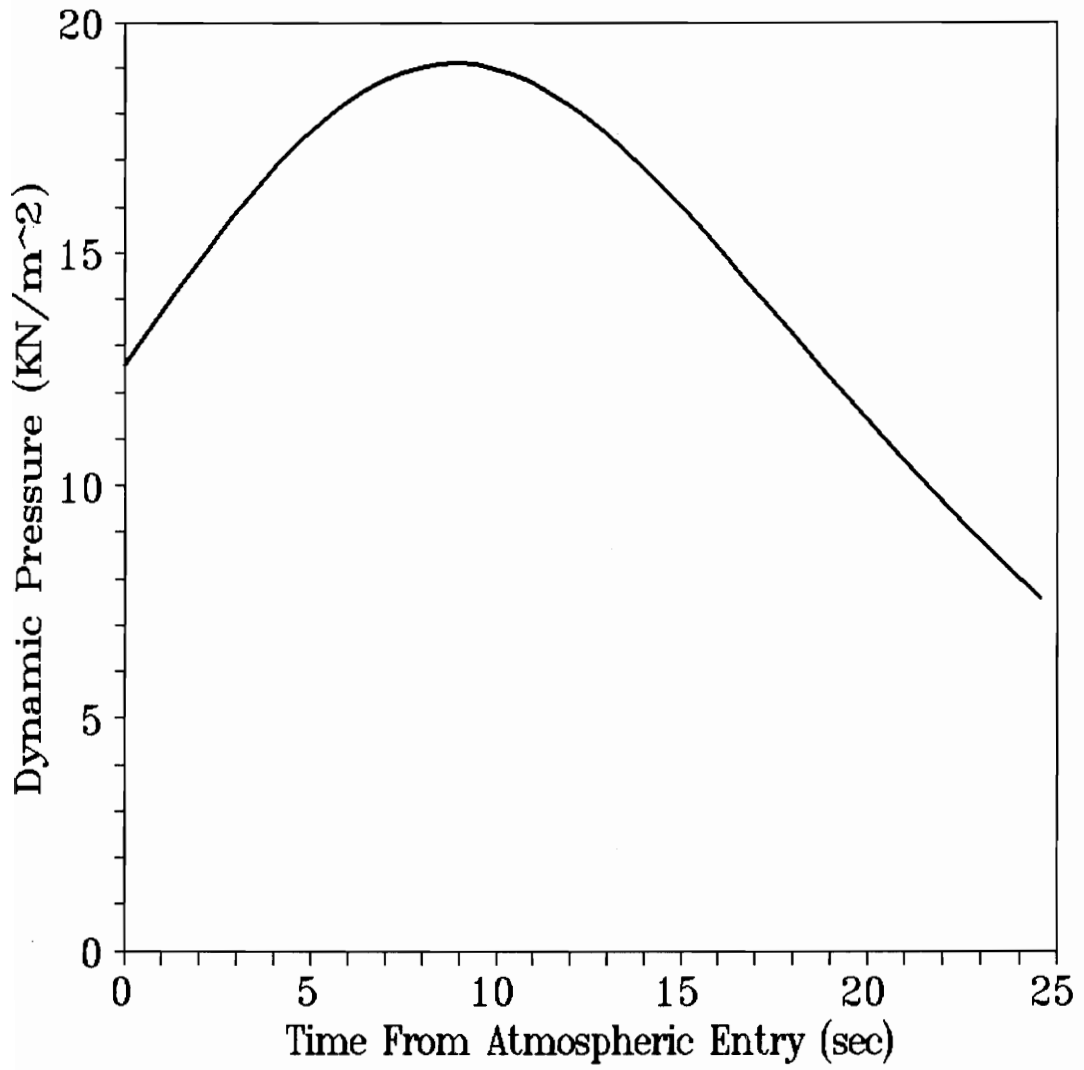


Figure 16. Dynamic Pressure vs. Time for $\chi = 5.75$ (Coplanar)

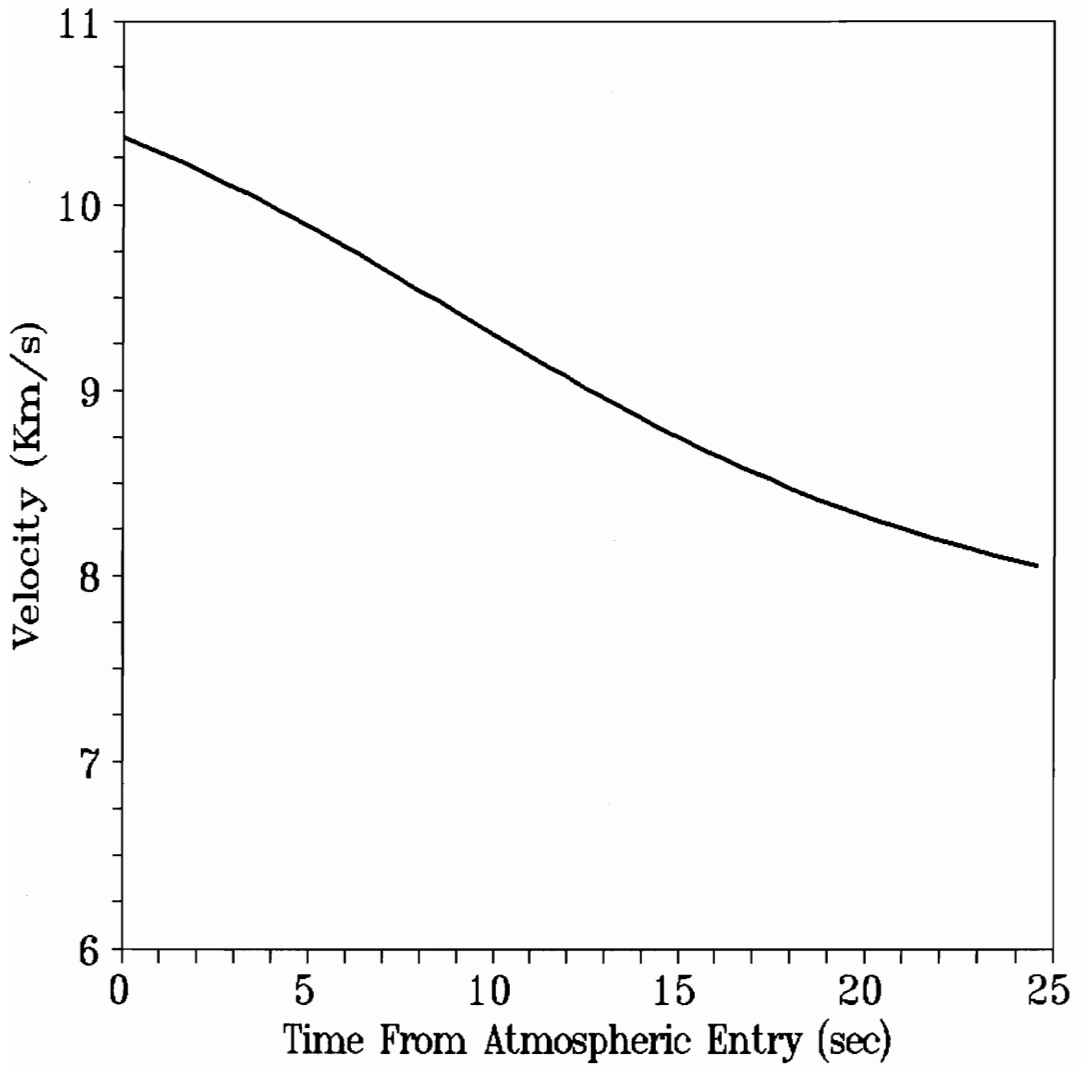


Figure 17. Velocity vs. Time for $\chi = 5.75$ (Coplanar)

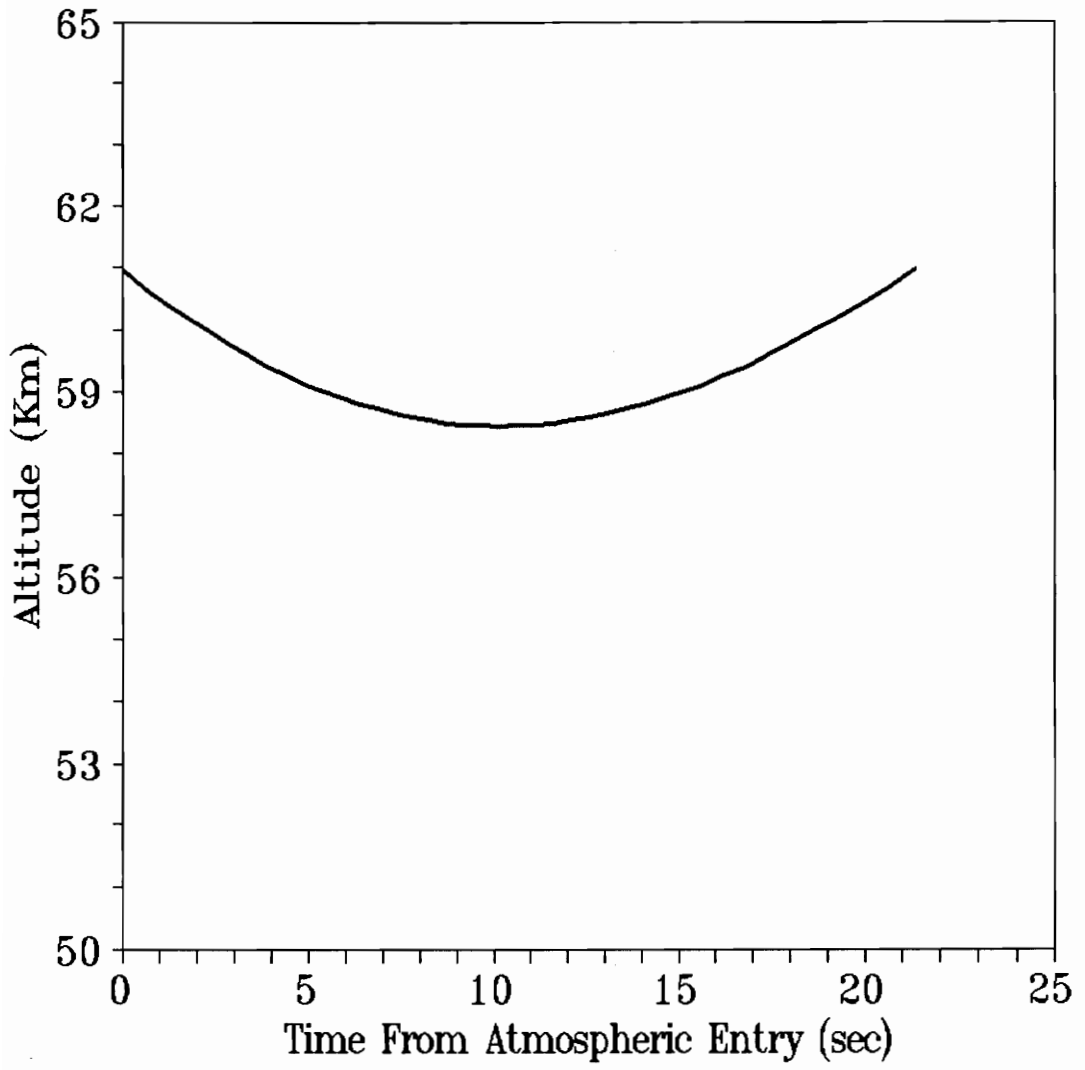


Figure 18. Altitude vs. Time for $\chi = 2.61$ (Coplanar)

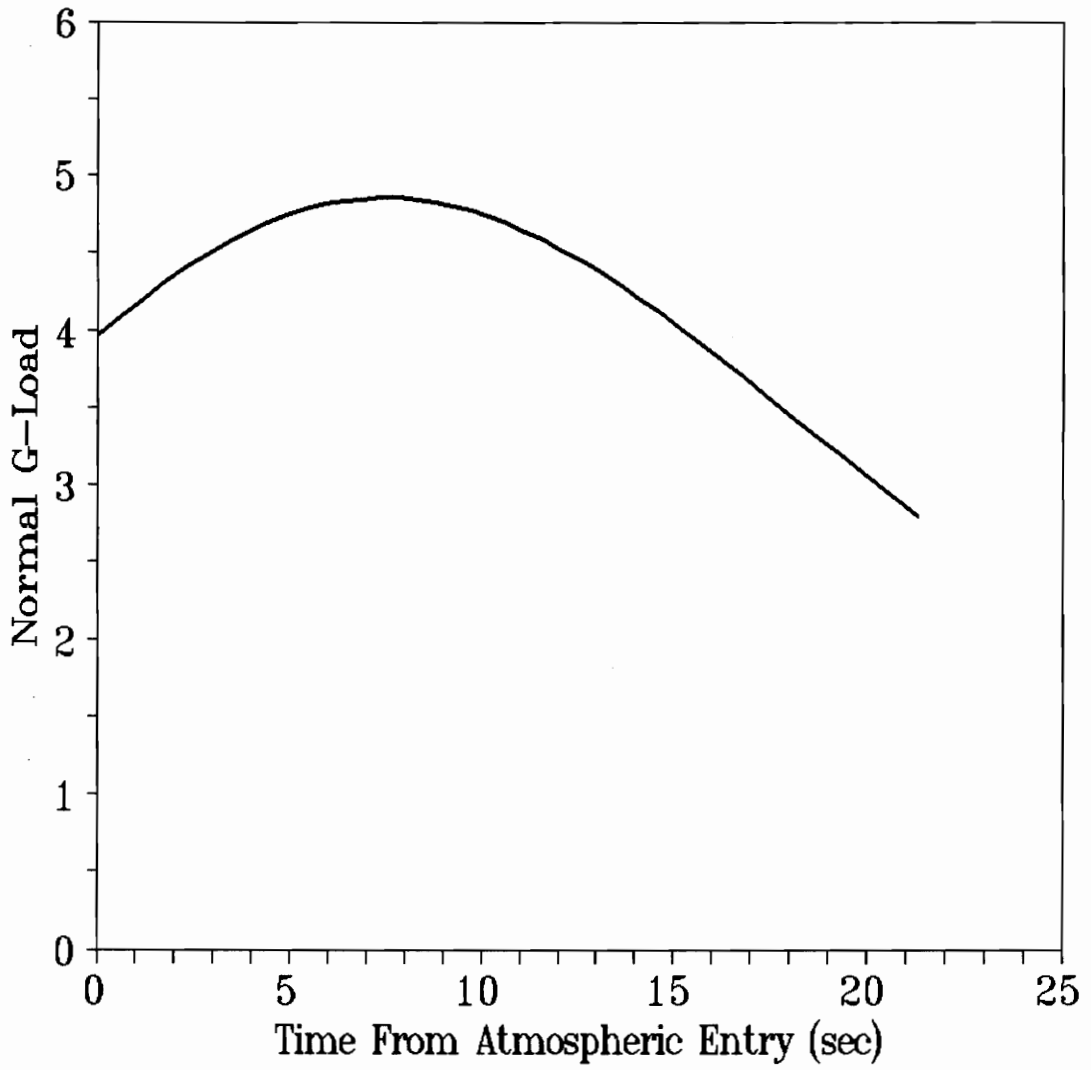


Figure 19. Normal G-Load vs. Time for $\chi = 2.61$ (Coplanar)

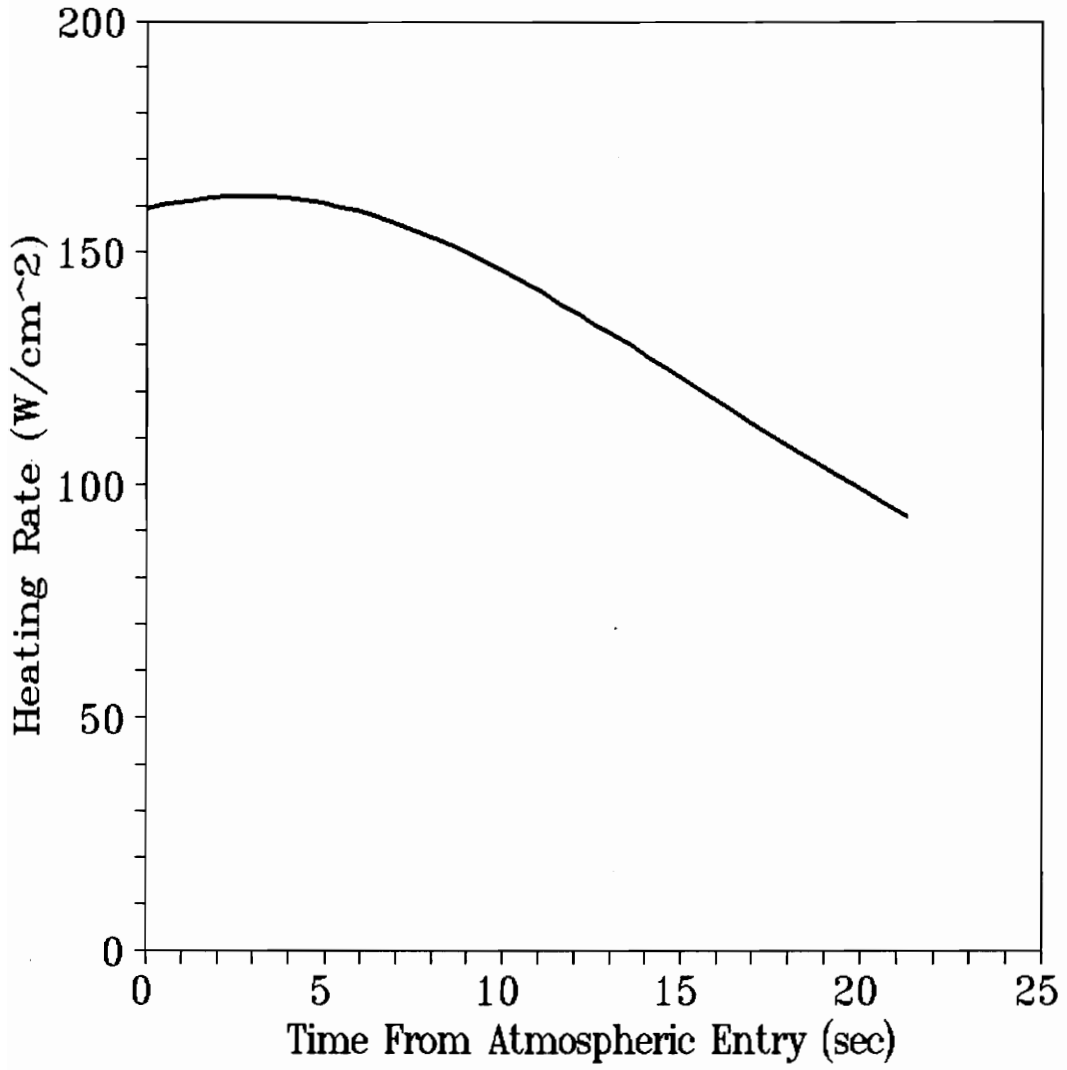


Figure 20. Convective Heating Rate vs. Time for $\chi = 2.61$ (Coplanar)

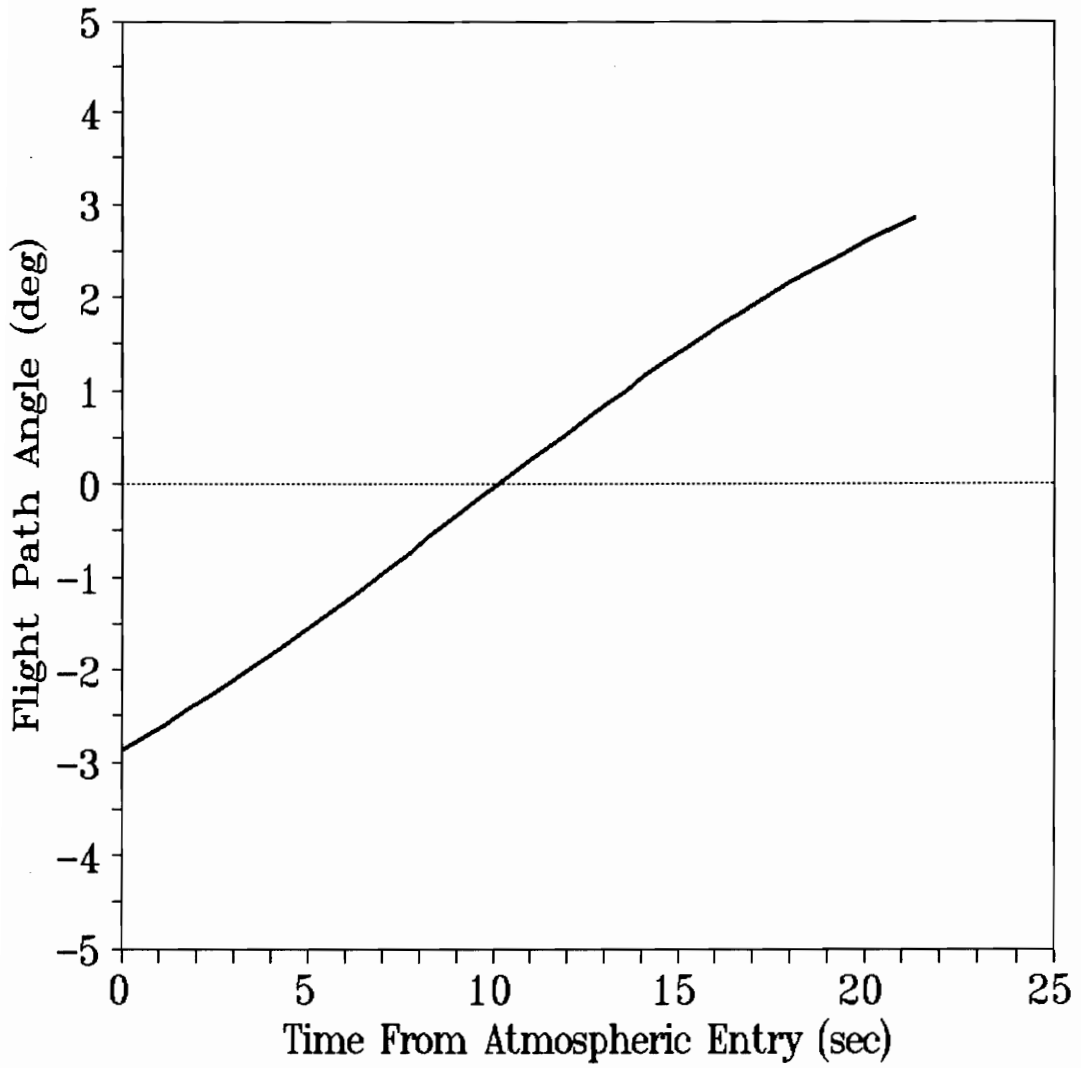


Figure 21. Flight Path Angle vs. Time for $\chi = 2.61$ (Coplanar)

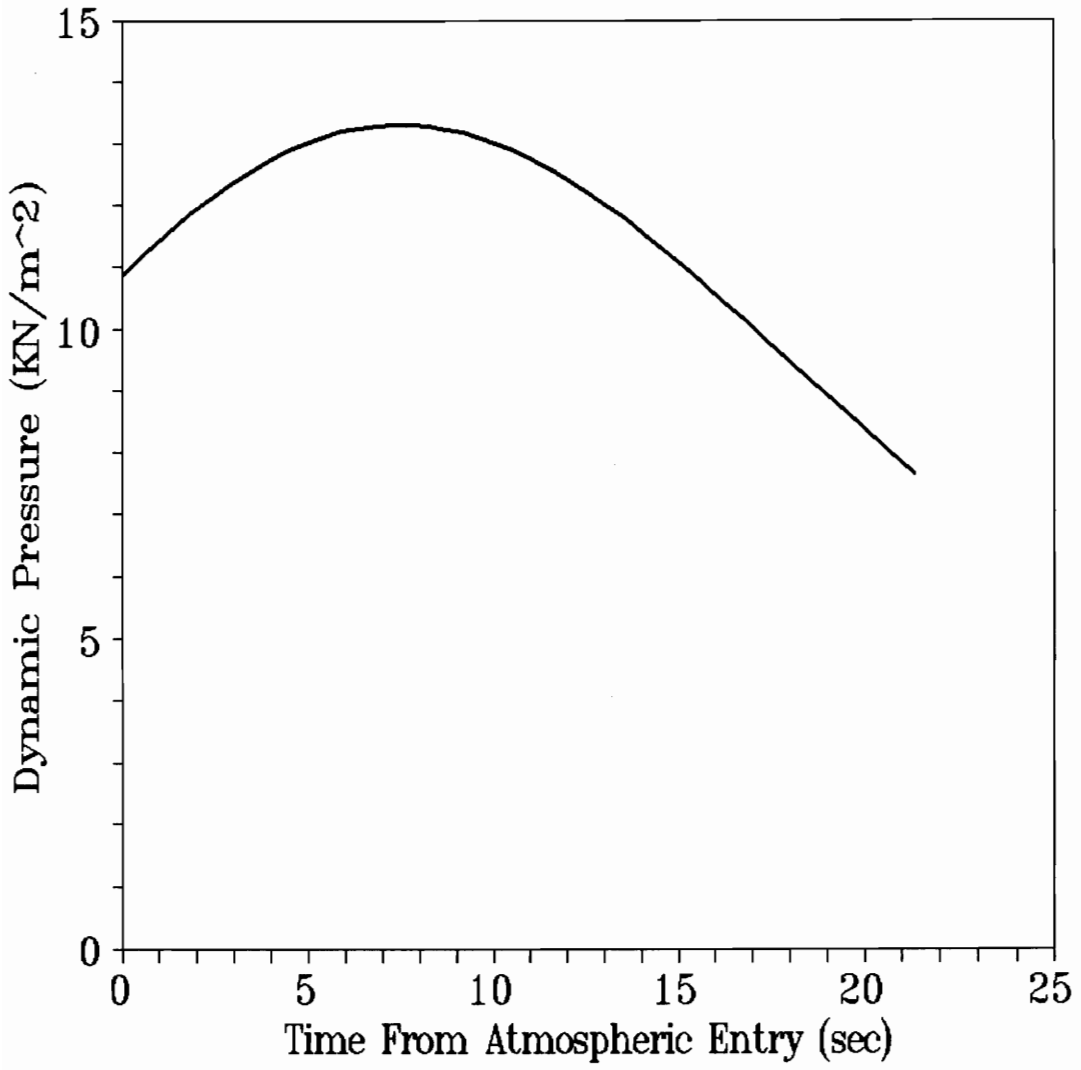


Figure 22. Dynamic Pressure vs. Time for $\chi = 2.61$ (Coplanar)

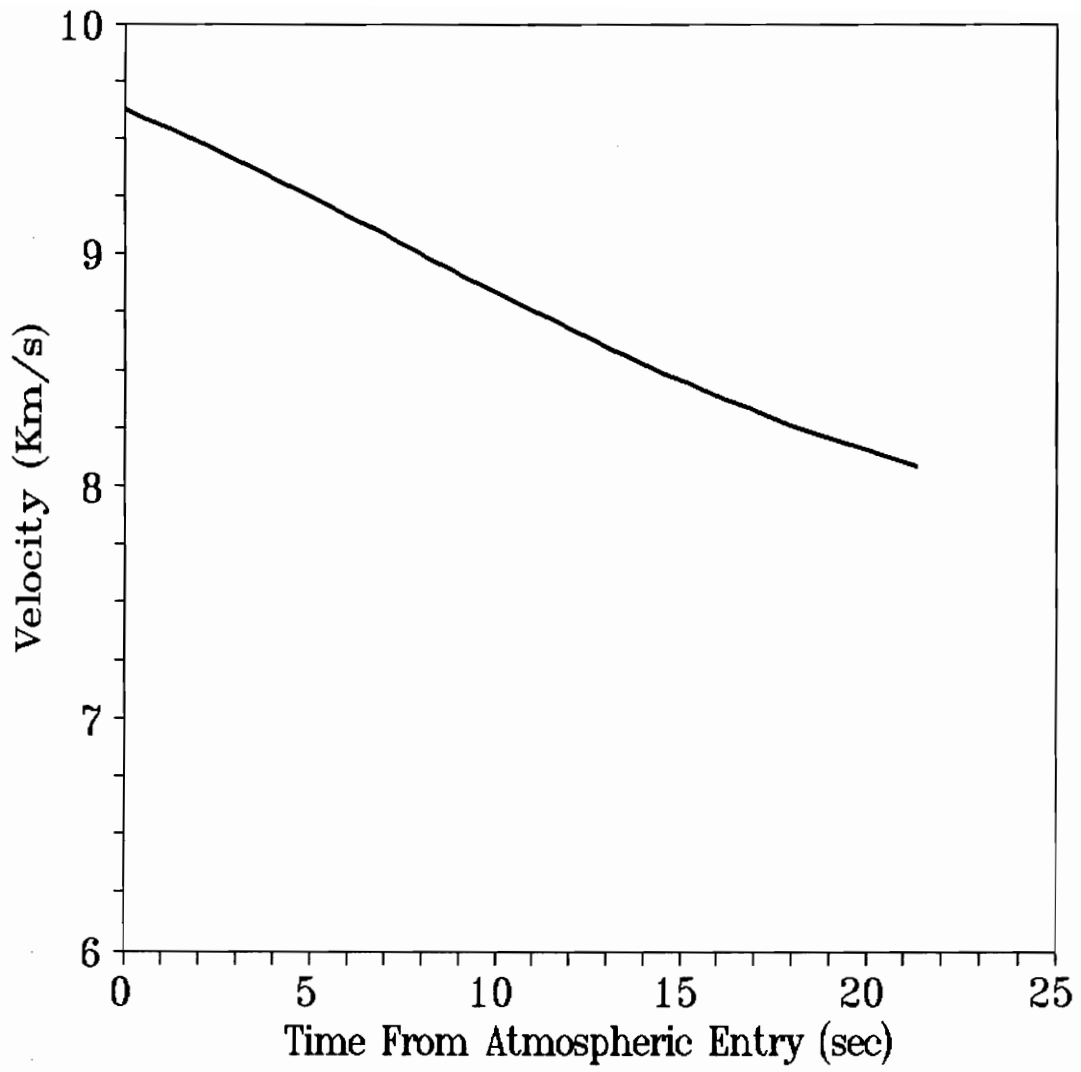


Figure 23. Velocity vs. Time for $\chi = 2.61$ (Coplanar)

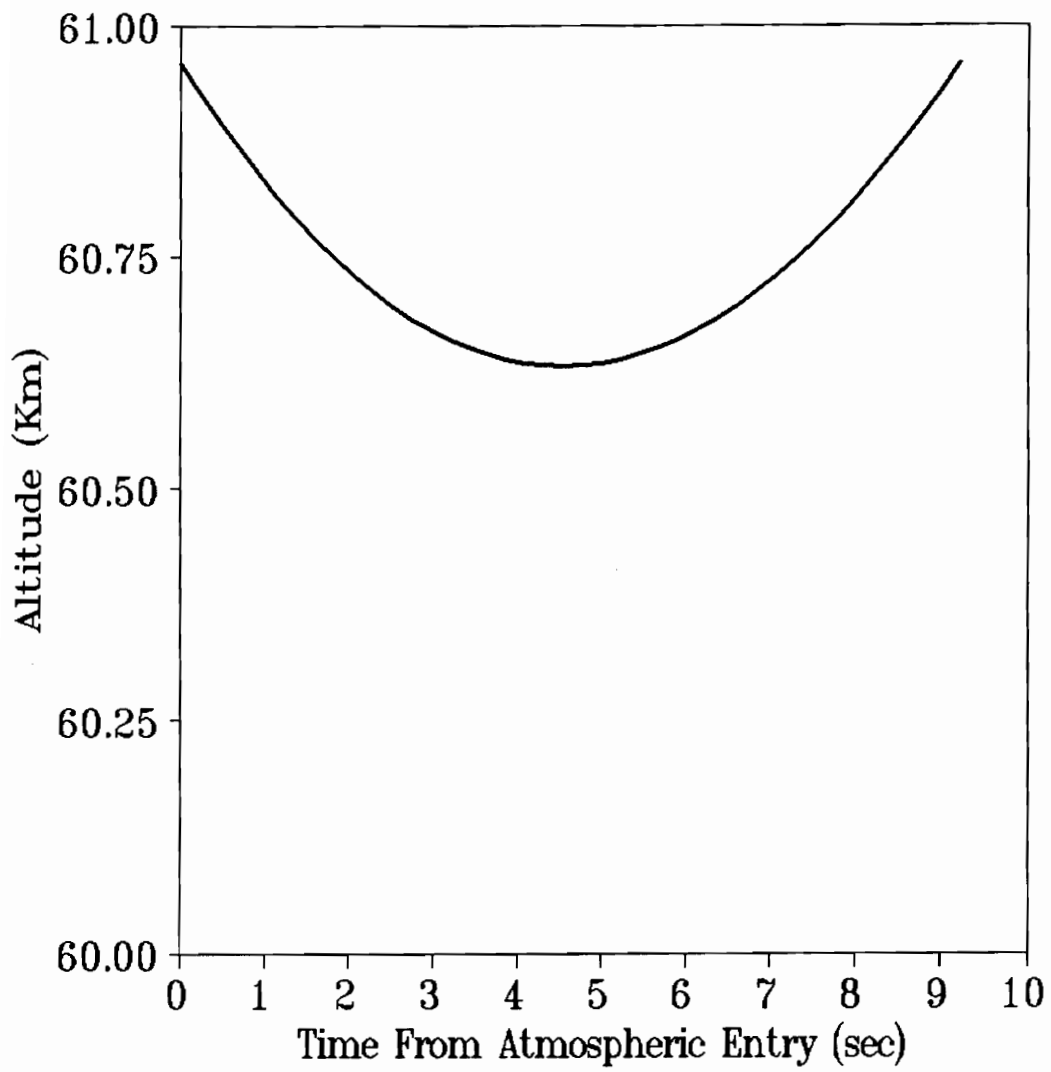


Figure 24. Altitude vs. Time for $\chi = 1.30$ (Coplanar)

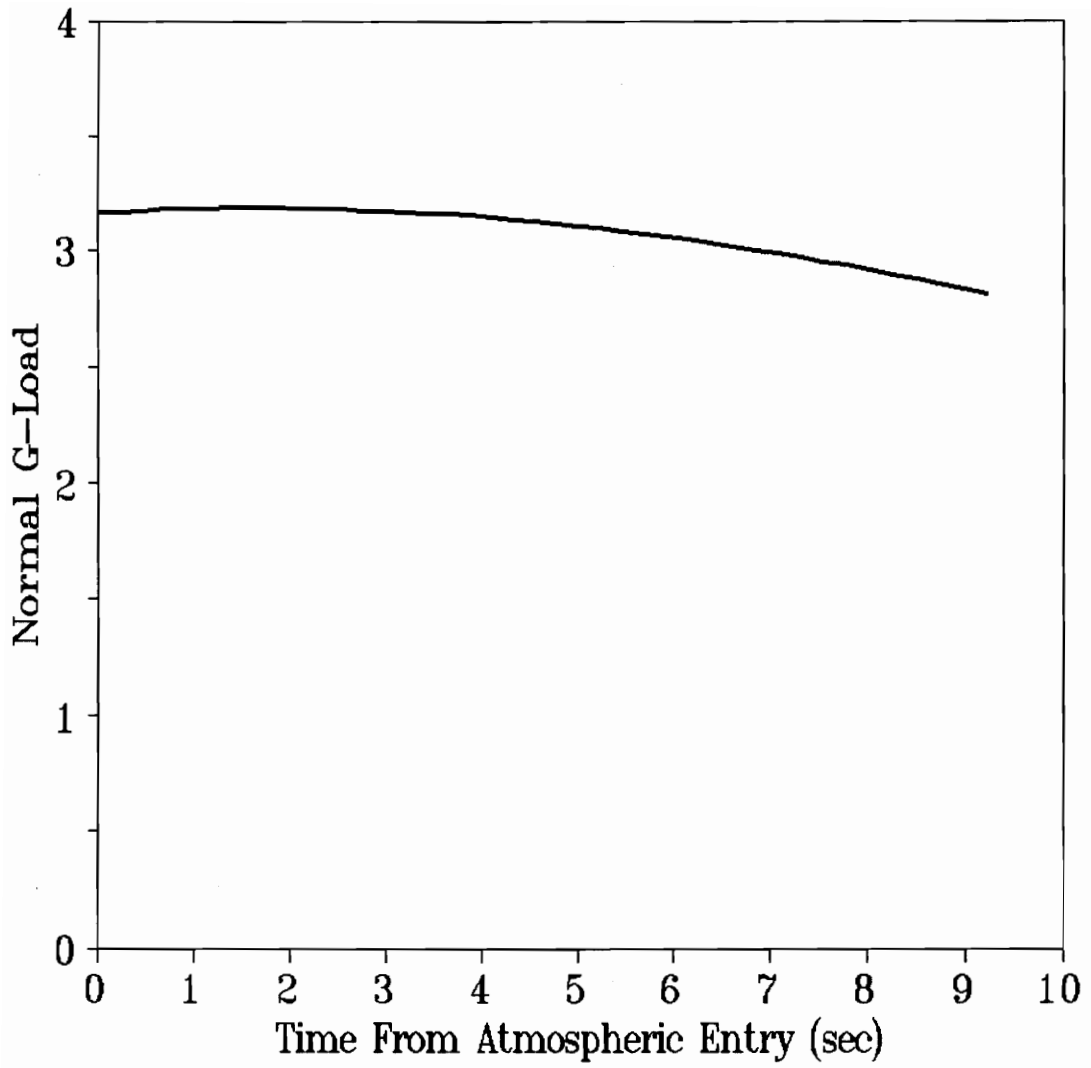


Figure 25. Normal G-Load vs. Time for $\chi = 1.30$ (Coplanar)

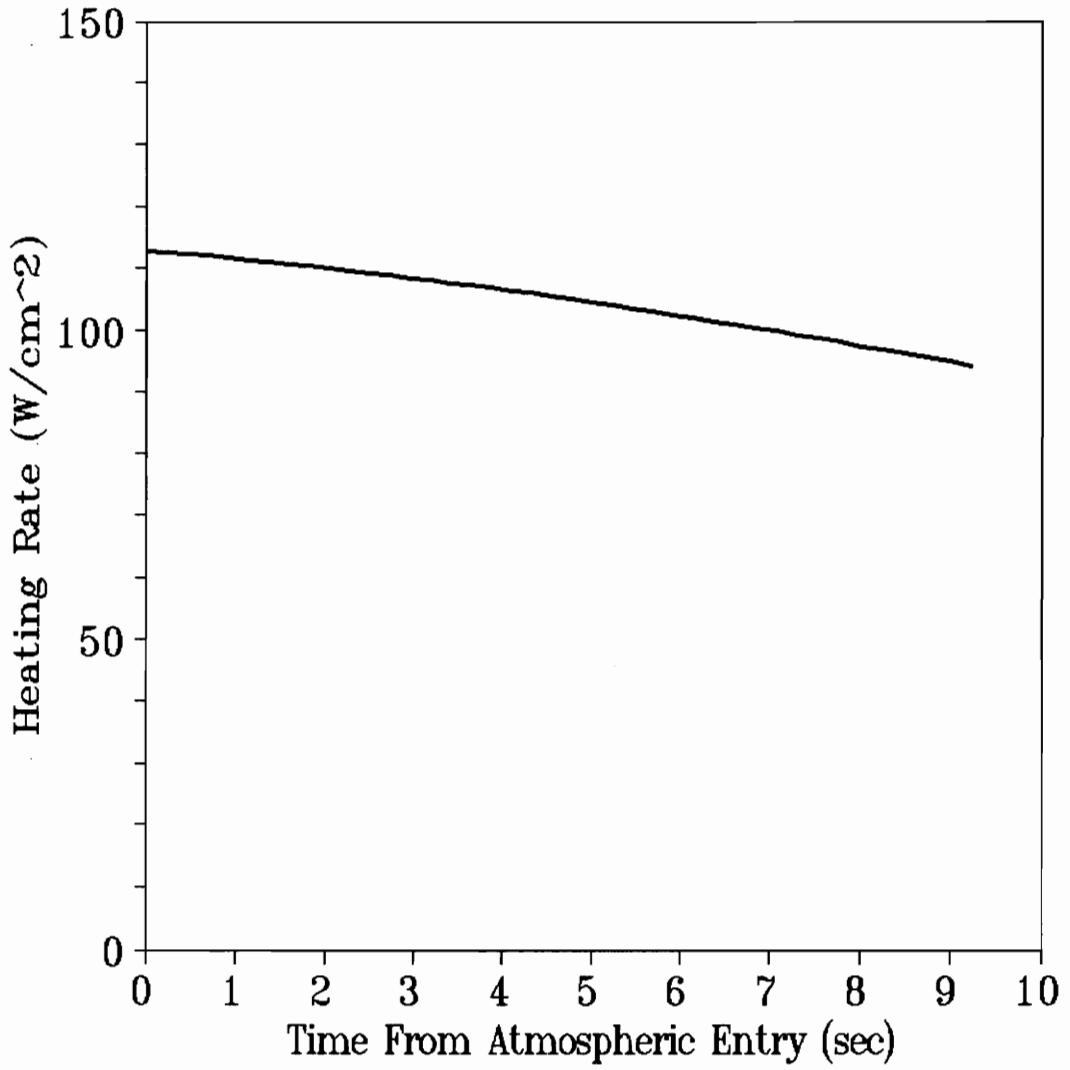


Figure 26. Convective Heating Rate vs. Time for $\chi = 1.30$ (Coplanar)

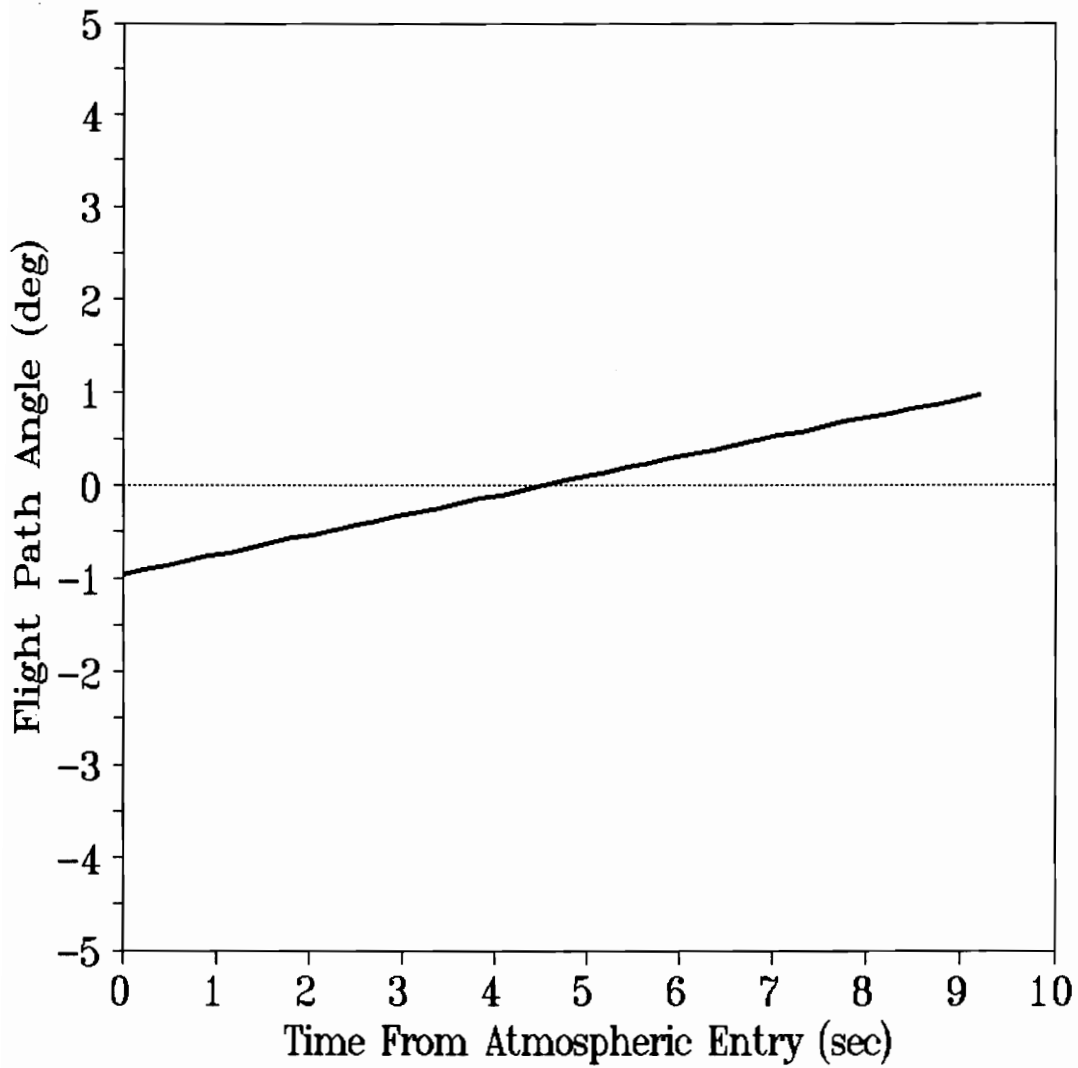


Figure 27. Flight Path Angle vs. Time for $\chi = 1.30$ (Coplanar)

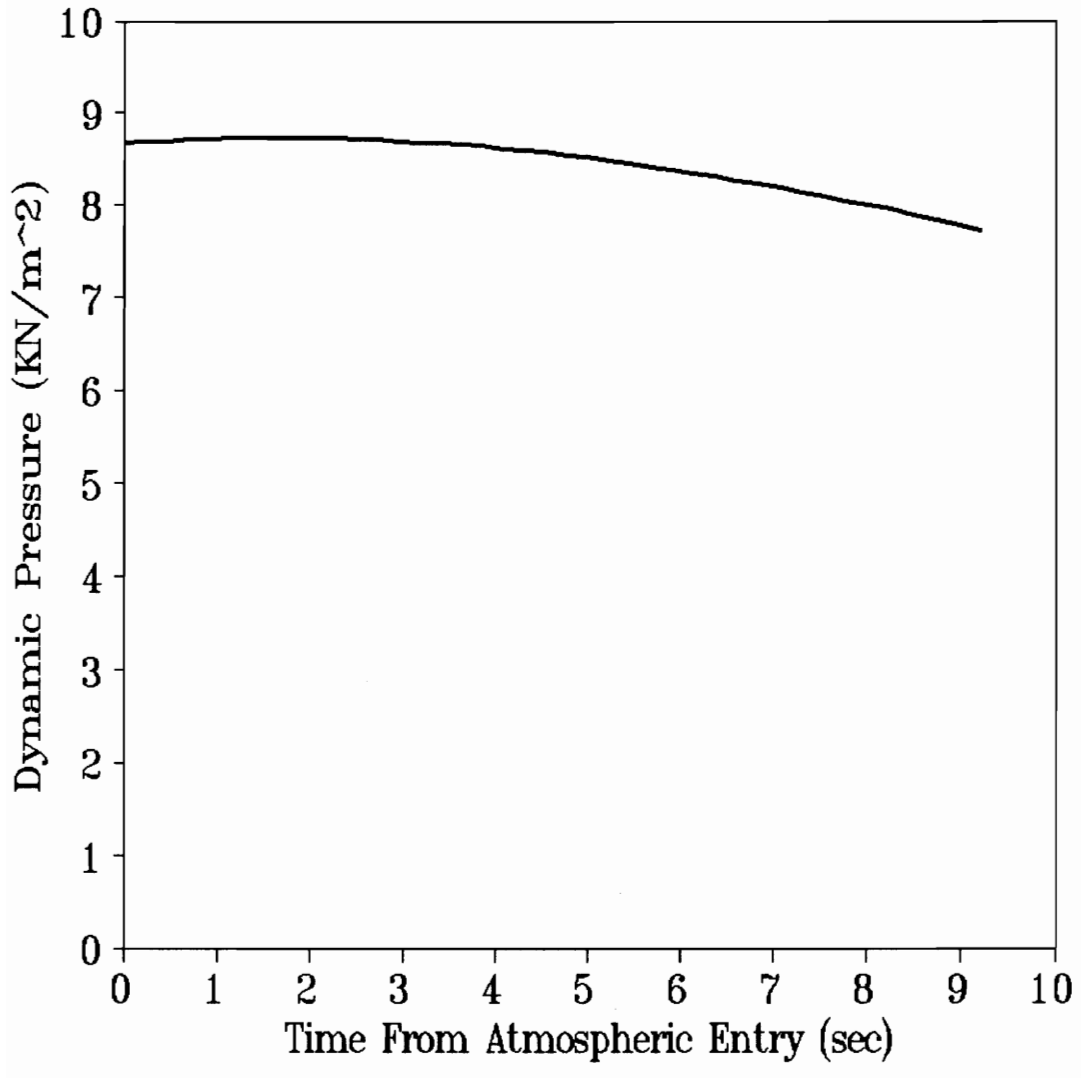


Figure 28. Dynamic Pressure vs. Time for $\chi = 1.30$ (Coplanar)

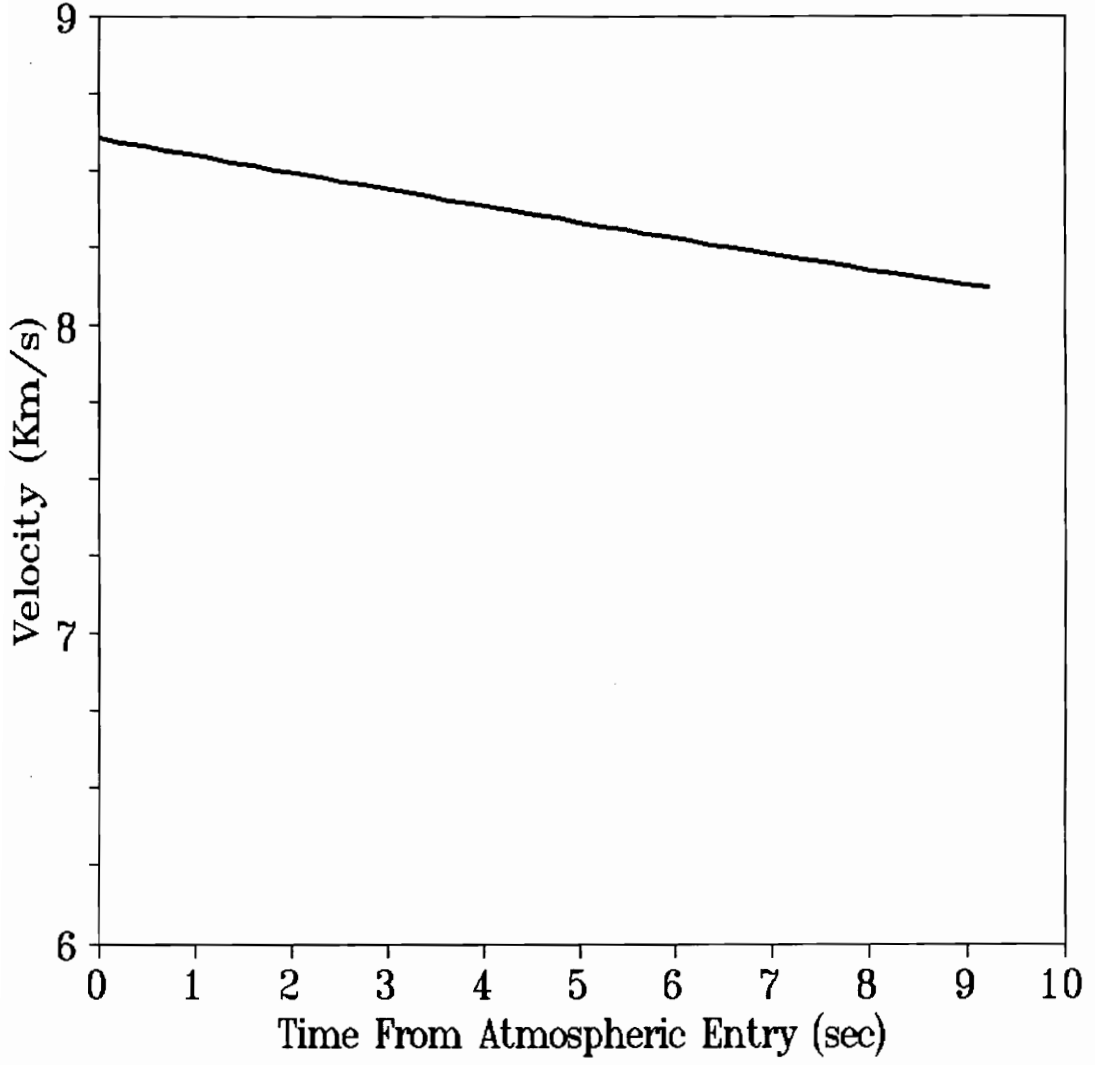


Figure 29. Velocity vs. Time for $\chi = 1.30$ (Coplanar)

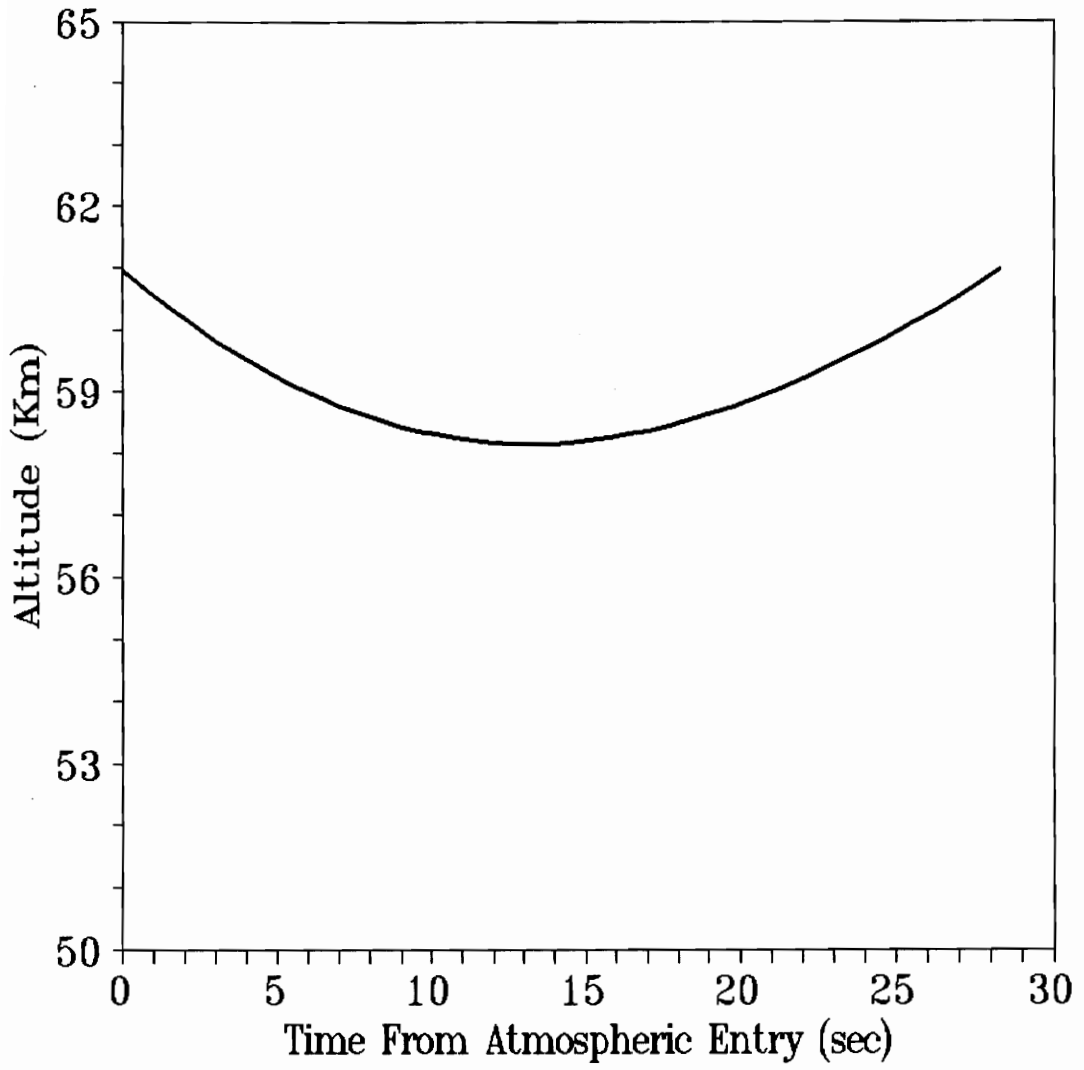


Figure 30. Altitude vs. Time for $\chi = 5.75$ (Noncoplanar $\Delta i = 5^\circ$)

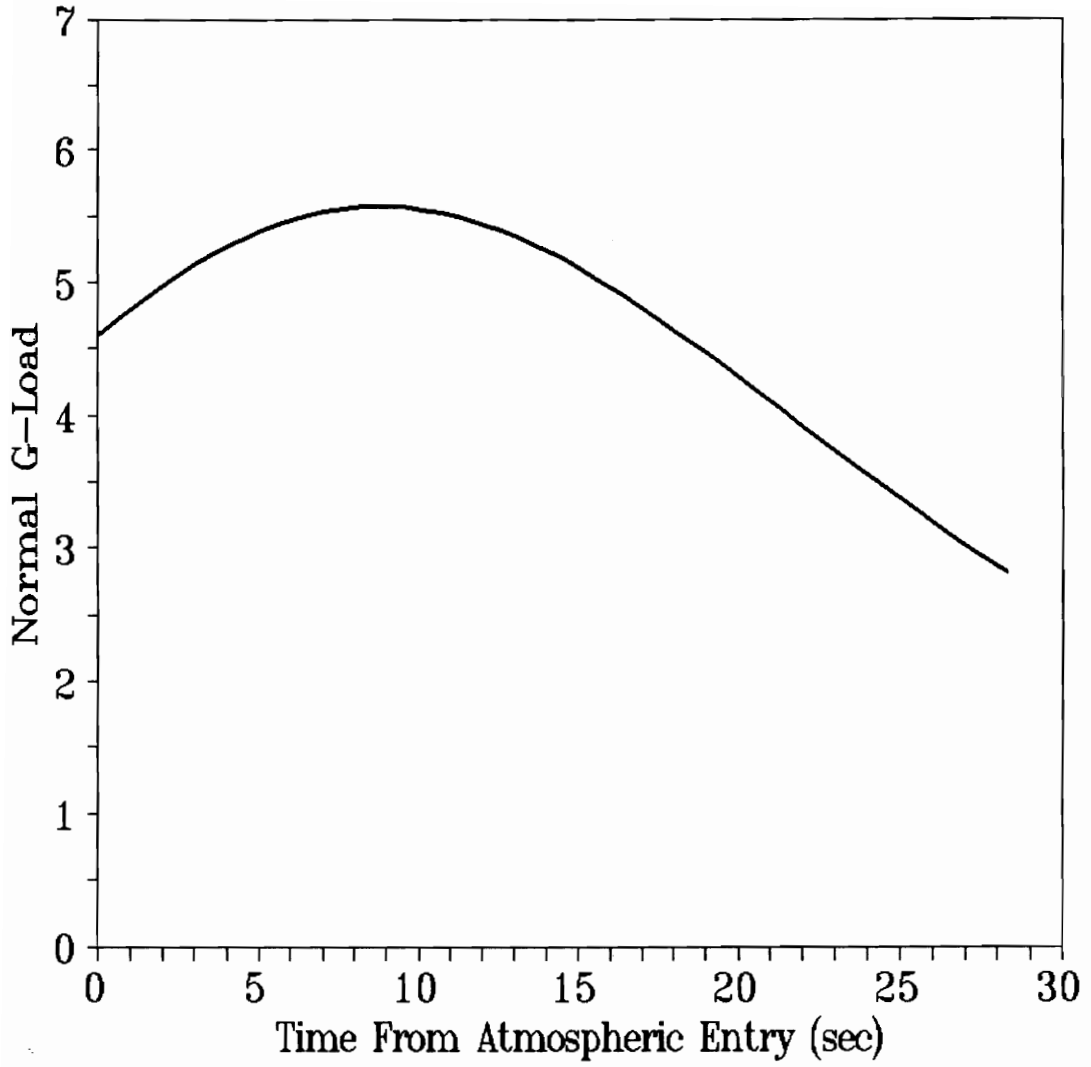


Figure 31. Normal G-Load vs. Time for $\chi = 5.75$ (Noncoplanar $\Delta i = 5^\circ$)

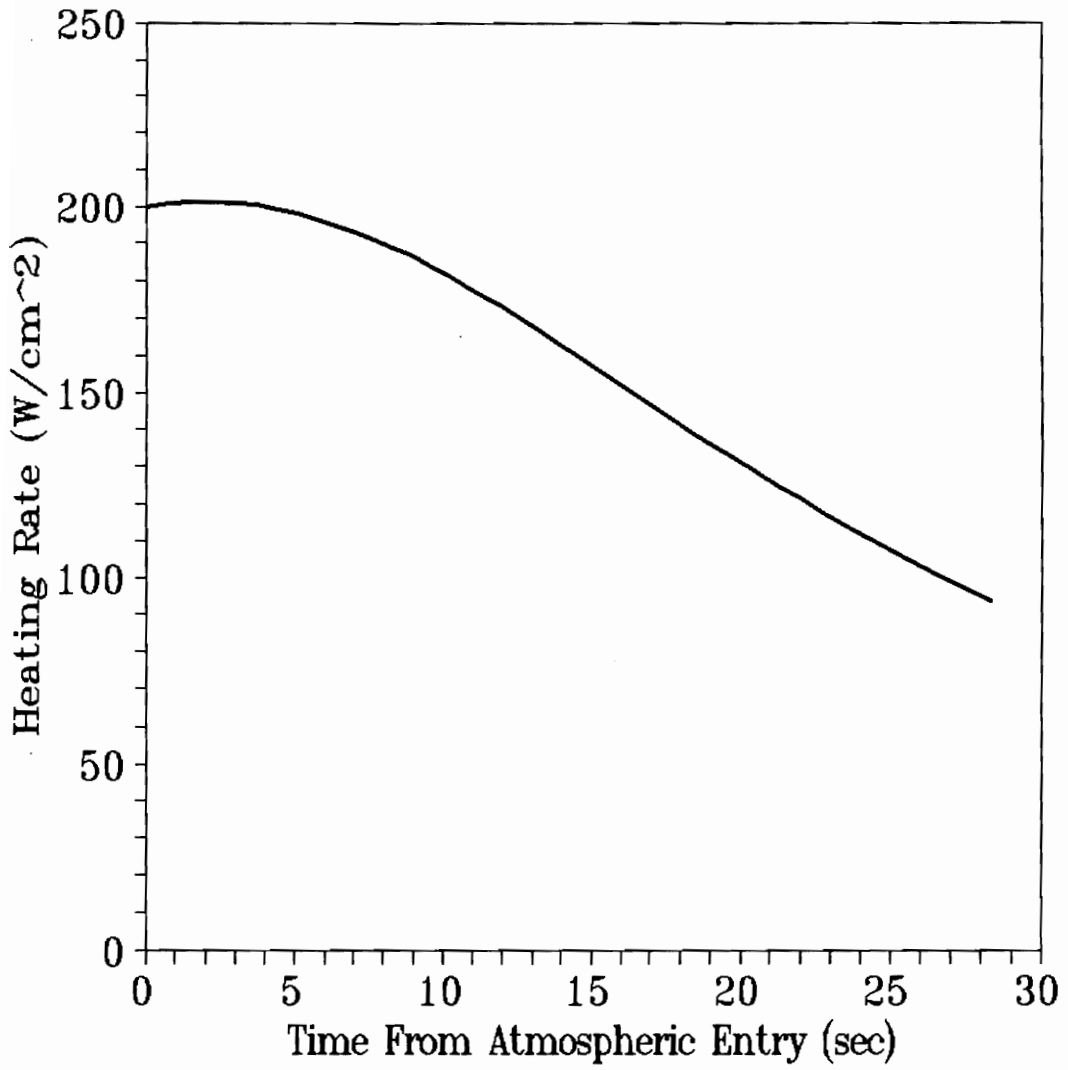


Figure 32. Convective Heating Rate vs. Time for $\chi = 5.75$ (Noncoplanar $\Delta i = 5^\circ$)

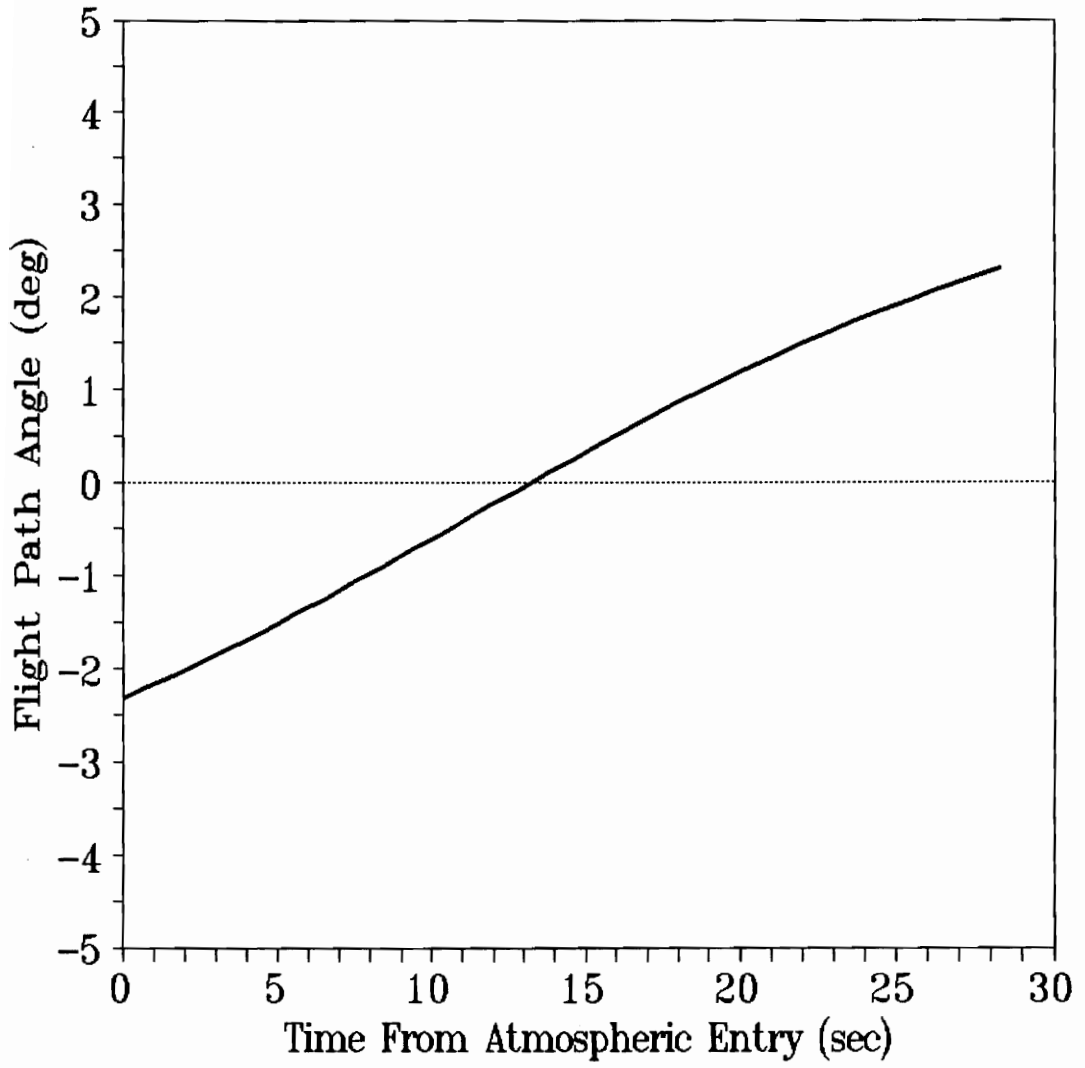


Figure 33. Flight Path Angle vs. Time for $\chi = 5.75$ (Noncoplanar $\Delta i = 5^\circ$)

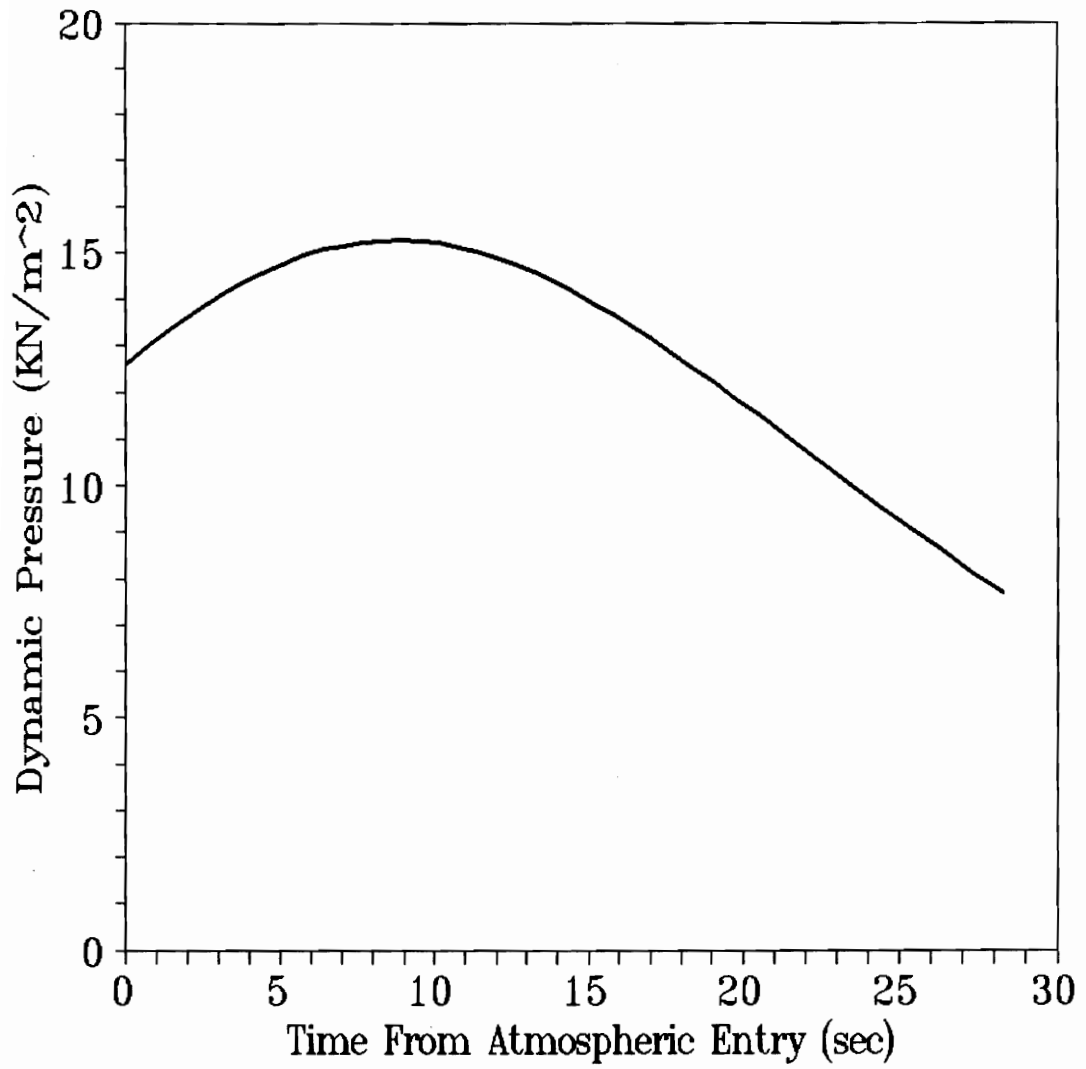


Figure 34. Dynamic Pressure vs. Time for $\chi = 5.75$ (Noncoplanar $\Delta i = 5^\circ$)

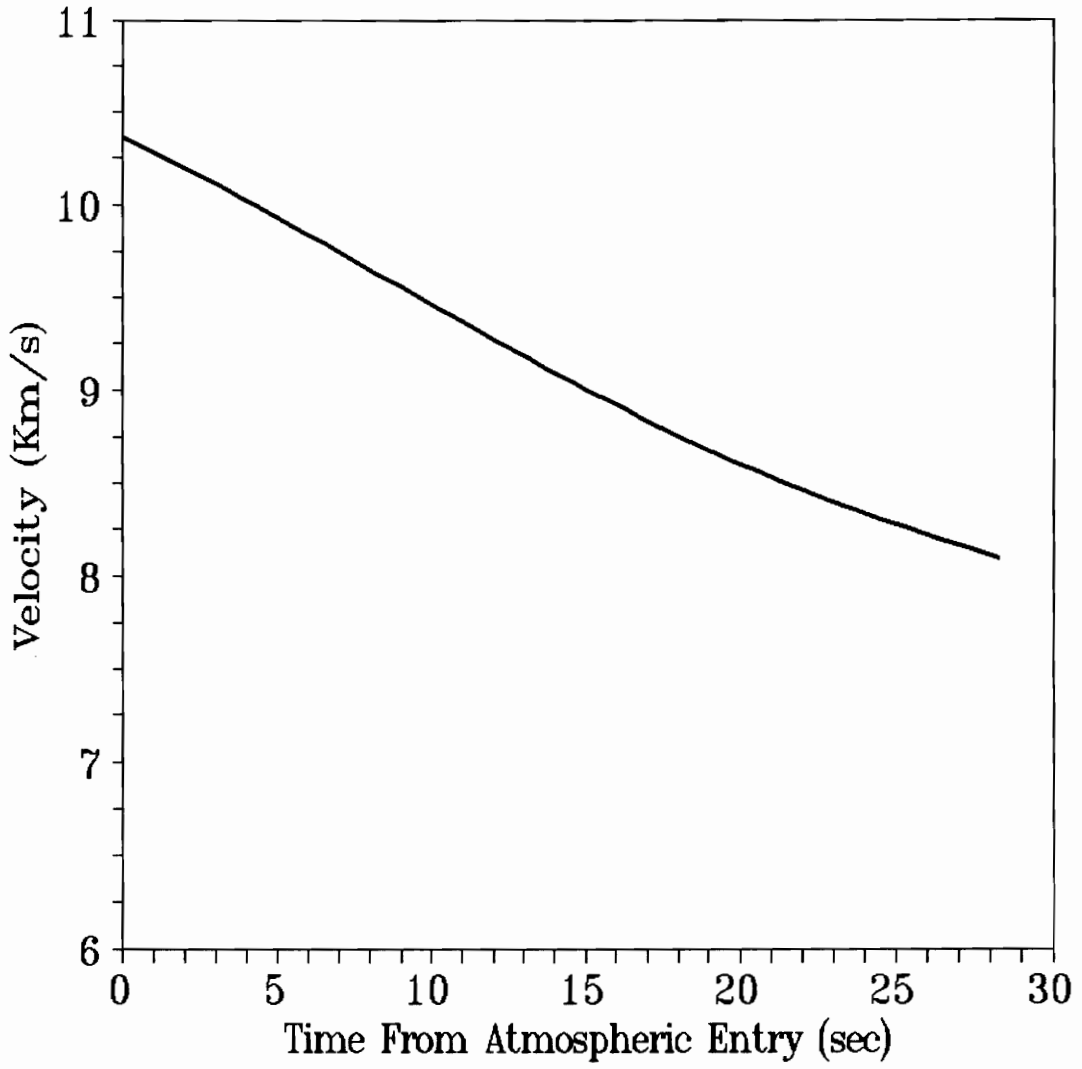


Figure 35. Velocity vs. Time for $\chi = 5.75$ (Noncoplanar $\Delta i = 5^\circ$)

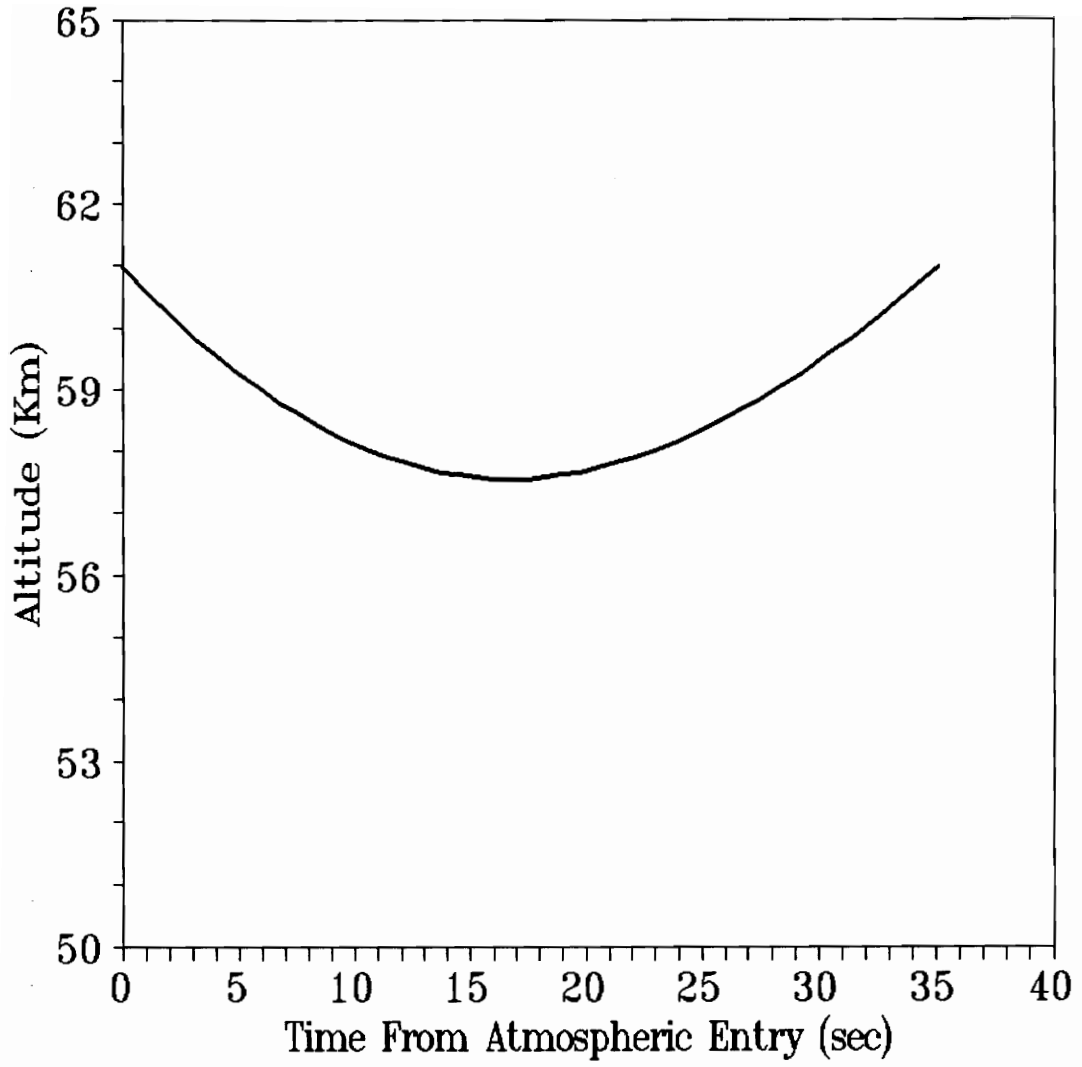


Figure 36. Altitude vs. Time for $\chi = 2.61$ (Noncoplanar $\Delta i = 5^\circ$)

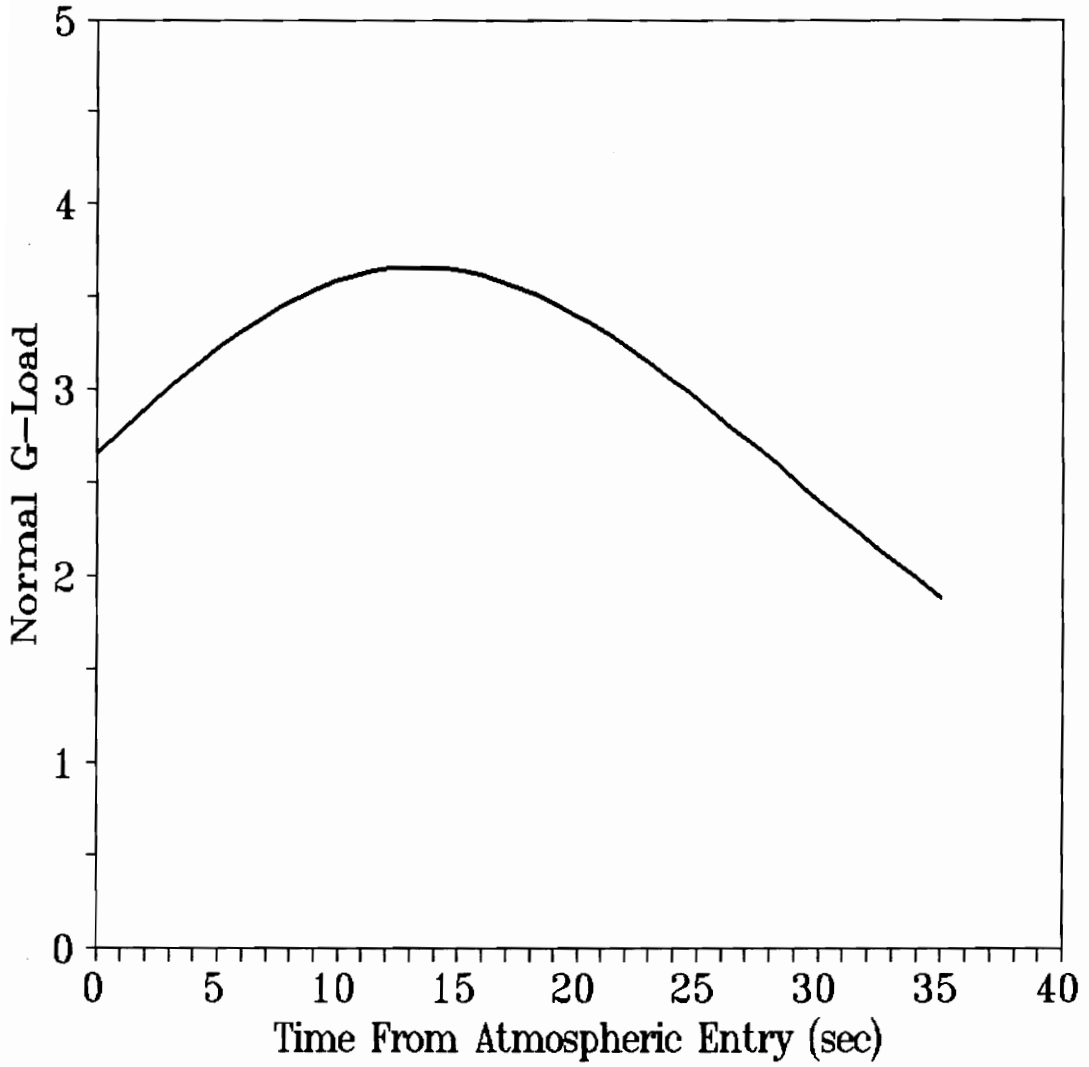


Figure 37. Normal G-Load vs. Time for $\chi = 2.61$ (Noncoplanar $\Delta i = 5^\circ$)

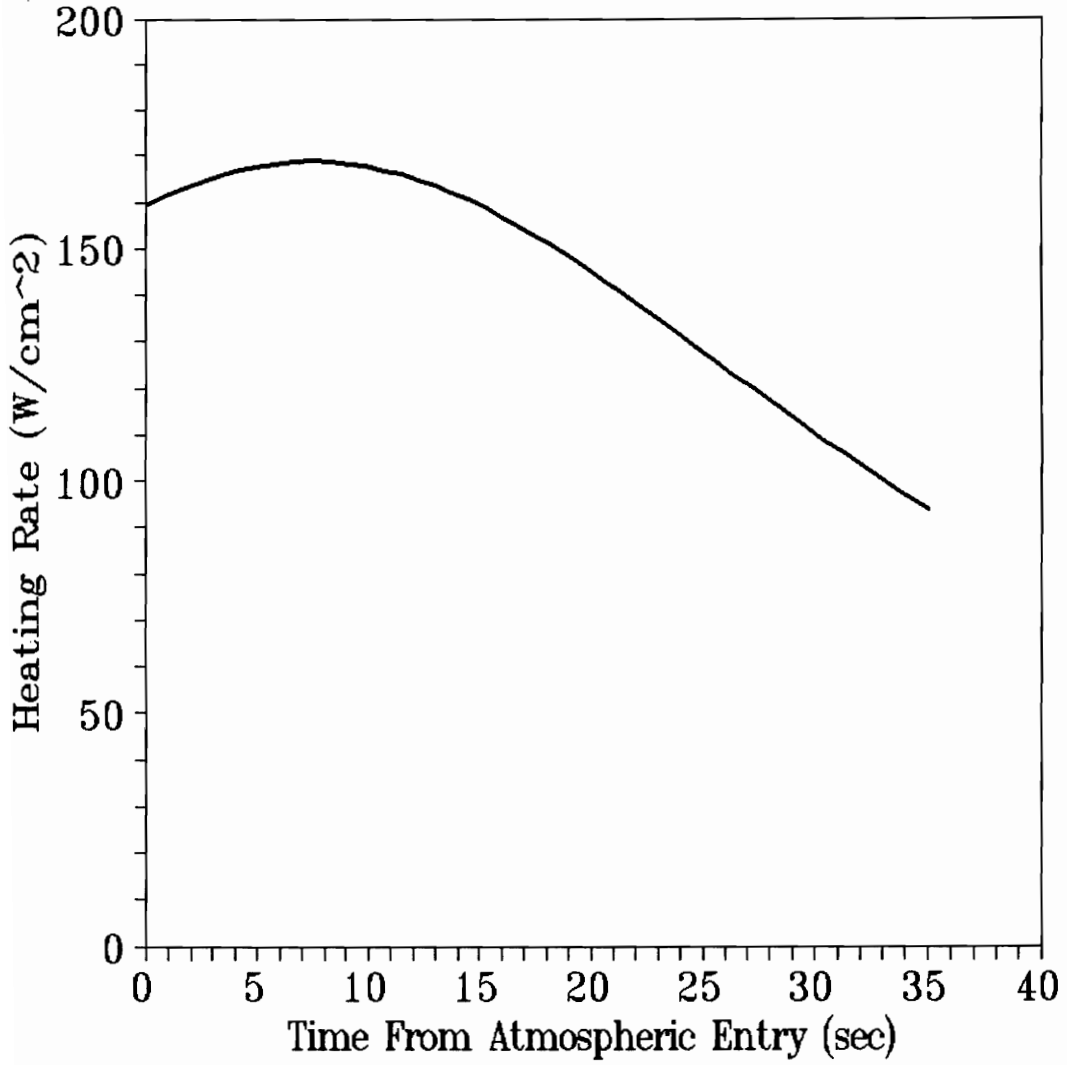


Figure 38. Convective Heating Rate vs. Time for $\chi = 2.61$ (Noncoplanar $\Delta i = 5^\circ$)

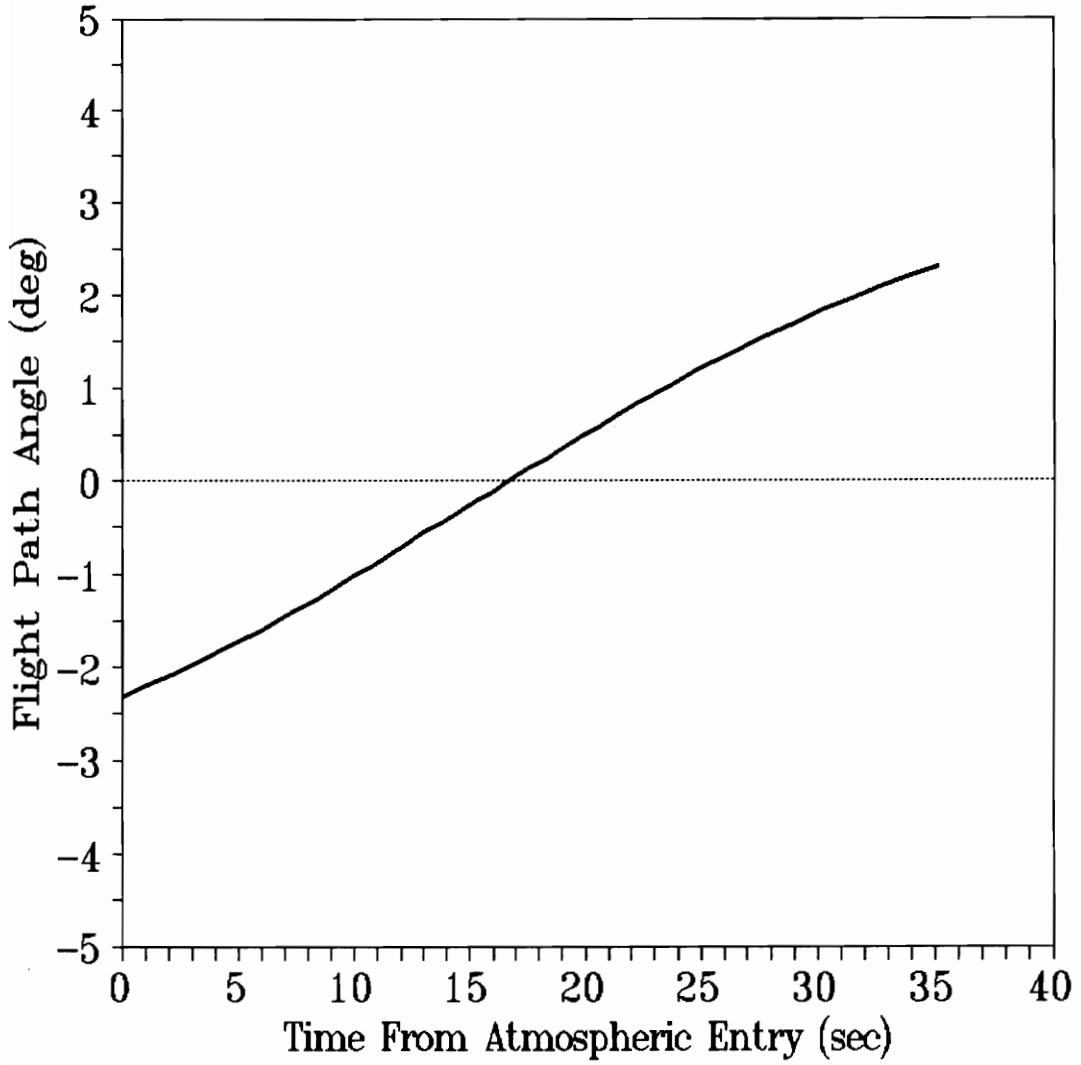


Figure 39. Flight Path Angle vs. Time for $\chi = 2.61$ (Noncoplanar $\Delta i = 5^\circ$)

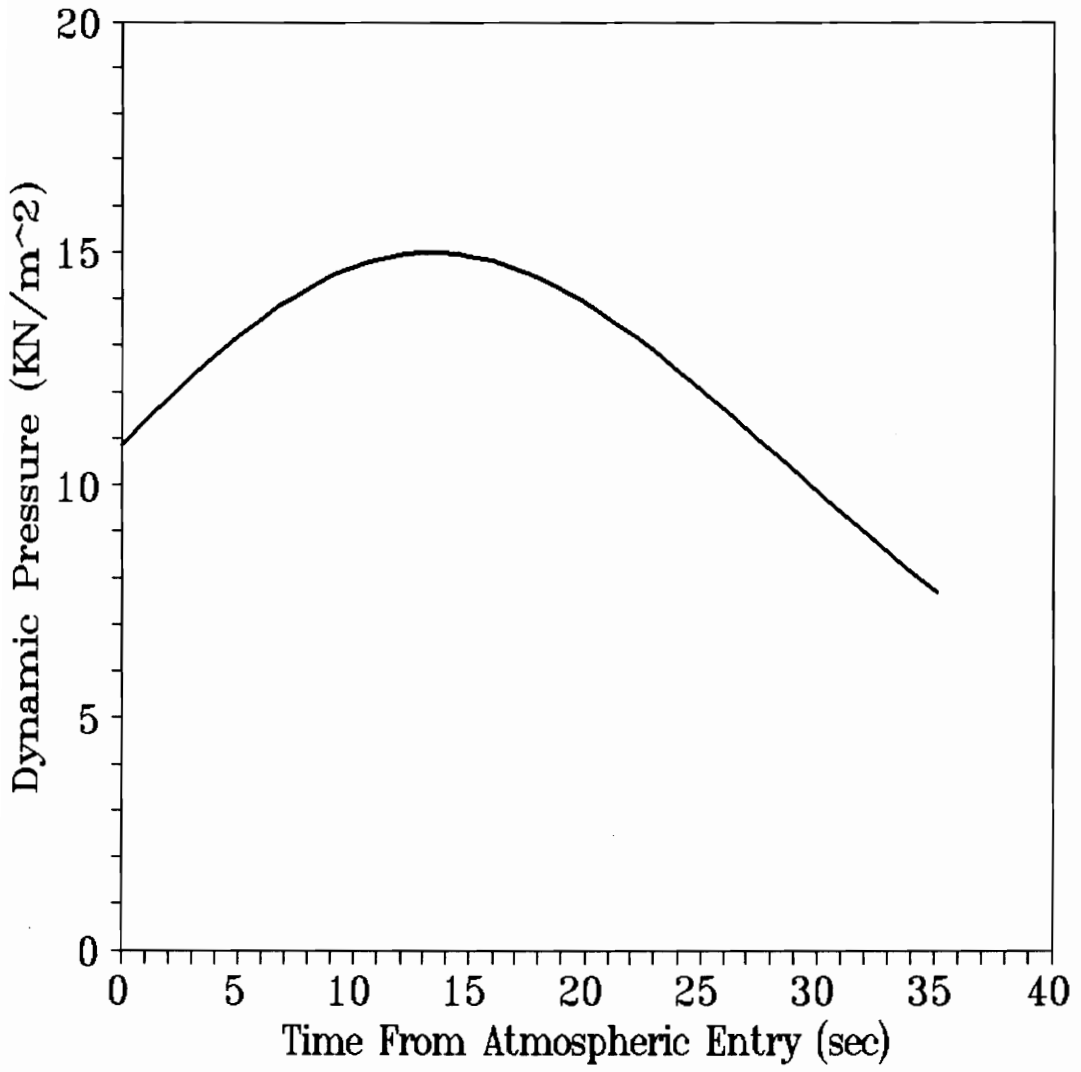


Figure 40. Dynamic Pressure vs. Time for $\chi = 2.61$ (Noncoplanar $\Delta i = 5^\circ$)

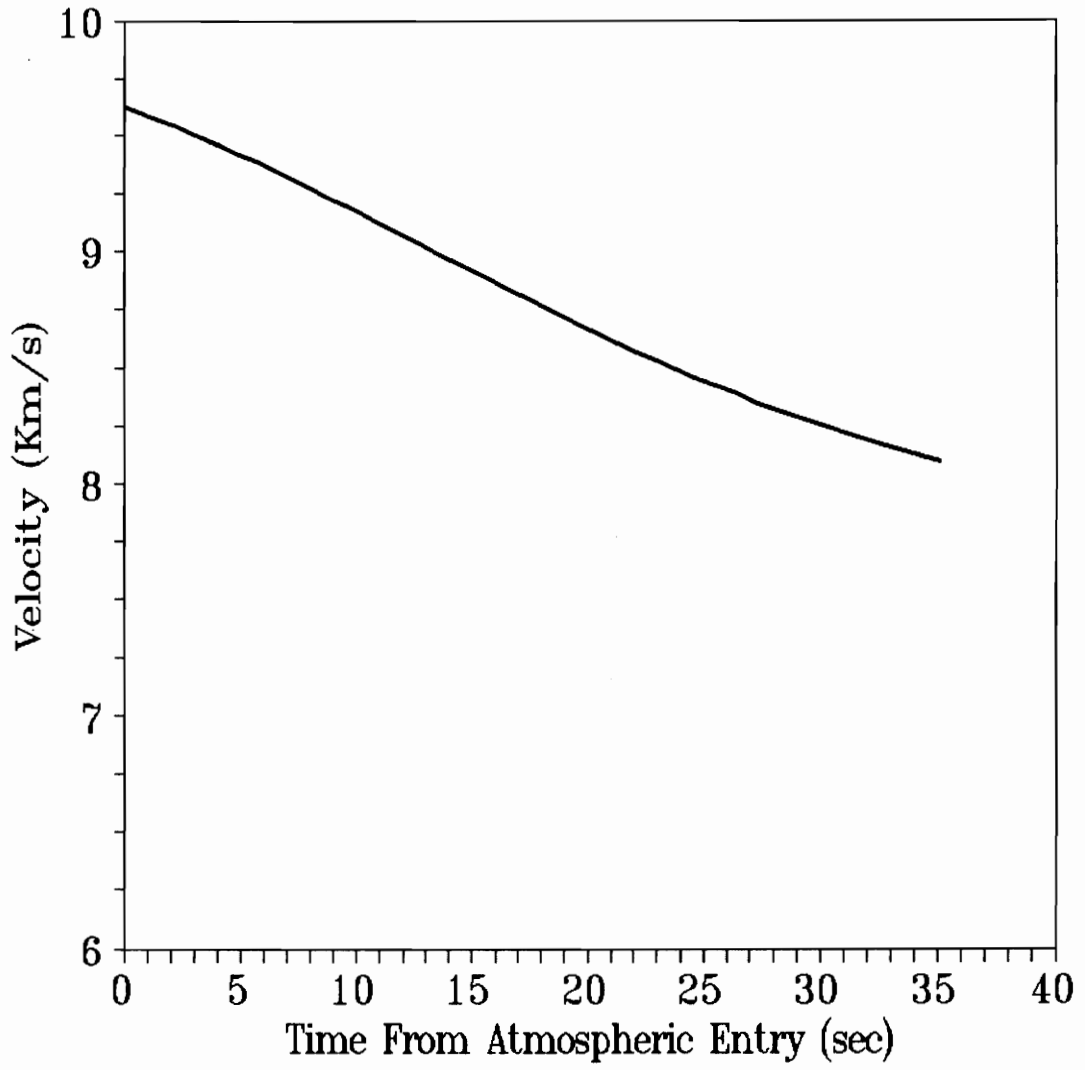


Figure 41. Velocity vs. Time for $\chi = 2.61$ (Noncoplanar $\Delta i = 5^\circ$)

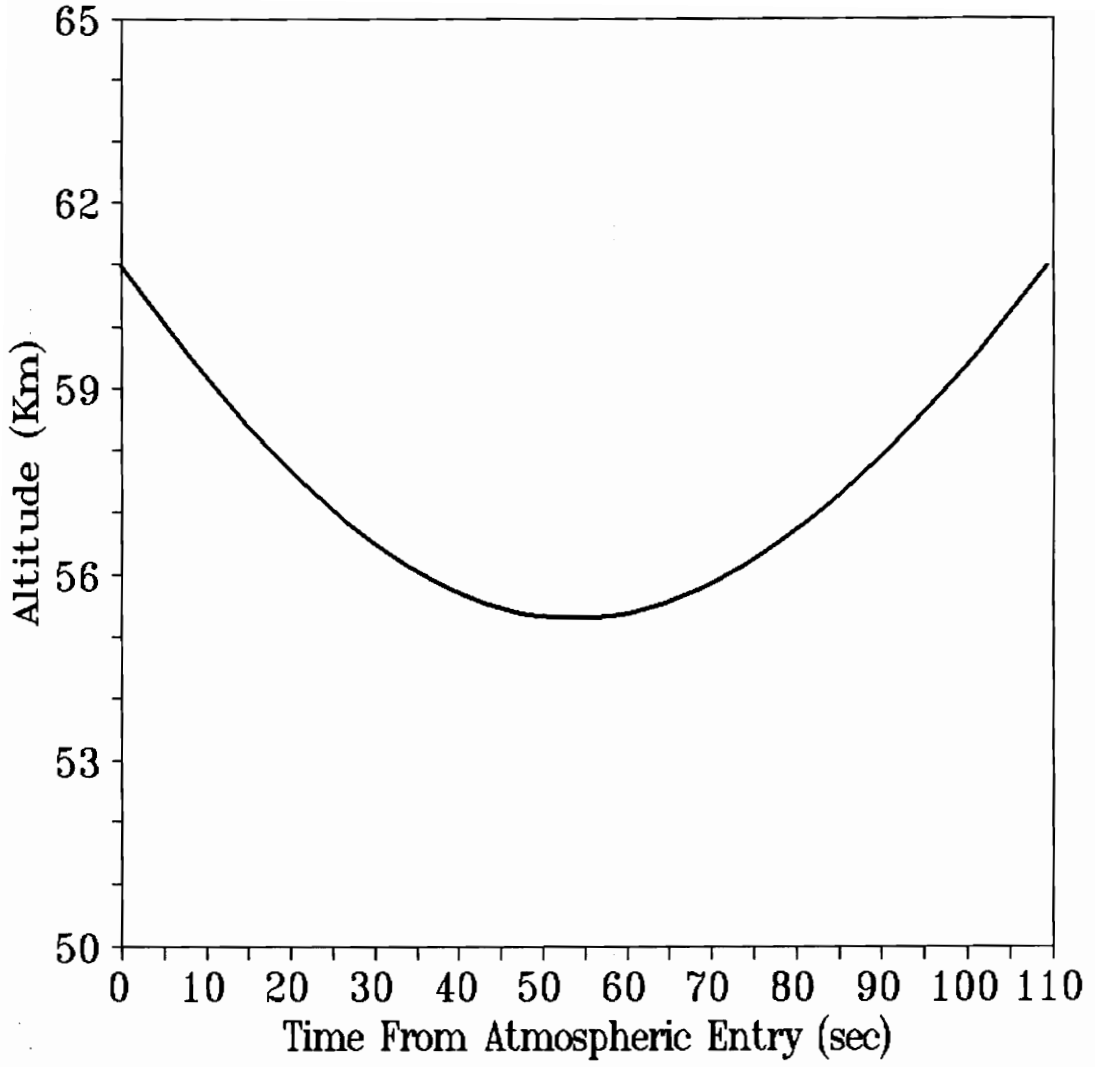


Figure 42. Altitude vs. Time for $\chi = 1.30$ (Noncoplanar $\Delta i = 5^\circ$)

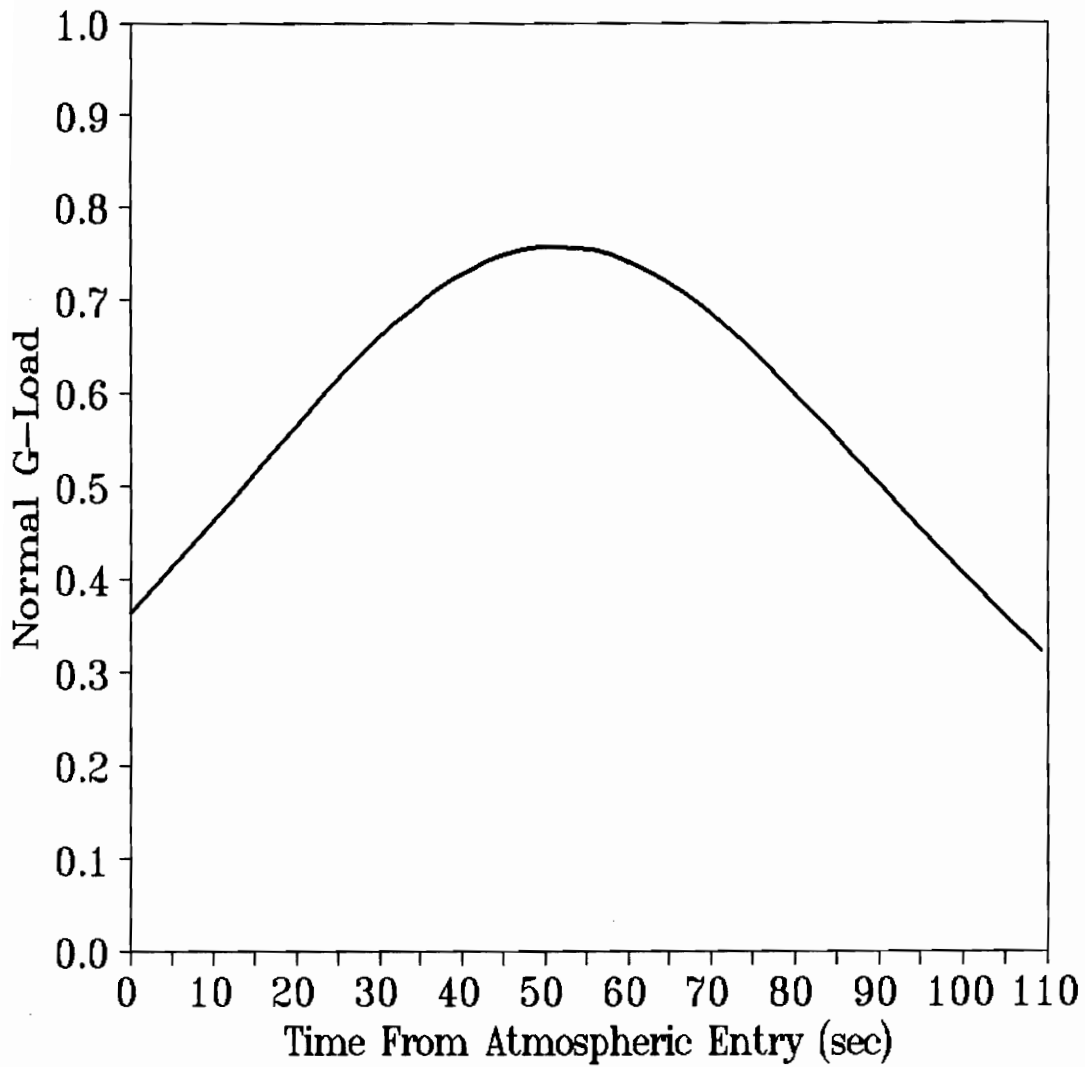


Figure 43. Normal G-Load vs. Time for $\chi = 1.30$ (Noncoplanar $\Delta i = 5^\circ$)

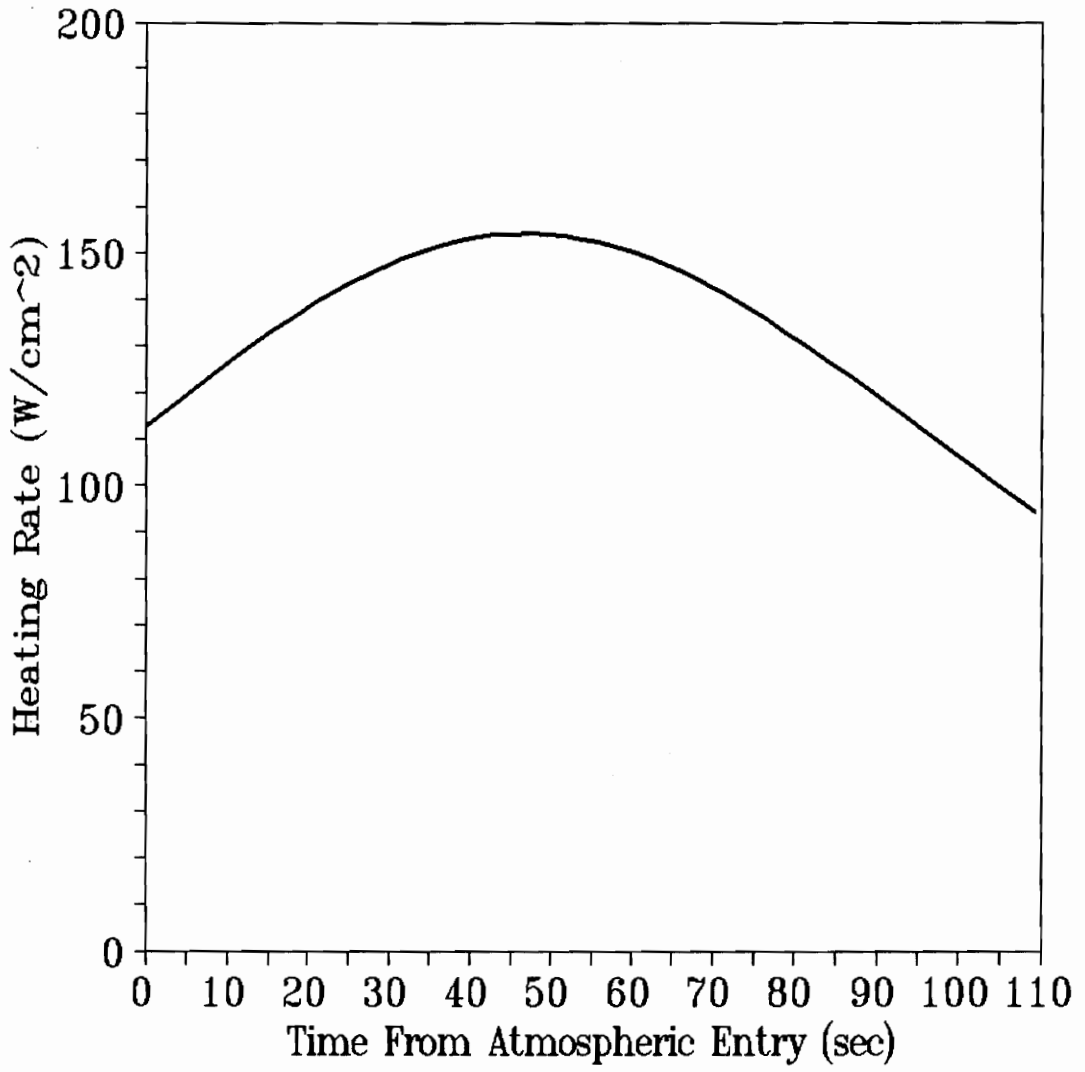


Figure 44. Convective Heating Rate vs. Time for $\chi = 1.30$ (Noncoplanar $\Delta i = 5^\circ$)

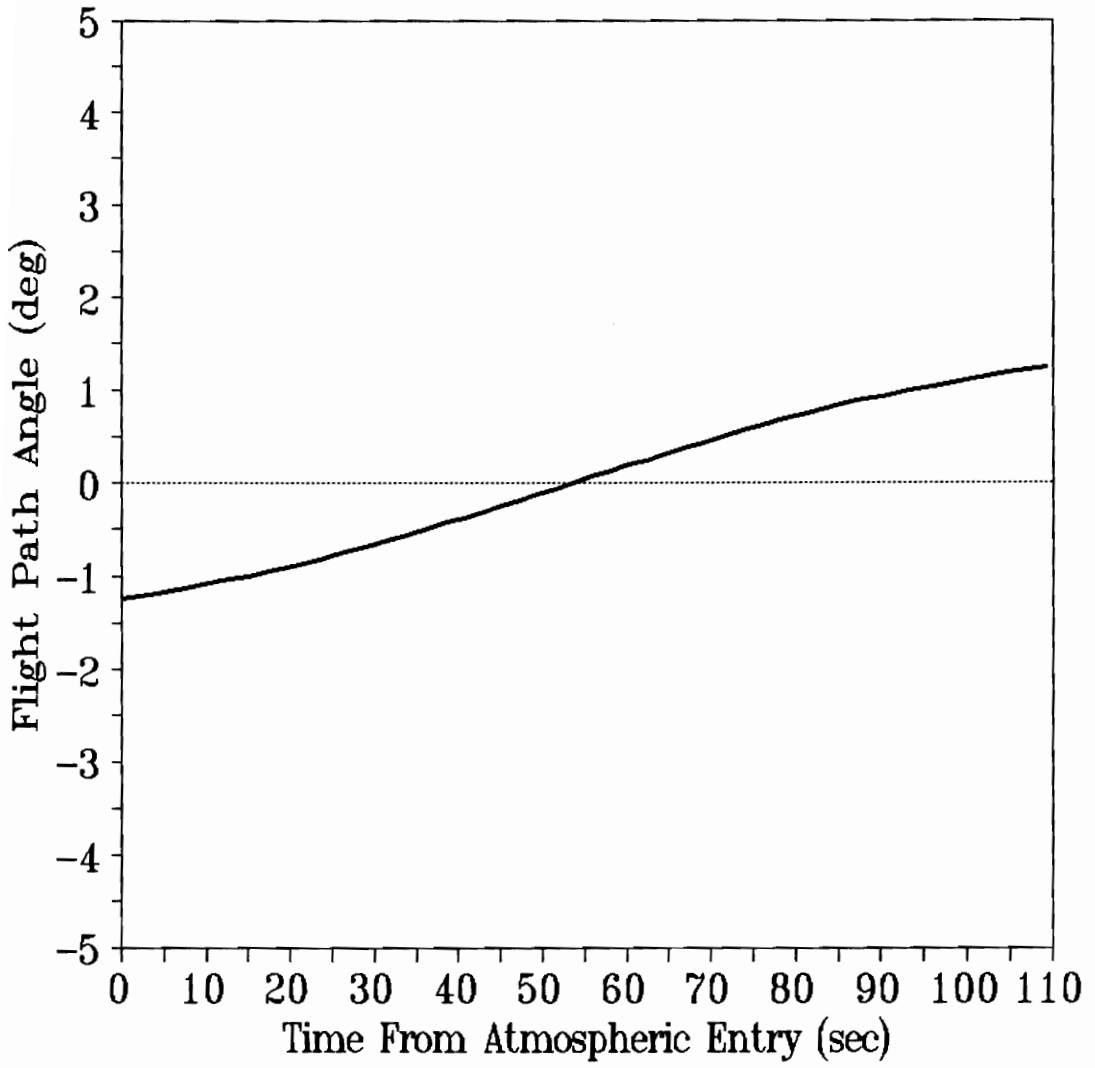


Figure 45. Flight Path Angle vs. Time for $\chi = 1.30$ (Noncoplanar $\Delta i = 5^\circ$)

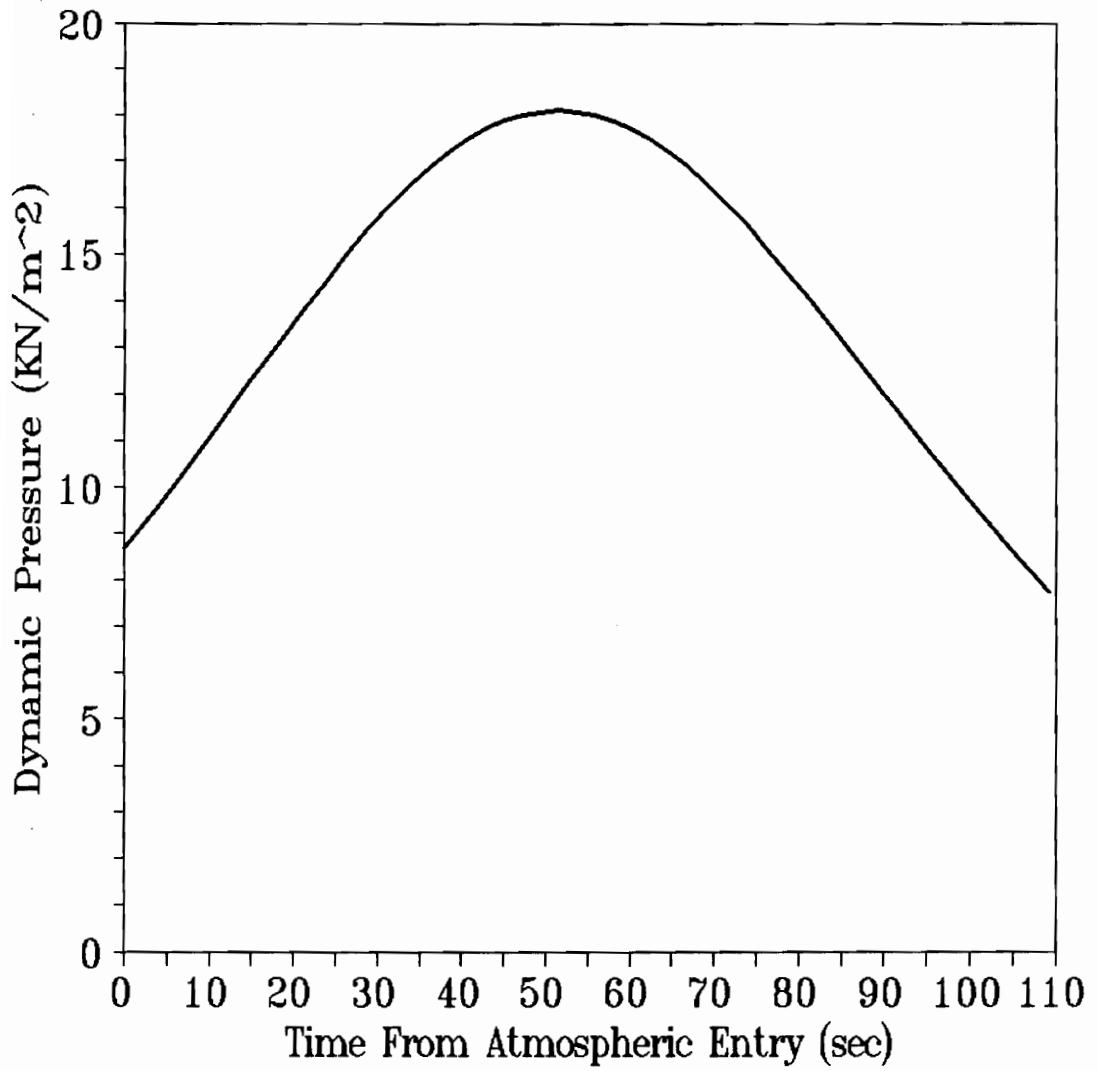


Figure 46. Dynamic Pressure vs. Time for $\chi = 1.30$ (Noncoplanar $\Delta i = 5^\circ$)

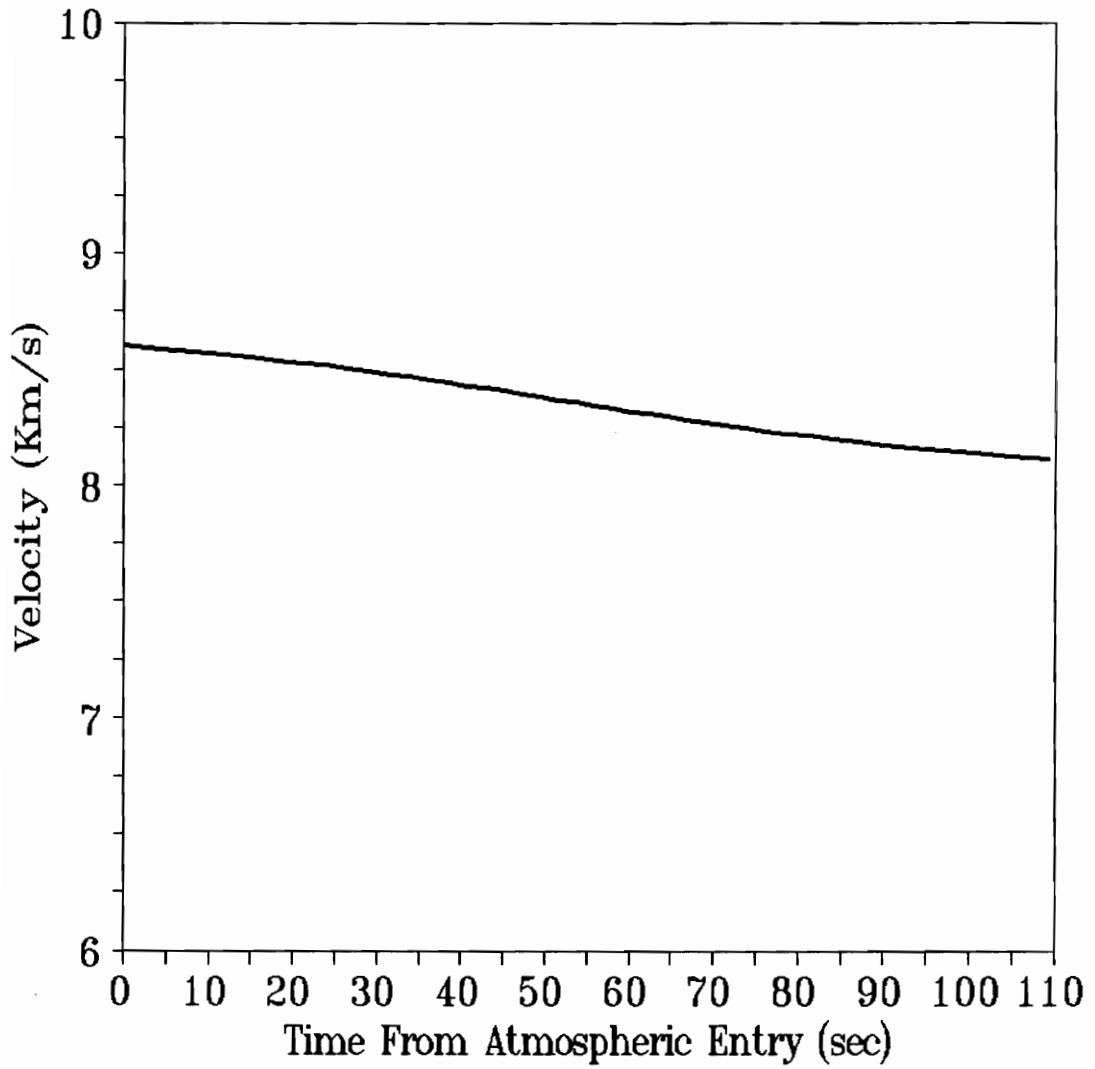


Figure 47. Velocity vs. Time for $\chi = 1.30$ (Noncoplanar $\Delta i = 5^\circ$)

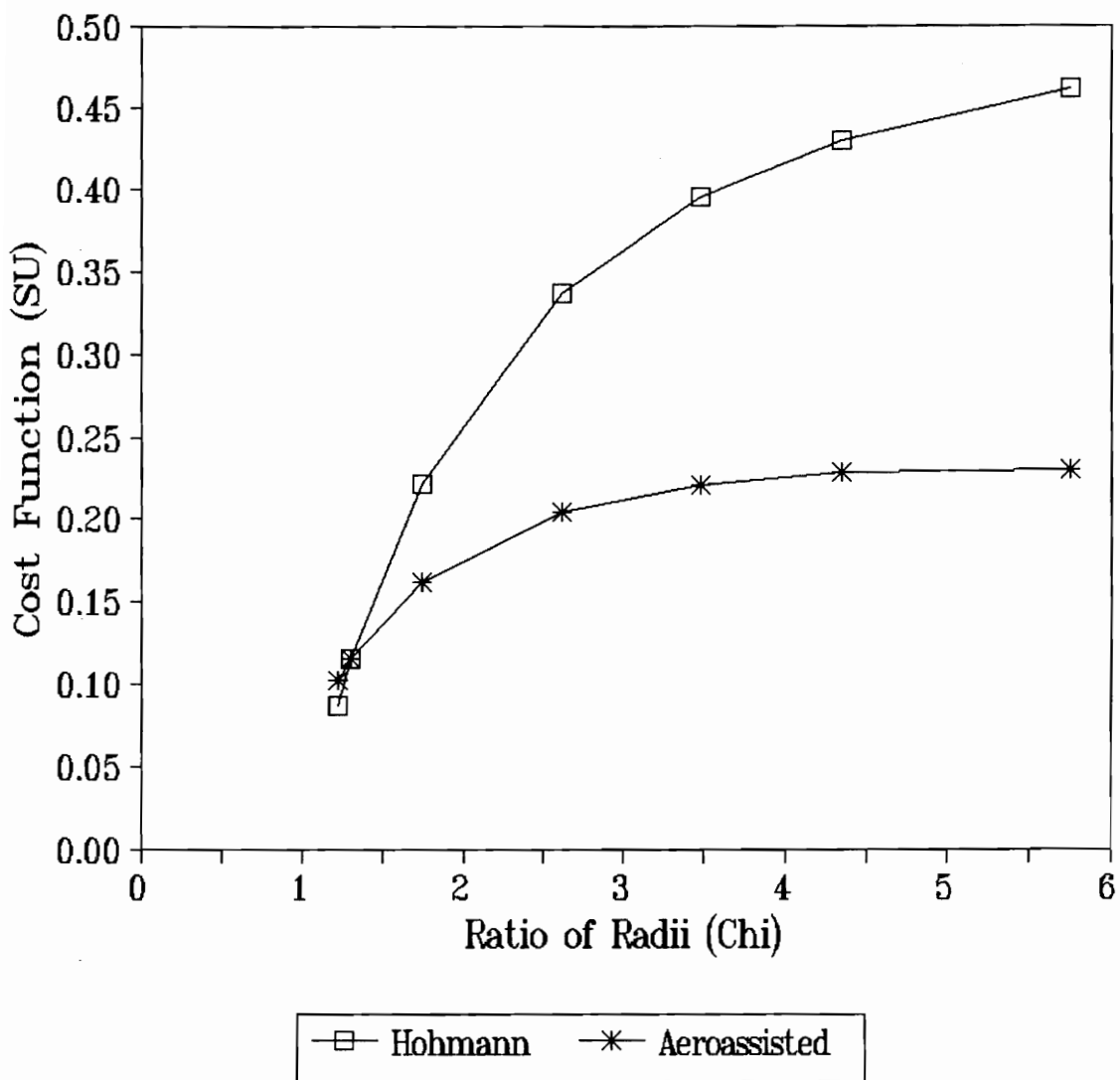


Figure 48. Cost Function vs. χ for Coplanar Transfer Methods

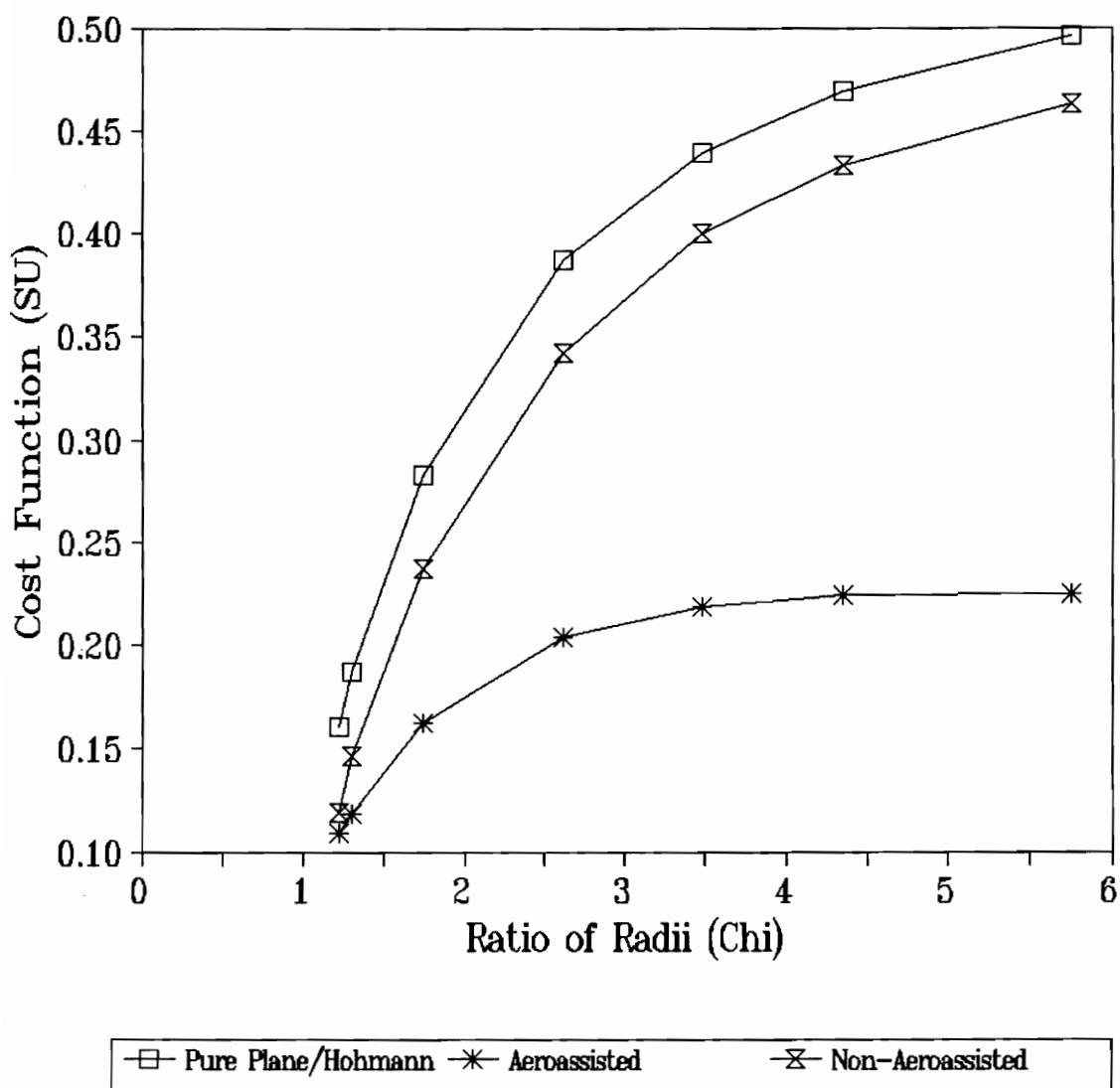


Figure 49. Cost Function vs. χ for Noncoplanar Transfer Methods ($\Delta i = 5^\circ$)

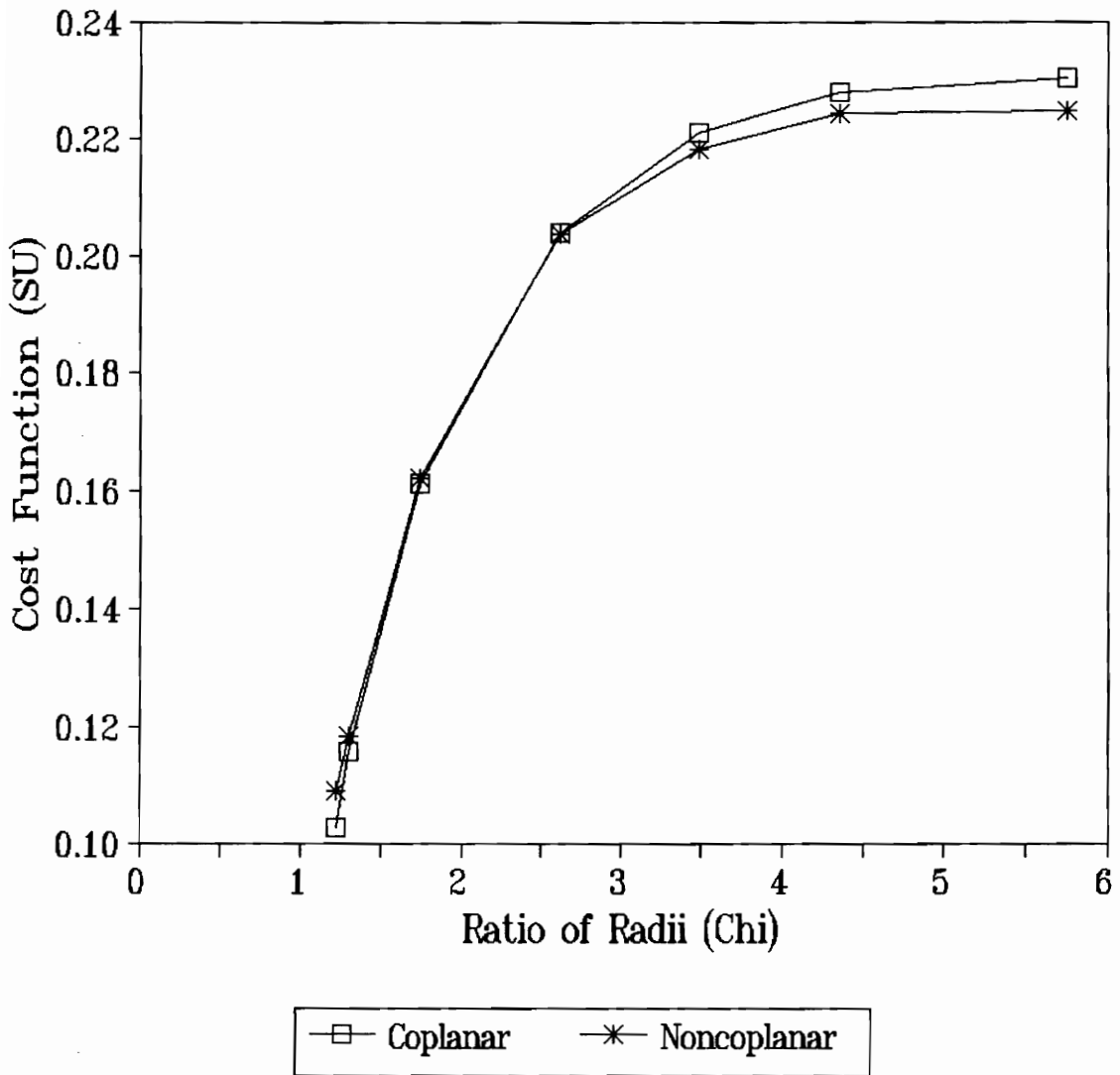
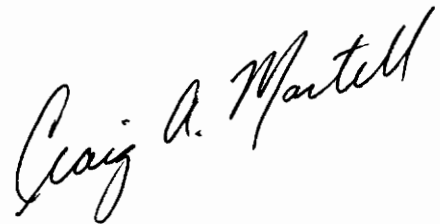


Figure 50. Coplanar and Noncoplanar Aeroassisted Transfer Cost Functions vs. χ

Vita

The author was born in Baltimore, Maryland on May twenty-third, nineteen hundred and sixty six. He received a Bachelor of Science degree in Aerospace Engineering from Virginia Polytechnic Institute and State University, Blacksburg, Virginia in May 1989. As well as attending the university at Blacksburg, the author also gained practical professional work experience working at Aberdeen Proving Grounds while enrolled in the university Co-Operative Education program. Upon completion of the Master of Science program, the author began his professional career at the Naval Surface Warfare Center in Dahlgren, Virginia.

This work is part of the requirements towards the degree of Master of Science in Aerospace Engineering at Virginia Polytechnic Institute and State University.

A handwritten signature in black ink that reads "Craig A. Martell". The signature is written in a cursive style and is positioned in the lower right quadrant of the page.